EXPLORING PHYSICS BEYOND THE STANDARD MODEL WITH NEUTRINO OSCILLATION

Ph. D. Thesis

Rudra Majhi

School of Physics,
Univrsity of Hyderabad

August, 2022

EXPLORING PHYSICS BEYOND THE STANDARD MODEL WITH NEUTRINO OSCILLATION

by

RUDRA MAJHI

17PHPH03

A thesis submitted in partial fulfillment for the degree of

DOCTOR OF PHILOSOPHY IN PHYSICS

School of Physics

University of Hyderabad

Hyderabad 500 046, INDIA

August 2022

DECLARATION

I hereby declare that, this thesis titled **Exploring Physics Beyond the Standard Model with Neutrino Oscillation** submitted by me, under the guidance and supervision of **Prof. Rukmani Mohanta**, is a bonafide research work and is free from plagiarism. I also declare that it has not been submitted previously, in part or in full to this University or any other University or Institution, for the award of any degree or diploma. I hereby agree that my thesis can be deposited in Shodhganga/INFLIBNET.

A report on plagiarism statistics from the University Librarian is enclosed.

Rudra Majhi

Hyderabad
Date: 22.08.2022

(Rudra Majhi)
Reg. No.: 17PHPH03

CERTIFICATE

This is to certify that the thesis entitled **Exploring Physics Beyond the Standard Model with Neutrino Oscillation** submitted by Rudra Majhi bearing registration number 17PHPH03 in partial fulfilment of the requirements for award of Doctor of Philosophy in the School of Physics is a bonafide work carried out by her under my supervision and guidance.

This thesis is free from plagiarism and has not been submitted previously in part or in full to this or any other University or Institution for award of any degree or diploma.

Further, the student has the following publications before the submission of the thesis for adjudication.

1) R. Majhi, S. Chembra and R. Mohanta, J. Phys. G 47, no.9, 095002 (2020) [arXiv:1911.10952 [hep-ph]], (ISSN No: 0954-3899 (online)), Chapter 3.

2) R. Majhi, D. K. Singha, K. N. Deepthi and R. Mohanta, Phys. Rev. D 104, no.5, 055002 (2021) doi:10.1103/PhysRevD.104.055002 [arXiv:2101.08202 [hep-ph]], (ISSN No: 2470-0029 (online)), Chapter 4.

3) R. Majhi, S. Chembra and R. Mohanta, Eur. Phys. J. C 80, no.5, 364 (2020) [arXiv:1907.09145 [hep-ph]], (ISSN No: 1434-605 (online)), Chapter 5.

Further, the student has passed the following courses towards fulfilment of course-work requirement for Ph.D:

Course Code	Name	Credits	Pass/Fail
PY801	Research Methodology	4	Pass
PY802	Advanced Quantum Mechanics	4	Pass
PY803	Advanced Experimental Techniques	4	Pass
PY804	Advanced Condensed Matter Physics	4	Pass

Rukmani Mohanta

Prof. Rukmani Mohanta
Thesis Supervisor
School of Physics
University of Hyderabad

Date: 22.08.2022

22/8/2022

Prof. K.C. James Raju
Dean
School of Physics
University of Hyderabad

DEAN
School of Physics
University of Hyderabad
HYDERABAD - 500 046

Acknowledgements

I would like to express my heartful gratitude to many people for their continuous support and encouragement throughout my research career.

First among these is my supervisor, Prof. Rukmani Mohanta, whom I would like to thank for allowing me to work with her. This thesis is possible only due to her endless guidance and support. It was a great pleasure to work with her. I also wish to thank her for her patience and for support throughout the Ph. D. duration.

I would like to convey my special thank to our Dean, Prof. K.C. James Raju for his encouraging words to pursue research. With the same respect, I wish to thank our former Dean of the School, Prof. A. Chatterjee, Prof. V. Seshubai and Prof. B. A. Bambah. Special thanks to Prof. B. A. Bambah for her inspiration in particle physics research.

I am extremely thankful to my doctoral committee members, Prof. E. Harikumar and Prof. Soma Sanyal for their support and suggestion during this period. In addition, I would like to convey my thanks to all the faculty members of our school.

Also I want to express my thanks to Prof. A. K. Giri, Indian Institute of Technology, Hyderabad for his guidance. Also I am very much fortunate to work with my collaborators Dr. Soumya C. and Dr. K. N. Deepthi, want to convey my thanks for their help and suggestion.

I acknowledge CMSD HPC facility of University of Hyderabad to carry out computations.

I acknowledge all the non-teaching staff of our School. My special thank goes to Mr. P. Narsimha Rao, Mr. Sudarshanam and former staffs Mrs. Saileja, Ms. Deepika for their patience and help in the academic activities.

I acknowledge the Innovation in Science Pursuit for Inspired Research (INSPIRE) for the financial support during my research period. Also thanks to " Collaboration by Indian Physicist on Neutrino Projects at Fermilab" sponsored by DST.

I would like to express my gratitude to my teachers (from School to University) for their support at different stages of my academic life. I am extremely thankful to them.

I would like to thank my seniors for their constant support during my research career. I am thankful to Dr. Monojit Ghosh, Dr. Suchismita Sahoo, Dr. S. Shiva Rama Krishna, Dr. S. Robertson and Dr. Atasi Ray for their encouraging words for research.

I want to thank Dinesh Bhai, Lipu Bhai, and my lab-mates Mitesh K. Behera and Akshaya Chatla, and Akash Tarai for spending a good time with me at university. I am extremely thankful to Aishwarya Bhatta, Dinesh, Priya and Papia.

I would also like to thank all my friends, specially Ph. D. friends Abhishek, Sovan, Nurul, Vishnu, Shiva, Debika, Susmita, Samir da, Najirul, Haritha, Suman. My M. Sc. friends Dipak, Ayusman, Bikash, Chinu, Rajesh, Yashobanta, Laxmi, Manaswini. B.Sc. friends Shantanu, Soumya, Akshaya, Diptiranjan. Also, I want to thank my childhood friends Satya, Dharamendra and Gopinath for being with me.

My family has been a source of unwavering support, and no words in these acknowledgements can adequately thank them. I would like to convey my love and special gratitude to my family members, without whose support and understanding, the success of my life journey was impossible.

Abstract

The tiny particle neutrino has a sizeable amount of idiosyncratic features. Neutrinos are neutral particles that possess tiny masses and participate in electroweak interactions. Although neutrinos are one of the most abundant particles in the universe, still conceal from the experimental detection due to the unusual behaviour. Recent observations from various experiments disclose the property of flavour changing process from one to another during the propagation of neutrinos, is known as Neutrino Oscillation. Neutrino oscillation confirmed the non-zero neutrino masses and mixing between different flavours and thus, opened up the gate for physics beyond standard model (BSM). The ceaseless efforts of highly dedicated neutrino experiments provide the results on precise measurement of solar and atmospheric neutrinos along with neutrino oscillation parameters. However, there are several unsettled issues like Mass Hierarchy, Octant of θ_{23}, CP violation in neutrino sector, exact value of CP phase δ_{CP}, absolute mass scale of neutrinos, etc. Additionally many well developed theoretical models illustrate that neutrino oscillation can be affected by various BSM physics such as existence of sterile neutrino, CPT violation, Lorentz violation, Non-standard interactions, Neutrino decay, etc. All these open questions create a boundless scientific interest for neutrino enthusiasts.

All the neutrino experiments have the primary objectives of measuring the oscillation parameters with great accuracy, studying the unknowns of this sector, and explaining different BSM scenarios. Long-baseline neutrino oscillation experiments have a crucial role in this regards. There are several currently running experiment (NOvA and T2K) and future based planned experiments (DUNE, T2HK, T2HKK, ESSnuSB, P2O). This thesis is based on the study of physics beyond standard model at long-baseline experiments.

Based on the anomalous results from short-baseline experiments, we have considered a light sterile neutrino to standard three flavor neutrinos. The impact of sterile neutrino on neutrino oscillation as well as on the sensitivity of NOvA and T2K experiments. Implication of light sterile neutrino on Neutrinoless Double Beta Decay have been discussed briefly. Further the CPT violation has been studied for future long-baseline experiments (T2HK, T2HKK, DUNE, ESSnuSB) in a model independent way. Also, obtained the bounds on the CPT violating parameters for these experiments. Future experiments will be able to establish CPT

violating signals if it exist in nature in neutrino sector. Also, we have studied the CPT violation originating from Lorentz invariance violation at NOvA and T2K experiments. Found that Lorentz violation can affect the neutrino oscillation both at probability and sensitivity levels. Furthermore, the sensitivity limits on the Lorentz violating parameters are obtained for NOvA, T2K and synergy of NOvA and T2K.

Contents

List of Figures

List of Tables

Dedicated to my family,
specially to my beloved father and mother.

Chapter 1

Introduction

1.1 Standard Model of particle physics

Efforts of thousands of Physicists brought some remarkable explanations of fundamental symmetry and structure of the universe. Our universe is made up of elementary particles which are inter-connected through four fundamental forces. Standard Model (SM) is a well established theoretical model narrates the fundamental particles and the three fundamental forces (i.e. electromagnetic, weak and strong forces) out of four. Also, it is a low energy effective field theory emerged from unified description of gravity and quantum physics at Planck scale. SM is able to predict various phenomena and explains most of the experimental results in Particle physics. Hence, it has been established as one of the most successful theories in physics.

1.1.1 Particle content

SM is a gauge theory, based on the gauge symmetry $SU(3)_C \times SU(2)_L \times U(1)_Y$ [1–3], where the subscripts C, L and Y represent the color, left handedness and hyper charge, respectively. The gauge theory describes the strong, electromagnetic and weak interactions among the fundamental particles. The particle content of the SM is given in the Table [1.1]. Elementary particles are categorised into Fermions and Bosons depending on the spin quantum number. Fundamental particles having half-integral spin i.e., Fermions are classified as Quarks and Leptons. These

particles appear in three families and two particles in each family. Quarks exist in six flavours namely *up (u), down (d), charm (c), strong (s), top (t)* and *bottom (b)* quarks. Correspondingly there exist six antiquarks for six flavours. Combination of two or more quarks with the help of strong interaction results to some subatomic particles called hadrons. Hadrons are grouped into two categories, meson and baryon. Mesons are made up of quark and anti-quark pair while Baryons are constructed from three quarks. According to Pauli-exclusion principle "color" charge introduced for quarks are Red (R), Green (G) and Blue (B). These colors are changed to corresponding anti-colors for antiquarks. A combination of the three colors or a combination of color and anti-color can result in a colorless particle; hence the observed hadrons are colorless in nature. The other fundamental spin-half particles in SM are Leptons, classified as charged leptons (electron (e), muon (μ), tau (τ)) and neutral leptons (electron-neutrino (ν_e), muon-neutrino (ν_μ), tau-neutrino (ν_τ)).

The gauge group $SU(3)_C$ contains both left and right handed quark triplets having color charges to participate in strong interactions. Left handed particles are doublets and right handed particles are singlets under $SU(2)_L$ symmetry. Left handed particles only take part in weak interaction through $SU(2)_L$ symmetry. Both the left and right handed charged particles participate in electromagnetic interaction under $U(1)_{em}$ gauge group. The unification of weak and electromagnetic interactions is known as electroweak interaction represented as $SU(2)_L \times U(1)_Y$ gauge group.

In addition to these, there are four types of gauge bosons, which are the force carriers. Gluons (g) and photon (γ) mediate strong and electromagnetic interactions, respectively. Weak force is mediated by the charged gauge bosons $W^{\pm}$ and neutral boson Z^0. The spin-less particle Higgs boson, which is doublet under the $SU(2)_L$ is responsible for the origin of mass for the fundamental particles.

1.2 Symmetries in gauge theory

Symmetry of a physical system under a continuous transformation leads to a conservation law by Noether's theorem and also implies some unmeasurable quantities. Gauge symmetry is the basic underlying symmetry of SM. Any quantum

Particles	Fields	$SU(3)_C$	$SU(2)_L$	$U(1)_Y$	Q
Quarks	$Q_L \equiv \begin{pmatrix} u \\ d \end{pmatrix}_L \begin{pmatrix} c \\ s \end{pmatrix}_L \begin{pmatrix} t \\ b \end{pmatrix}_L$	3	2	1/6	$\begin{pmatrix} 2/3 \\ -1/3 \end{pmatrix}$
	u_R, c_R, t_R	3	1	2/3	2/3
	d_R, s_R, b_R	3	1	$-1/3$	$-1/3$
Leptons	$\ell_L \equiv \begin{pmatrix} \nu_e \\ e \end{pmatrix}_L \begin{pmatrix} \nu_\mu \\ \mu \end{pmatrix}_L \begin{pmatrix} \nu_\tau \\ \tau \end{pmatrix}_L$	1	2	$-1/2$	$\begin{pmatrix} 0 \\ -1 \end{pmatrix}$
	$\ell_R \equiv e_R, \mu_R, \tau_R$	1	1	-1	-1
Scalar	H	1	2	1/2	$\begin{pmatrix} 1 \\ 0 \end{pmatrix}$

TABLE 1.1: Particle content of SM and their quantum numbers.

state $\psi(x)$ can be gauged by some arbitrary phase α:

$$\psi(x) \to \psi'(x) = \psi(x)e^{i\alpha} \,, \tag{1.1}$$

where α is a non-physical and unmeasurable parameter. Invariance of SM interactions in terms of gauge fields is known as global gauge invariance.

Let us first consider the gauge invariance in the fermionic sector. The Dirac Lagrangian for fermionic field is given as,

$$\mathcal{L} = i\overline{\psi}\gamma^\mu\partial_\mu\psi - m\overline{\psi}\psi \,, \tag{1.2}$$

which is invariant under global gauge transformation Eqn. (1.1). However, under $U(1)$ local phase transformation i.e., for a space time dependent arbitrary phase $\alpha(x)$, the states will transform as

$$\psi \to \psi' = \psi e^{i\alpha(x)Q}, \tag{1.3}$$

where Q is the generator for the $U(1)$ group. The Dirac Lagrangian Eqn. (1.2) transforms as

$$\mathcal{L} \to \mathcal{L}' = \overline{\psi}\left(i\gamma^\mu\partial_\mu - \gamma^\mu\partial_\mu\alpha(x)Q - m\right)\psi \,, \tag{1.4}$$

and hence, is not invariant under this local gauge transformation. In order to

preserve its invariance, demands the introduction of a new bosonic gauge field A_μ, having transformation property

$$A_\mu \to A'_\mu = A_\mu + \frac{1}{e}\partial_\mu \alpha(x) \ . \tag{1.5}$$

At the same time, the ordinary derivative has to be replaced by the covariant derivative, defined as

$$D_\mu = \partial_\mu - ieA_\mu \ . \tag{1.6}$$

Thus, the $U(1)$ invariant Lagrangian in terms of covariant derivative is expressed as,

$$\mathcal{L} = \overline{\psi}(i\gamma^\mu D_\mu - m)\psi. \tag{1.7}$$

The new gauge field A_μ can be identified as the massless photon as one can't write a gauge invariant mass term $\frac{1}{2}m^2 A_\mu A^\mu$ for it. As the Lagrangian in Eqn. (1.7) represents the interaction between the Dirac and the electromagnetic fields, hence identified as the Lagrangian for Quantum Electrodynamics (QED),

$$\mathcal{L}_{QED} = \overline{\psi}(i\gamma^\mu \partial_\mu - m)\psi - e\overline{\psi}\gamma^\mu Q\psi A_\mu - \frac{1}{4}F^{\mu\nu}F_{\mu\nu} \ , \tag{1.8}$$

where $F_{\mu\nu} = \partial_\mu A_\nu - \partial_\nu A_\mu$ is the field tensor and $-\frac{1}{4}F^{\mu\nu}F_{\mu\nu}$ is the kinetic energy for the photon. The term (e) represents the electric charge.

In a similar manner like $U(1)$, one can do local gauge invariance for $SU(N)$, under which any fermionic filed $\psi(x)$ can be transformed as

$$\psi(x) \to e^{i\alpha_a(x)T_a}\psi(x) \ , \tag{1.9}$$

where T_a's are the generators of $SU(N)$ group. These generators satisfy the Lee-algebra

$$[T_a, T_b] = if_{abc}T_c \ , \tag{1.10}$$

where f_{abc}'s are the structure constants. The covariant derivative for this local gauge transformation after introducing the gauge fields G^a_μ is given as,

$$D_\mu = \partial_\mu + igT_a G^a_\mu \ , \tag{1.11}$$

and the transformation rule for the field G^a_μ is

$$G^a_\mu \to G^a_\mu - \frac{1}{g}\partial_\mu \alpha_a - f_{abc}\alpha_b G^c_\mu \, . \tag{1.12}$$

Thus, the invariant Lagrangian under local gauge transformation $SU(N)$ becomes

$$\mathcal{L}_{SU(N)} = \overline{\psi}(i\gamma^\mu \partial_\mu - m)\psi - g\left(\overline{\psi}\gamma^\mu T_a \psi\right) G^a_\mu \, . \tag{1.13}$$

Realising Eqn. (1.9) for local gauge transformation in $SU(3)$, the Lagrangian for strong interaction, referred to as Quantum Chromodynamics (QCD) is given as,

$$\mathcal{L}_{QCD} = \overline{\psi}(i\gamma^\mu \partial_\mu - m)\psi - g\left(\overline{\psi}\gamma^\mu T_a \psi\right) G^a_\mu - \frac{1}{4} G^a_{\mu\nu} G^{\mu\nu}_a, \tag{1.14}$$

where G^a_μ fields are representation of massless gluons which interact with quarks by coupling constant g. There are eight such gluons as $a = 1, 2, 3, ..8$ and the field strength tensor $G^a_{\mu\nu}$ for $SU(3)$ is expressed as

$$G^a_{\mu\nu} = \partial_\mu G^a_\nu - \partial_\nu G^a_\mu - g f_{abc} G^b_\mu G^c_\nu \, . \tag{1.15}$$

In 1961, Glashow introduced an enlarged symmetry group by including $SU(2)_L$ and $U(1)_Y$ as $SU(2)_L \times U(1)_Y$, prior to the discovery of Electro-Weak interactions by Weinberg and Salam. This gauge symmetry explains the electromagnetic and weak interactions in an unified picture, known as the Weinberg-Salam model.

In electromagnetic interaction, under local gauge transformation as described in Eqn. (1.8), the current element and interaction Lagrangian can be written as

$$\begin{aligned} J^{em}_\mu &= e\overline{\psi}\gamma_\mu Q\psi, \\ \mathcal{L}_I &= -ieJ^{em}_\mu A^\mu = -ie(\overline{\psi}\gamma_\mu Q\psi)A^\mu \, , \end{aligned} \tag{1.16}$$

where Q is the charge operator for $U(1)_{em}$ group and $Q = -1$ for electron.

In a similar fashion one can write the interaction term for a weak process in two ways.
(i) Coupling of weak current J_μ to three vector bosons W_μ for $SU(2)_L$

$$-igJ_\mu \cdot W^\mu = -ig\overline{\psi}_L \gamma_\mu \mathbf{T} \cdot \mathbf{W}^\mu \psi_L \, . \tag{1.17}$$

(ii) Coupling of weak hypercharge current J_μ^Y to the vector bosons B_μ for $U(1)_Y$

$$-i\frac{g'}{2}J_\mu^Y B^\mu = -ig'\overline{\psi}\gamma_\mu\frac{Y}{2}\psi B^\mu \ , \tag{1.18}$$

where $\mathbf{T}$ and Y are the generators while g and g' are the coupling strengths for $SU(2)_L$ and $U(1)_Y$ groups, respectively. ψ_L and ψ_R are the left and right handed components of the state ψ and their gauge transformations are,

$$\psi_L \to \psi'_L = \psi_L e^{i(\alpha_b(x)T_b+\beta(x)Y)}, \tag{1.19}$$

$$\psi_R \to \psi'_R = \psi_R e^{i\beta(x)Y} \ , \tag{1.20}$$

with T_b $(b = 1, 2, 3)$ represent the different components of the generator $\mathbf{T}$. The generators satisfy the relation,

$$\begin{aligned} Q &= T^3 + \frac{Y}{2} \ , \\ \text{hence, } J_\mu^{em} &= J_\mu^3 + \frac{1}{2}J_\mu^Y \ . \end{aligned} \tag{1.21}$$

Equation (1.21) shows that the electromagnetic interaction is combination of the neutral currents J_μ^3 and J_μ^Y. The observable neutral gauge fields A_μ and Z_μ are orthogonal combination of the two gauge fields W_μ^3 and B_μ.

The corresponding gauge invariant Lagrangian is given as

$$\begin{aligned} \mathcal{L} = \overline{\psi}_L\gamma^\mu\left(i\partial_\mu - g\mathbf{T}\cdot\mathbf{W}_\mu - g'\left(\frac{-1}{2}\right)B_\mu\right)\psi_L + \overline{\psi}_R\gamma^\mu\left(i\partial_\mu - g'(-1)B_\mu\right)\psi_R \\ - \frac{1}{4}W_{\mu\nu}.W^{\mu\nu} - \frac{1}{4}B_{\mu\nu}B^{\mu\nu} \ , \end{aligned} \tag{1.22}$$

where $W_{\mu\nu} = \partial_\mu W_\nu - \partial_\nu W_\mu - gW_\mu \times W_\nu$ and $B_{\mu\nu} = \partial_\mu B_\nu - \partial_\nu B_\mu$ are the kinetic energy terms for W_μ and B_μ fields, respectively. This extended symmetry $SU(2)_L \times U(1)_Y$ breaks down spontaneously to the symmetry group $U(1)_{em}$ through Higgs mechanism, generating massive weak gauge bosons $W^\pm$ and Z^0.

1.3 Higgs Mechanism

Spontaneous symmetry breaking (SSB) is an ingenious way to get the mass of a particle, which is also known as Higgs Mechanism [4–7]. Let's understand the SSB

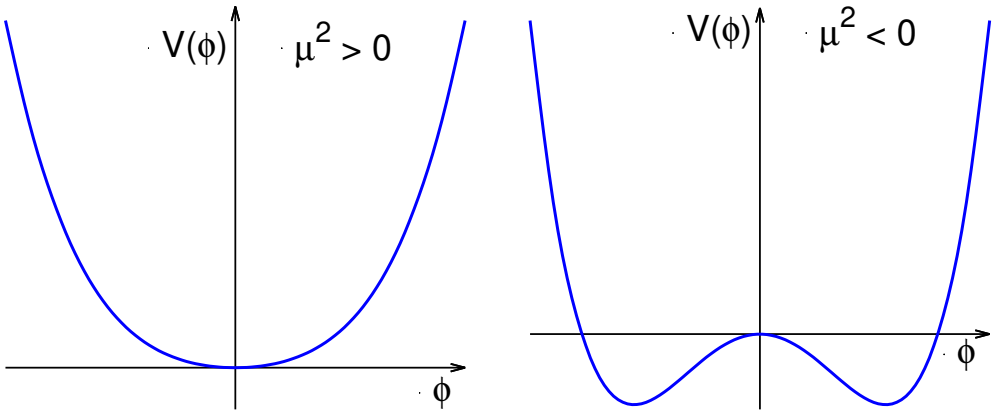

FIGURE 1.1: Potential Energy $V(\phi) = (\frac{1}{2}\mu^2\phi^2 + \frac{1}{4}\lambda\phi^4)$ as a function of ϕ with $\mu^2 > 0$ in left panel and $\mu^2 < 0$ in the right panel.

by considering a simple scalar field ϕ having the Lagrangian,

$$\mathcal{L} = \underbrace{\frac{1}{2}(\partial_\mu\phi)^2}_{\text{Kinetic Energy}} - \underbrace{\left(\frac{1}{2}\mu^2\phi^2 + \frac{1}{4}\lambda\phi^4\right)}_{\text{Potential Energy}} . \tag{1.23}$$

This Lagrangian is invariant under $U(1)$ symmetry and has a reflection symmetry around the field $\phi = 0$. For a value of $\mu^2 > 0$, it will represent the mass of a scalar particle in potential term. The interaction term ϕ^4 is four particle interaction with coupling λ. As usual, the minimum point for this particular choice of potential will be at $\phi = 0$ which will have the reflection symmetry as shown in the left panel of Fig. 1.1.

However, the choice of $\mu^2 < 0$ and $\lambda > 0$ will lead to an intriguing feature. The potential will have the non-zero minima as shown in right panel of Fig.1.1 at

$$\phi = \pm\sqrt{\frac{-\mu^2}{\lambda}} = \pm v . \tag{1.24}$$

A perturbation around the minimum point v can be induced through a quantum fluctuation $\eta(x)$ as

$$\phi = v + \eta(x) . \tag{1.25}$$

Incorporating Eqn. (1.25) into Eqn. (1.23), the Lagrangian can be expressed in terms of η as

$$\mathcal{L}' = \frac{1}{2}(\partial_\mu \eta)^2 - \lambda v^2 \eta^2 - \lambda v \eta^3 - \frac{1}{4}\lambda \eta^4 + \text{const.} \tag{1.26}$$

One can thus obtain the mass of the field η as $m_\eta = \sqrt{2\lambda v^2} = \sqrt{-2\mu^2}$. Other higher order terms of η correspond to its self interacting terms. Here the reflection symmetry is broken due to our choice of ground state and as a consequence generated mass for the field η. This phenomenon is known as the "Spontaneous Symmetry Breaking".

In a similar fashion, for a complex field one can perturb the ground state by field η and ξ to generate the mass, i.e.,

$$\phi(x) = \sqrt{\frac{1}{2}}(v + \eta + i\xi) \ . \tag{1.27}$$

As in the previous case, the mass for η can be generated as $m_\eta = \sqrt{-2\mu^2}$, but the field ξ will appear as a massless particle, known as Goldstone Boson.

Similarly, considering a complex scalar field ϕ, doublet under $SU(2)$, one can show the SSB of $SU(2)$ gauge symmetry. Also, we will get mass for the three gauge fields.

1.3.1 Gauge Boson mass

Higgs mechanism has been discussed in detail for only $U(1)$ and $SU(2)$ symmetries in the previous section. Analogously, in $SU(2) \times U(1)$ symmetry, we can generate the masses for $W^\pm$ and Z^0 bosons and massless photon by introducing four scalar fields ϕ_i through Higgs mechanism. In order to have gauge invariant Lagrangian these four fields will be arranged as a doublet under $SU(2)$ having unit hypercharge quantum number,

$$\phi = \begin{pmatrix} \phi^+ \\ \phi^0 \end{pmatrix}, \tag{1.28}$$

where

$$\phi^+ = (\phi_1 + i\phi_2)/\sqrt{2}\,, \qquad (1.29)$$
$$\phi^0 = (\phi_3 + i\phi_4)/\sqrt{2}\,.$$

This is one most effective choice of ϕ made by Weinberg in 1967. The gauge invariant Lagrangian in $SU(2) \times U(1)$ is given as

$$\mathcal{L}_I = \left| \left(i\partial_\mu - g\mathbf{T}\cdot\mathbf{W}_\mu - g'\frac{Y}{2}B_\mu \right)\phi \right|^2 - \left(\frac{1}{2}\mu^2\phi^2 - \frac{1}{4}\lambda\phi^4 \right)\,. \qquad (1.30)$$

With the choice of Higgs potential for $\mu^2 < 0$ and $\lambda > 0$, one can generate the masses for the gauge bosons, by choosing the vacuum expectation value of ϕ as ϕ_0

$$\phi_0 = \sqrt{\frac{1}{2}}\begin{pmatrix} 0 \\ v \end{pmatrix}. \qquad (1.31)$$

Under this particular choice of ϕ_0, the $SU(2) \times U(1)$ spontaneously breaks down to $U(1)_{em}$.

Substituting the vacuum expectation value of ϕ in Eqn. (1.30), one can generate masses for the gauge bosons as shown below:

$$\begin{aligned}
&\left| \left(-g\mathbf{T}\cdot\mathbf{W}_\mu - g'\frac{Y}{2}B_\mu \right)\phi \right|^2 \\
&= \frac{1}{8}\left| \begin{pmatrix} gW_\mu^3 + g'B_\mu & g(W_\mu^1 - iW_\mu^2) \\ g(W_\mu^1 + iW_\mu^2) & -gW_\mu^3 + g'B_\mu \end{pmatrix} \begin{pmatrix} 0 \\ v \end{pmatrix} \right|^2 \\
&= \frac{1}{8}v^2g^2\left[(W_\mu^1)^2 + (W_\mu^2)^2 \right] + \frac{1}{2}v^2\left(-gW_\mu^3 + g'B_\mu \right)\left(-gW^{3\mu} + g'B^\mu \right) \\
&= \frac{1}{4}v^2g^2W_\mu^+W^{-\mu} + \frac{1}{8}v^2\left(gW_\mu^3 - g'B_\mu \right)^2 + 0\left(g'W_\mu^3 + gB_\mu \right)^2\,, \qquad (1.32)
\end{aligned}$$

where $\mathbf{T} = \boldsymbol{\tau}/2$ and $W^\pm = (W^1 \mp iW^2)/\sqrt{2}$. The first term in the Eqn. (1.32) can be identified as the mass term for gauge boson W, with mass

$$M_W = \frac{1}{2}vg\,. \qquad (1.33)$$

In Eqn. (1.32), the second and third terms can be identified as mass terms for the orthogonal combination of W_μ^3 and B_μ fields. The normalised state of these

combination of fields are

$$A_\mu = \frac{g' W_\mu^3 + g B_\mu}{\sqrt{g^2 + g'^2}} \text{ and } Z_\mu = \frac{g' W_\mu^3 - g B_\mu}{\sqrt{g^2 + g'^2}} \, . \tag{1.34}$$

The fields A_μ and Z_μ are neutral physical fields and the 2nd and 3rd terms in Eqn. (1.32) can be identified as their mass terms

$$\frac{1}{2} M_Z^2 Z_\mu^2 + \frac{1}{2} M_A^2 A_\mu^2 \, , \tag{1.35}$$

with $M_A = 0$ and $M_Z = \frac{1}{2} v \sqrt{g^2 + g'^2}$. Using the value of Fermi coupling constant in weak interaction

$$\frac{G}{\sqrt{2}} = \frac{g^2}{8 M_W^2} = \frac{1}{2v^2} \, , \tag{1.36}$$

one can calculate the vacuum expectation value for Higgs particle as $v/\sqrt{2} = 174$ GeV.

Interestingly, in terms of the weak mixing angle $(g'/g) = \tan\theta_W$ the physical fields can be written in terms of gauge boson W_μ^3 and B_μ basis,

$$\begin{pmatrix} A_\mu \\ B_\mu \end{pmatrix} = \begin{pmatrix} \cos\theta_W & \sin\theta_W \\ -\sin\theta_W & \cos\theta_W \end{pmatrix} \begin{pmatrix} B_\mu \\ W_\mu^3 \end{pmatrix} . \tag{1.37}$$

In this way, by Higgs mechanism we can get the massive gauge bosons $W_\mu^\pm$ and Z_μ and massless photon A_μ.

1.3.2 Fermion mass

Higgs mechanism is well enough to generate the mass for leptons and quarks with same choice of Higgs field as we choose for generating the gauge boson masses. Gauge invariant Lagrangian involving the mass terms for leptons and quarks is

$$\mathcal{L}_Y = -\left(Y_\ell \bar{L}_L \phi \ell_R + Y_d \bar{Q}_L \phi d_R + Y_u \bar{Q}_L \tilde{\phi} u_R + \text{h.c.} \right) \, , \tag{1.38}$$

where Q_L and L_L are the left-handed quark and lepton doublets, while u_R (d_R) and ℓ_R are the right handed up (down) type quark and charged-lepton singlets. The coefficients Y_ℓ, Y_u and Y_d represent the Yukawa couplings. The field $\tilde{\phi}$ denotes

the conjugate Higgs doublet of ϕ. Both ϕ and $\tilde{\phi}$ can be written as

$$\phi = \begin{pmatrix} \phi^+ \\ \phi^0 \end{pmatrix}, \tag{1.39}$$

$$\tilde{\phi} = -i\tau_2\phi^* = \begin{pmatrix} -\overline{\phi}^{\,0} \\ \phi^- \end{pmatrix}. \tag{1.40}$$

The symmetry can be broken spontaneously by perturbating our choice of vacuum expectation value for ϕ. The ground states for ϕ and $\tilde{\phi}$ are given as

$$\phi = \sqrt{\frac{1}{2}} \begin{pmatrix} 0 \\ v + h(x) \end{pmatrix} \text{ and } \tilde{\phi} = \sqrt{\frac{1}{2}} \begin{pmatrix} v + h(x) \\ 0 \end{pmatrix}, \tag{1.41}$$

where $h(x)$ is a neutral Higgs field. Neglecting the interaction of $h(x)$ with leptons, one can generate the masses as

$$\text{Mass of leptons: } M_l = \frac{Y_\ell}{2} v \,, \tag{1.42}$$

$$\text{Mass of quarks: } M_q = \frac{Y_q}{\sqrt{2}} v \,. \tag{1.43}$$

1.4 Neutrinos in the Standard Model

Neutrinos are one of the most fundamental and mysterious particles found in our universe. These fermions being chargeless and colourless in nature, participate only in weak interactions. Although neutrinos are the second most abundant particles in nature, it is very hard to detect them due to their extremely feeble interaction, and hence they are the least understood particles of nature due to their perplexing properties. In the SM of particle physics neutrinos are considered to be massless unlike other fermions. Neutrinos are considered to be the most fascinating particles in nature, posses many unique and interesting features in contrast to the other SM fermions. Indeed, we now know that neutrinos are massive albeit extremely light, and change their flavour as they propagate. This characteristic is known as Neutrino Oscillation, the understanding of which requires physics beyond the SM (BSM). Neutrinos can be used as a tool to probe new physics beyond the SM. Last

couple of decades have witnessed the emergence of many fascinating properties of neutrinos by different experiments.

1.5 History of Neutrinos

Although neutrino is a very tiny particle, it has a long history [8]. The idea of existence of neutrinos proposed by Wolfgang Pauli in 1930 to save the conservation of energy in Beta decay. He introduced a neutral lightly massive particle, which he named as "neutron", to explain the missing energy in the Beta decay process. This tiny particle carried away the missing energy results to the observation of continuous energy spectrum of electrons. He made a statement for non-observation of this particle in any experiment that, "I have done a terrible thing. I have postulated a particle that can not be detected."

In the year 1932, James Chadwick discovered a neutral particle named as neutron very heavy compare to Pauli's particle. Two years later, Enrico Fermi developed the theory of weak interaction, where he renamed Pauli's particle as neutrino means "little neutral one". After two decades of Pauli's prediction in 1956, the first experimental evidence for neutrino given by Fedrick Reines and Cylde Cowan at Los Alamos National Laboratory [9]. They discovered electron anti neutrino ($\overline{\nu}_e$) by observing inverse beta decay process ($\overline{\nu}_e + p \rightarrow n + e^+$) using organic liquid scintillators. This positron (e^+) gets annihilated with the electron to produce two gamma rays. Thereafter, a delayed gamma ray is produced due to the capture of the neutron by atomic nucleus. Observation of these two signals is the signature of existence of neutrino. In a telegram to W. Pauli, they mentioned their success as "We are happy to inform you that we have definitively detected neutrinos". Later Fedrick Reines awarded Nobel prize in physics for the year 1995.

In between, the prediction of double beta decay with neutrinos given by Maria Goeppert Mayer in 1935. Two years later, Ettore Majorana gave the concept of Majoran nature for neutrinos. Wendell Furry combined the idea of G. Mayer and E. Majorana to suggest the special decay process Neutrinoless double beta decay can explain the Majorana nature of neutrinos.

Golden period for neutrino sector started from mid 19th century. Concept of neutrino oscillation introduced by Burno Pontecorvo in 1957 before the discovery of

other flavor of neutrinos. Later in 1962, the second type of neutrino ν_μ discovered by a group of scientists under the leadership of Lederman, Mel Schwartz and Jack Steinberger at Brookhaven National Laboratory, and they were awarded with Nobel Prize in 1988. In 1968, the first ever solar neutrinos observed by the Homestake experiment. It observed only one-third of predicted solar neutrinos, and this anomalous result is known as "solar neutrino anomaly". Similarly the collaboration of Kamiokande and IMB in 1985 observed the discrepancy in atmospheric neutrinos. The ratio of ν_μ to ν_e is smaller than the predicted ratio, known as the atmospheric neutrino anomaly. In the year of 1998, the first ever evidence for neutrino oscillation observed at Super-Kamiokande experiment. DONUT (Direct observation of Nu Tau) experiment discovered the third type of neutrino, i.e., tau neutrino (ν_τ) in the mid of 2000. Another Nobel Prize to neutrino sector came in the year 2002 for the detection of cosmic neutrinos at Kamiokande experiment. Half of the Nobel prize in physics for this year shared by Ray Davis and Masatoshi Koshiba. In the year 2015, the Nobel Prize has been awarded jointly to Arthur B. McDonald from SNO experiment and Takaki Kajita from Super-Kamiokande experiment, for the discovery of Neutrino Oscillation. Nowadays there are several type of neutrino experiments are there to explore properties of neutrinos.

1.6 Neutrinos Beyond the Standard Model

From different well established experimental observations, it is found that neutrinos show flavor transition behaviour during propagation called neutrino oscillation, suggests that neutrinos do posses small but non-zero mass and mixing. This clearly indicates that SM is not the complete theory of nature and has to be extended. Neutrinos can be considered as a gateway to various BSM physics.

1.6.1 Neutrino Mass

Neutrinos are considered as massless fermions in the SM, and do not have mass unlike other fermions. For fermions, mass can be realized as the coupling between right and left handed helicity states through Youkawa coupling as discussed in section 1.3.2, and the mass term in the Lagrangian is given as

$$-\mathcal{L}_{\text{mass}} = M_D \overline{\psi}_L \psi_R + h.c.. \tag{1.44}$$

In order to have mass for neutrinos, we have to look beyond SM, as there are no right-handed neutrino states in the SM.

In other way Majorana mass for neutrinos can be expressed as

$$-\mathcal{L}_{\text{mass}} = M_M \psi_L^T C^{-1} \psi_L \ . \tag{1.45}$$

Right-handed neutrino state can be realised by the same way as the left handed antineutrino state, but this mass term violates lepton number by two units. In the SM, lepton number is an exact symmetry, hence neutrinos have no Majorana mass. Majorana mass cann't be accommodated through perturbation theory. Hence, neutrinos are massless in all orders of perturbation theory.

The mass can be obtained through some special mechanism. Before that let's have an idea about the Dirac and Majorana mass terms for neutrinos in beyond the SM framework.

1.6.1.1 Dirac mass for Neutrino

For charged fermions, the mass term is only the Dirac mass as given in Eqn. (1.44). For neutrinos, the Dirac mass can be obtained by considering a right-handed neutral lepton field ν_R, which is singlet under $SU(3)_C \times SU(2)_L \times U(1)_Y$ symmetry. The corresponding Lagrangian density is given as

$$-\mathcal{L}_{\text{mass}} = \sum_{\ell,\ell'} Y_{ll'} \overline{\psi}_{\ell L} \phi \nu_{\ell' R} + h.c. \tag{1.46}$$

After SSB, the mass matrix elements can be obtained as,

$$M_{\ell\ell'} = Y_{\ell\ell'} \frac{v}{\sqrt{2}} \ . \tag{1.47}$$

After standard diagonalisation of this 3×3 mass matrix, neutrino masses can be obtained. The generation of mass in this mechanism leading to an open question regarding the extraordinary small mass for neutrinos.

1.6.1.2 Majorana mass for Neutrino

Majorana proposed that for neutral particles, the right handed state of the particle can be identified as the left handed state of anti-particle in a Lorentz invariant way, i.e.,

$$\nu_R = (\nu_L)^c = C\overline{\nu_l}^T = C\gamma_0\nu_L^* \, . \tag{1.48}$$

In order to have mass in a gauge invariant way, we have to consider the coupling of neutrinos to two Higgs fields as in Fig 1.2. Thus, the two left-handed states coupled to the two Higgs fields through dimension-five operator given as [10]

$$-\mathcal{L}_{\text{mass}} = \frac{\alpha_\nu}{M} L_L^T C\tilde{\phi}^T \tilde{\phi} L_L + h.c., \tag{1.49}$$

where, ϕ is the Higgs field and α_ν is the dimensionless coupling constant. For renormalizable purpose, the factor M is introduced which has dimension of mass. After SSB, one can get the mass term as,

$$m_\nu = \alpha_\nu \frac{v^2}{M} \, . \tag{1.50}$$

The smallness of neutrino mass can be explained through this model by con-

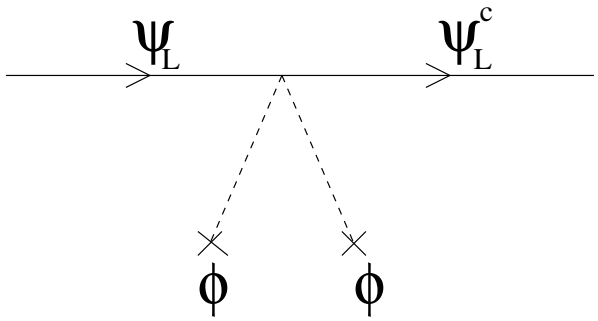

FIGURE 1.2: Majorana coupling between neutrinos and Higgs fields.

sidering M as much heavier compared to the scale of vacuum expectation value v.

1.6.2 Seesaw Mechanism

In order to generate the masses for neutrinos, the commonly used framework is the seesaw mechanism [11–13]. In the SM, dimension $d = 4$ terms in the Lagrangian are unable to generate the mass terms, so we need an effective Lagrangian which contains terms of order $d > 4$. The corresponding effective Lagrangian is expressed as,

$$\begin{aligned} \mathcal{L} &= \mathcal{L}_{SM} + \mathcal{L}_{eff}^{d=5} + \mathcal{L}_{eff}^{d=6} + .. \,, \\ \mathcal{L} &= \mathcal{L}_{SM} + \sum_{n=5}^{\infty} \sum_{i=1} \left(\frac{b_i^n}{\Lambda_i^{n-4}} O_i^n + h.c. \right) \,. \end{aligned} \tag{1.51}$$

Higher order terms are suppressed by a factor $\frac{b_i^n}{\Lambda^{n-4}}$, where Λ is the new physics scale. The lowest possible dimension term $d = 5$ will dominate over other higher order terms. The corresponding dimension five operators are called Weinberg Operators $\mathcal{O}^{d=5} = (\bar{L}^c \tilde{\phi}^*)(\tilde{\phi}^\dagger L)$. These operators generate Majorana mass for neutrinos by SSB and can be mediated by singlet fermion or by triplet scalar or by triplet fermion. In all these processes, light neutrino mass will be generated at the cost of a heavy particle, hence the mechanism is known as see-saw mechanism. See-saw mechanism categorised into three types as i) Type-I, ii) Type-II, iii) Type-III, depending upon the mediated particle in the Weinberg operator.

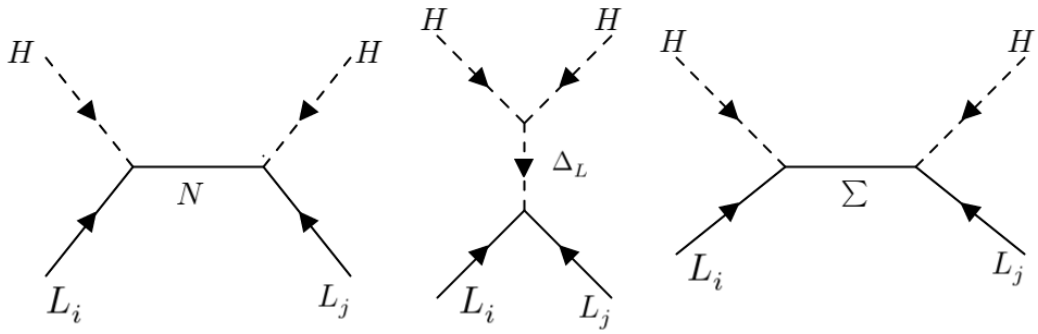

FIGURE 1.3: Neutrino masses through i) Type-I, ii) Type-II and iii) Type-III seesaw model (from left to right).

1.6.2.1 Type-I seesaw

Three singlet right-handed neutrinos (N_{Ri}) added to SM to generate tiny masses for neutrinos. These N_{Ri} will mediate the interaction of neutrinos with Higgs as

shown in the left panel of Fig. 1.3. The effective Lagrangian will be

$$\mathcal{L} = \mathcal{L}_{\mathcal{SM}} + \mathcal{L}_{N_R} \ , \tag{1.52}$$

where $\mathcal{L}_{N_R}$ is the Lagrangian term for N_R given as

$$\mathcal{L}_{N_R} = i\bar{N}_R \not{\partial} N_R - (\bar{L}_L \tilde{\phi} Y_\nu N_R + h.c.) - \frac{Y_\nu}{\Lambda}(\bar{L}^c \tilde{\phi}^*)(\tilde{\phi}^\dagger L) \ . \tag{1.53}$$

Here Y_ν is the Yukawa coupling. After spontaneous symmetry breaking through Higgs field, the Yukawa coupling term gives the Dirac mass term and Weinberg term gives the Majorana mass term as

$$-\mathcal{L}_{mass} = \frac{1}{2}\Big[M_D \bar{\nu}_L N_R + M_D \bar{N}_R^c \nu_L^c + M_m \bar{N}_R^c N_R + h.c.\Big] \ , \tag{1.54}$$

where Dirac mass: $M_D = \dfrac{Y_\nu v}{\sqrt{2}}$ and Majorana mass: $M_m = \dfrac{Y_\nu^2 v^2}{2\Lambda}$.

Thus, the neutrino mass matrix (M_ν) in the basis (ν_L^c, N_R) is given as

$$M_\nu = \begin{bmatrix} 0 & M_D \\ M_D^T & M_m \end{bmatrix} \ . \tag{1.55}$$

Constraining the number of right handed neutrino to one,

$$M_\nu = \begin{bmatrix} 0 & M \\ M & B \end{bmatrix} , \tag{1.56}$$

where M is the Dirac mass, B is Majorana mass, are simply numbers. After diagonalising mass matrix, one obtains the neutrino masses as

$$m_\nu = O M_\nu O^T = \begin{bmatrix} -m_1 & 0 \\ 0 & m_2 \end{bmatrix} , \tag{1.57}$$

where O is a 2-dimensional rotational matrix given as,

$$O = \begin{bmatrix} \cos\theta & -\sin\theta \\ \sin\theta & \cos\theta \end{bmatrix} . \tag{1.58}$$

Using the condition $\tan 2\theta = 2M/B$ one can get the eigenvalues of the mass matrix as,

$$m_{1,2} = \frac{1}{2}(\mp B + \sqrt{B^2 + 4M^2}). \tag{1.59}$$

Rearranging the mass matrix,

$$\begin{bmatrix} -m_1 & 0 \\ 0 & m_2 \end{bmatrix} = \begin{bmatrix} m_1 & 0 \\ 0 & m_2 \end{bmatrix} \begin{bmatrix} -1 & 0 \\ 0 & 1 \end{bmatrix} = mK^2. \tag{1.60}$$

Here the m contains the positive eigenvalues and K^2 a simply diagonal matrix with positive and negative unit eigenvalues. The mass M arises from the coupling of Higgs field to neutrino, it is of the order of ordinary fermionic mass. Considering a very heavy Majorana mass ($B \gg M$), eigenvalues of the matrix (Eqn. 1.59)

$$m_1 \simeq \frac{M^2}{B} \text{ and } m_2 \simeq B \ , \tag{1.61}$$

which will result a tiny mass for neutrino compared to other fermions $m_1 \ll M$, by considering the parameter B to be very heavy, roughly $\mathcal{O}(10^9)$ GeV. Thus, this model can successfully explain the smallness of neutrino families and in order to have ν_τ lighter than its present bound, the mass scale of B should be, $B \gtrsim 5 \times 10^9$ GeV. To summarize, type-I seesaw mechanism requires the mass scale of the right-handed fermions to be order of Grand Unified Theory (GUT) scale, for the explanation of light neutrino mass [14].

1.6.2.2 Type-II seesaw

The other way of creation of smallness of neutrino mass is the addition of Higgs triplet $(\Delta^{++}, \Delta^{+}, \Delta^{0})$ which couples to $(\nu, \ell)_L$ as shown in Fig 1.3. The relevant interaction term for mass can be written as [14, 15],

$$\frac{h_\nu}{2}\left[\nu\nu\Delta^0 - \left(\frac{\nu l + l\nu}{2}\right) + ll\Delta^{++}\right] \ , \tag{1.62}$$

where h_ν is the Yukawa coupling strength. With the consideration of a lighter VEV for Higgs triplet compared to Higgs doublet $\langle\Delta^0\rangle \ll \langle\phi^0\rangle$, gives the light

neutrino mass as

$$m_\nu = h_\nu \left\langle \Delta^0 \right\rangle . \tag{1.63}$$

1.6.2.3 Type-III seesaw

In this framework, a fermion triplet Σ_R $(\Sigma_R^+, \Sigma_R^0, \Sigma_R^-)$ with hypercharge zero added as a mediator to Weinberg operator as shown in right panel of Fig. 1.3. This mechanism is equivalent to Type-I except Σ_R in place of N_R. In a compact notation for an usual fermion triplet

$$\Sigma_R = \begin{bmatrix} \frac{\Sigma_R^0}{\sqrt{2}} & \Sigma_R^+ \\ \Sigma_R^- & -\frac{\Sigma_R^0}{\sqrt{2}} \end{bmatrix} , \tag{1.64}$$

the mass term in the Lagrangian is given as

$$-\mathcal{L}_{\text{mass}} = \sum_L \bar{L}_L \bar{\phi} Y_\nu \Sigma_R + h.c. - \frac{Y_v}{\Lambda} \bar{L}^c \bar{\phi}^* \bar{\phi}^\dagger L \, . \tag{1.65}$$

After spontaneous symmetry breaking, choosing VEV for standard Higgs boson as $\frac{v}{\sqrt{2}}$, symmetric mass matrix is

$$\begin{pmatrix} 0 & Y_\Sigma^T \frac{v}{2\sqrt{2}} \\ Y_\Sigma \frac{v}{2\sqrt{2}} & \frac{M_\Sigma}{2} \end{pmatrix} . \tag{1.66}$$

Diagonalization of mass matrix Eqn. (1.66), Majorana mass for neutrinos can be obtained as [16],

$$M_\nu = \frac{1}{2} Y_\Sigma \frac{v^2}{\Lambda} Y_\Sigma^T \, . \tag{1.67}$$

In all the above mentioned seesaw mechanisms, one of the important issue is the experimental signature of heavy particles. The drawbacks in TeV scale seesaw mechanism can be avoided by the Inverse See-Saw mechanism (ISS). In this mechanism, the light neutrino mass can be explained by considering the new physics scale at or below TeV scale. ISS requires addition of three right-handed neutrinos N_{iR} and three extra singlet neutral fermions, S_{iL} for three active neutrinos [17]. In addition to this, several other models which can generate neutrino mass through

loop corrections. Such models are Zee model [18], Zee-Babu model [19, 20], Ma model [21], etc.

1.7 Neutrinoless Double Beta Decay

Confirmation of non zero neutrino mass entails two unknowns: the absolute mass scale of neutrinos and the nature of neutrinos. Neutrinoless double beta decay process can answer to these questions, which will be discussed in this section.

Double beta decay ($\beta\beta_{2\nu}$) is a process where two beta particles along with two neutrinos are emitted from a nucleus as shown in Fig 1.4,

$$(A, Z) \rightarrow (A, Z+2) + e^- + e^- + \bar{\nu}_e + \bar{\nu}_e \ . \tag{1.68}$$

First ever experimental observation of $\beta\beta_{2\nu}$ process was done by Elliot, Hahn and Moe after a century of observation of beta decay process [22]. In general these processes are very rare, occur only when single beta decay processes are forbidden. Amplitude of these processes are weak as G_F^2 with a half-life time of $\sim 1.1 \times 10^{20}$ years [23].

While Neutrinoless double beta decay ($\beta\beta_{0\nu}$) is a lepton number violating process two beta particles are emitted from the nucleus without any neutrino as shown in right panel of Fig 1.4,

$$(A, Z) \rightarrow (A, Z+2) + e^- + e^- \ . \tag{1.69}$$

It violates the lepton number by two units. Observation of such signals can probe the Majorana nature of neutrino as the mass term $m_\nu \nu_L^T C^{-1} \nu_L$ violates lepton number by two units. Non observation of such signals put some bounds on the life time of this process. Obtained bounds on the half life time $\mathcal{T}_{1/2} \sim 10^{25}$ years for different nuclei from various experiments: KamLAND-Zen [24], GERDA [25], EXO-200 [26], CURCINO and CUORE [27]. Half-life time for $\beta\beta_{0\nu}$ [28, 29] can be expressed as

$$\mathcal{T}_{1/2}^{-1} = Q \left| \frac{M_\nu}{m_e} \right| |M_{ee}|^2 \ , \tag{1.70}$$

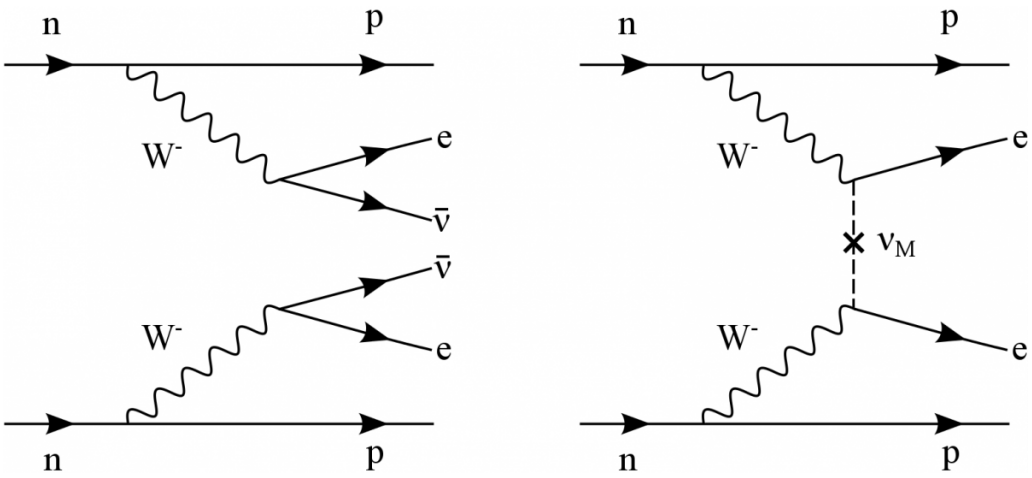

FIGURE 1.4: Feynman diagram for double beta decay (left) and Neutrinoless double beta decay (right).

where Q represents the phase space factor, M_ν is the nuclear matrix element, m_e is the electron mass and $\left|M_{ee}\right|$ is the effective Majorana mass parameter. The bounds on life time for $\beta\beta_{0\nu}$ can be reflected as limits on the $\left|M_{ee}\right|$ as $\sim (0.2-0.4)$ eV [30, 31]. Effective Majorana mass depends upon the neutrino mass and mixing parameters as

$$\left|M_{ee}\right| = \left|U_{e1}^2 m_1 + U_{e2}^2 m_2 e^{i\alpha} + U_{e3}^2 m_3 e^{i\beta}\right|, \tag{1.71}$$

where U_{ei} are the neutrino mixing matrix elements and α, β are the Majorana phases. Hence, the study of $\left|M_{ee}\right|$ can give idea about the nature and mass of neutrinos.

1.8 Thesis Overview

Current chapter gives the basic idea of the SM and its particle content. Neutrinos one of the most puzzling particles show the flavour transition properties called neutrino oscillation, which demands tiny mass and maxing for neutrinos. Various neutrino mass mechanism discussed in details. Measurement of neutrino mixing matrix elements is the primary goal of neutrino experiments. There are some degeneracies and unknowns among the oscillation parameters, can be answered by number of well known long baseline experiments T2K, NOvA, DUNE, T2HK, T2HKK, ESSnuSB, etc.

In this regard, we have explored neutrino oscillation and implications on various beyond SM hypothesis at long baseline experiments. Chapter-2, will be focused on the theory of neutrino oscillation in vacuum and matter, current status of neutrino oscillation parameters and brief discussion on various neutrino oscillation experiments. Next in chapter-3, light sterile neutrino and their implications on currently running long baseline experiments will be discussed. Considering an eV scale sterile neutrino, impact on parameter degeneracy and sensitivity of NOvA and T2K have been discussed. Also. its effect on Neutrino less double beta decay experiment has been investigated. A brief discussion on CPT symmetry, the fundamental symmetry of nature and violation CPT symmetry at future based long baseline experiments will be presented in chapter-4. Constraints on model-independent CPT violating parameters and sensitivities for discovery of CPT violation are obtained from different long baseline experiments. Chapter-5 is based on study of CPT violation through Lorentz invariance violation. Implications of Lorentz violation at currently running long baseline experiments NOvA and T2K have explored in details. Summary and conclusion of the whole thesis will be discussed in Chapter-6. Current and future scopes in neutrino studies will also be mentioned in this chapter.

Chapter 2

Theory of Neutrino Oscillation

2.1 Introduction to Neutrino Oscillation

Neutrino oscillation is a phenomenon of transition of neutrino flavors during their propagation. It is a quantum mechanical process of keen interest both theoretically and experimentally. In nature, neutrinos are produced in three flavors namely electron neutrino (ν_e), muon neutrino (ν_μ) and tau neutrino (ν_τ) in weak processes, in association with charged leptons. The flavor states are some combination of neutrino mass states, i.e., states with definite masses. In three flavor framework, neutrino flavor states (ν_e, ν_μ and ν_τ) can be related to mass states (ν_1, ν_2 and ν_3) through a complex unitary 3×3 mixing matrix called PMNS (Pontecorvo-Maki-Nakagwa-Sakata) matrix [32]. PMNS matrix is similar to the CKM (Cabibbo-Kobayashi-Maskawa) matrix in the quark sector. Neutrino Oscillation confirms the mixing of neutrinos and tiny mass for neutrinos.

As flavor states are the superposition of mass states of different masses, during the propagation of a given flavor state, the different components of mass states evolve differently with time and the combination of these evolved mass states at a later time, is not necessarily be the original flavor state, but might be some other flavor of neutrinos. Hence, in order to have neutrino oscillation, neutrinos must have non-zero mass. In the year 2015, Nobel Prize in Physics awarded jointly to Takaaki Kajita from Super-Kamiokande Collaboration and Arthur B. McDonald from Sudbury Neutrino Observatory Collaboration "for the discovery of neutrino oscillations, which shows that neutrinos have mass".

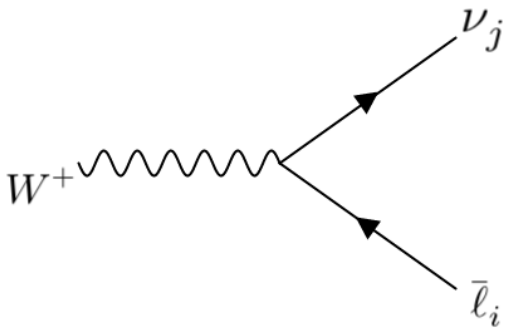

FIGURE 2.1: Feynman diagram for Lepton Mixing.

2.1.1 Neutrino Mixing

Non-zero neutrino mass in other words can be understood as neutrino mixing [33]. Hence, the Yukawa couplings for neutrino masses can be both diagonal and non-diagonal in flavor basis. Including the right-handed neutrinos, one can write the Lagrangian for the mass terms as

$$\begin{aligned}\mathcal{L}_{\text{Dirac}} &= \bar{\nu}_L^i (Y_\nu)_{ij} v \nu_R^j + h.c., \\ \mathcal{L}_{\text{Majorana}} &= \frac{v^2}{2M} {\nu_L^i}^T C (\alpha_\nu)_{ij} \nu_L^j + h.c.,\end{aligned} \tag{2.1}$$

where Y_ν and α_ν are the couplings. While in mass basis, neutral (charged) weak couplings are diagonal (non-diagonal) in nature (shown in Fig. 2.1):

$$\begin{aligned}\mathcal{L}_{\text{Dirac}} &= \bar{\ell}_L^i \gamma^\mu W_\mu^+ U_{mix}^{ij} \nu_L^j + \frac{1}{2} \bar{\nu}_L^i \gamma^\mu Z_\mu \nu_L^i + \bar{\nu}_L^i m_i \nu_R^i + h.c., \\ \mathcal{L}_{\text{Majorana}} &= \bar{\ell}_L^i \gamma^\mu W_\mu^+ \tilde{U}_{mix}^{ij} \nu_L^j + \frac{1}{2} \bar{\nu_L^i} \gamma^\mu Z_\mu \nu_L^i + \frac{1}{2} {\nu_L^i}^T C m_i \nu_L^i + h.c..\end{aligned} \tag{2.2}$$

The lepton mixing matrix $U_{mix}(\tilde{U}_{mix})$ can be identified as the PMNS matrix for Dirac (Majorana) case. The number of independent parameters in the mixing matrix is the sum of independent real and imaginary terms in the matrix. Independent parameters can be obtained by eliminating the dependent parameters after field redefinition. For a family with n number of leptons, there are $n(n-1)/2$ number of real and $(n-1)(n-2)/2$ number of imaginary independent parameters. For Majorana neutrino, the number of real and imaginary independent parameters are same and equal to $n(n-1)/2$ in the mixing matrix [34].

2.2 Neutrino Oscillation in Vacuum

Using the relation between flavor and mass states, one can calculate the oscillation probability in vacuum i.e., in a potential free space. It should be emphasized that the overall phases of the transition amplitude will not give any contribution towards the probability. Majorana phases appear as overall phases in the oscillation amplitude and hence, do not contribute to the oscillation probability.

In general for a n family system, the flavor states $|\nu_\alpha\rangle$ are the superposition of mass states $|\nu_j\rangle$

$$\big|\nu_\alpha\big\rangle = \sum_{j=1}^{n} U_{\alpha j}\big|\nu_j\big\rangle. \tag{2.3}$$

Similarly in a reverse transformation, mass states can be written in terms of flavor states

$$\big|\nu_j\big\rangle = \sum_{\alpha=1}^{n} U^*_{\alpha j}\big|\nu_\alpha\big\rangle. \tag{2.4}$$

The mass states satisfy Schrödinger equation in vacuum

$$H\big|\nu_j\big\rangle = \frac{d}{dt}\big|\nu_j\big\rangle = E_j\big|\nu_j\big\rangle, \tag{2.5}$$

where H is the Hamiltonian and $E_j = \sqrt{m_j^2 + \vec{p}_j^{\,2}}$ is the energy of a neutrino mass state with mass m_j and momentum $\vec{p}_j$. Matrix representation of Hamiltonian is

$$H = \frac{1}{2E}\mathrm{diag}(m_1^2, m_2^2, m_3^2, ..., m_n^2). \tag{2.6}$$

The time evolution of flavor and mass states can be written as

$$\big|\nu_\alpha, t\big\rangle = \sum_{j=1}^{n} U_{\alpha j}\big|\nu_j, t\big\rangle \tag{2.7}$$

and

$$\big|\nu_j, t\big\rangle = e^{-iE_j t}\big|\nu_j, 0\big\rangle, \tag{2.8}$$

where $\big|\nu_j, 0\big\rangle$ is the mass eigenstate at initial time $t = 0$ and also denoted as $\big|\nu_j\big\rangle$. Similarly $\big|\nu_\alpha, 0\big\rangle = \big|\nu_\alpha\big\rangle$ is the initial flavor state. Therefore, flavor states can be

written as

$$\big|\nu_\alpha, t\big\rangle = \sum_{j=1}^{n} U_{\alpha j} e^{-iE_j t} \big|\nu_j, 0\big\rangle. \tag{2.9}$$

Using Eqn. (2.4) in (2.9), one obtains

$$\big|\nu_\alpha, t\big\rangle = \sum_{\beta=1}^{n} \left(\sum_{j=1}^{n} U_{\alpha j} e^{-iE_j t} U^*_{\beta j} \right) \big|\nu_\beta\big\rangle. \tag{2.10}$$

Transition amplitude for α type neutrino (ν_α) at an initial time ($t = 0$) to β type neutrino (ν_β) at a time t is

$$\mathcal{A}_{\alpha\beta} = \langle \nu_\alpha, 0 \big| \nu_\beta, t \rangle = \sum_{\gamma=1}^{n} \left(\sum_{j=1}^{n} U_{\beta j} e^{-iE_j t} U^*_{\gamma j} \right) \langle \nu_\alpha, 0 \big| \nu_\gamma, 0 \rangle. \tag{2.11}$$

The orthogonality condition $\langle \nu_\alpha, 0 \big| \nu_\gamma, 0 \rangle = \delta_{\alpha\gamma}$ in flavor space implies that

$$\mathcal{A}_{\alpha\beta} = \sum_{j=1}^{n} U_{\beta j} e^{-iE_j t} U^*_{\alpha j}. \tag{2.12}$$

Probability of oscillation for $\nu_\alpha \to \nu_\beta$ process is

$$\begin{aligned} P_{\nu_\alpha \to \nu_\beta} = \big|\mathcal{A}_{\alpha\beta}\big|^2 &= \sum_{j=1}^{n} U_{\beta j} e^{-iE_j t} U^*_{\alpha j} \sum_{k=1}^{n} U^*_{\beta k} e^{iE_k t} U_{\alpha k}, \\ &= \sum_{j,k=1}^{n} U_{\beta j} U^*_{\alpha j} U^*_{\beta k} U_{\alpha k} e^{-i(E_j - E_k)t}. \end{aligned} \tag{2.13}$$

Neutrino energy can be expressed as

$$\begin{aligned} E_j = \sqrt{p_j^2 + m_j^2} &= p_j (1 + \frac{m_j^2}{p_j^2})^{1/2} \\ &\simeq p_j \left(1 + \frac{m_j^2}{2p_j^2} \right) = p_j + \frac{m_j^2}{2p_j}, \end{aligned} \tag{2.14}$$

where p_j represents the magnitude of the momentum of the mass state $|\nu_j\rangle$. Considering neutrino as a relativistic particle, time and space can be treated with equal footing i.e., $t = L$, where t is the travel time of neutrino between the point of source to detector and distance between the source and detector point is L. Further assuming equal momentum for all the mass states as p, the phase expression

in Eqn. (2.13) will reduce to

$$\begin{aligned}(E_j - E_k)t &= \left(p + \frac{m_j^2}{2p} - p - \frac{m_k^2}{2p}\right) L \\ &= \frac{(m_j^2 - m_k^2)}{2p} L. \end{aligned} \tag{2.15}$$

Assuming the mass states have same energy as $E \simeq p$ and denoting the mass squared difference as $\Delta m_{jk}^2 = m_j^2 - m_k^2$, one obtains

$$\frac{(m_j^2 - m_k^2)}{2p} L = \frac{\Delta m_{jk}^2 L}{2E}. \tag{2.16}$$

Using the expression of phase from Eqn. (2.16) in Eqn. (2.13), oscillation probability as a function of E and L is

$$P_{\nu_\alpha \to \nu_\beta}(L, E) = \sum_{j=1}^{n} \sum_{k=1}^{n} U_{\beta j} U_{\alpha j}^* U_{\beta k}^* U_{\alpha k} e^{-i \frac{\Delta m_{jk}^2 L}{2E}} \tag{2.17}$$

$$= \sum_{j=k=1}^{n} \left|U_{\beta j}\right|^2 \left|U_{\alpha j}\right|^2 + \sum_{j \neq k}^{n} U_{\beta j} U_{\alpha j}^* U_{\beta k}^* U_{\alpha k} e^{-i \frac{\Delta m_{jk}^2 L}{2E}}. \tag{2.18}$$

One can find the relation

$$\begin{aligned} \Big| \sum_{j=1}^{n} U_{\beta j} U_{\alpha j}^* \Big|^2 &= \sum_{j=1}^{n} U_{\beta j} U_{\alpha j}^* \sum_{k=1}^{n} U_{\beta k}^* U_{\alpha k} \\ &= \sum_{j=k} \left|U_{\beta j}\right|^2 \left|U_{\alpha j}\right|^2 + \sum_{j \neq k}^{n} U_{\beta j} U_{\alpha j}^* U_{\beta k}^* U_{\alpha k}. \end{aligned} \tag{2.19}$$

Using the unitary relation between the mixing matrix element

$$\sum_{j=1}^{n} U_{\beta j} U_{\alpha j}^* = \delta_{\beta \alpha} \ , \tag{2.20}$$

in Eqn. (2.19), one can obtain

$$\sum_{j=k} \left|U_{\beta j}\right|^2 \left|U_{\alpha j}\right|^2 = \delta_{\beta \alpha} - \sum_{j \neq k}^{n} U_{\beta j} U_{\alpha j}^* U_{\beta k}^* U_{\alpha k} \ . \tag{2.21}$$

Using the above relation, Eqn. (2.18) can be rewritten as

$$\begin{aligned} P_{\nu_\alpha\to\nu_\beta}(L,E) &= \delta_{\beta\alpha} - \sum_{j\neq k}^{n} U_{\beta j}U^*_{\alpha j}U^*_{\beta k}U_{\alpha k} + \sum_{j\neq k}^{n} U_{\beta j}U^*_{\alpha j}U^*_{\beta k}U_{\alpha k}\exp\left(-i\frac{\Delta m^2_{jk}L}{2E}\right) \\ &= \delta_{\beta\alpha} - \left[\sum_{j>k}^{n} U_{\beta j}U^*_{\alpha j}U^*_{\beta k}U_{\alpha k} + \sum_{j>k}^{n} U^*_{\beta j}U_{\alpha j}U_{\beta k}U^*_{\alpha k}\right] \text{[1]} \\ &+ \left[\sum_{j>k}^{n} U_{\beta j}U^*_{\alpha j}U^*_{\beta k}U_{\alpha k}\exp\left(-i\frac{\Delta m^2_{jk}L}{2E}\right) + \sum_{j>k}^{n} U^*_{\beta j}U_{\alpha j}U_{\beta k}U^*_{\alpha k}\exp\left(i\frac{\Delta m^2_{jk}L}{2E}\right)\right]. \end{aligned} \tag{2.22}$$

For a complex number z, we know $z + z^* = 2\text{Re}(z)$ and $z - z^* = 2\text{Im}(z)$. Using the Euler's formula $e^{i\phi} = \cos\phi + i\sin\phi$ in the above equation, we obtain

$$\begin{aligned} P_{\nu_\alpha\to\nu_\beta}(L,E) &= \delta_{\beta\alpha} - 2\sum_{j>k}^{n}\text{Re}(U_{\beta j}U^*_{\alpha j}U^*_{\beta k}U_{\alpha k})\left[1-\cos\left(\frac{\Delta m^2_{jk}L}{2E}\right)\right] \\ &+ 2\sum_{j>k}^{n}\text{Im}(U_{\beta j}U^*_{\alpha j}U^*_{\beta k}U_{\alpha k})\sin\left(\frac{\Delta m^2_{jk}L}{2E}\right). \end{aligned} \tag{2.23}$$

Using the trigonometric identity $1-\cos\phi = 2\sin^2\frac{\phi}{2}$ in Eqn. (2.23), gives

$$\begin{aligned} P_{\nu_\alpha\to\nu_\beta}(L,E) &= \delta_{\beta\alpha} - 4\sum_{j>k}^{n}\text{Re}(U_{\beta j}U^*_{\alpha j}U^*_{\beta k}U_{\alpha k})\sin^2\left(\frac{\Delta m^2_{jk}L}{4E}\right) \\ &+ 2\sum_{j>k}^{n}\text{Im}(U_{\beta j}U^*_{\alpha j}U^*_{\beta k}U_{\alpha k})\sin\left(\frac{\Delta m^2_{jk}L}{2E}\right). \end{aligned} \tag{2.24}$$

Eqn. (2.24) is the expression for oscillation probability in vacuum for three flavor scenario. Anti neutrino oscillation probability can be obtained by replacing the matrix element $U_{\alpha i}$ with $U^*_{\alpha i}$. The second term in Eqn. (2.24) is CP conserving as it is same for both neutrino and anti-neutrino while the third term is opposite for neutrino and anti-neutrino, is a CP violating term.

---

[1]

$$\begin{aligned} \sum_{j\neq k}^{n} U_{\beta j}U^*_{\alpha j}U^*_{\beta k}U_{\alpha k} &= \left[\sum_{j>k}^{n} U_{\beta j}U^*_{\alpha j}U^*_{\beta k}U_{\alpha k} + \sum_{j<k}^{n} U_{\beta j}U^*_{\alpha j}U^*_{\beta k}U_{\alpha k}\right] \\ &= \left[\sum_{j>k}^{n} U_{\beta j}U^*_{\alpha j}U^*_{\beta k}U_{\alpha k} + \sum_{j<k}^{n} U^*_{\beta j}U_{\alpha j}U_{\beta k}U^*_{\alpha k}\right]. \end{aligned}$$

The survival probability is the probability of getting ν_α at detector from ν_α at source point. Substituting $\alpha = \beta$ in Eqn. (2.24), the probability expression reduces to

$$P_{\nu_\alpha \to \nu_\alpha}(L, E) = \delta_{\beta\alpha} - 4 \sum_{j>k}^{n} \left|U_{\alpha j}\right|^2 \left|U_{\alpha k}\right|^2 \sin^2 \left(\frac{\Delta m^2_{jk} L}{4E}\right). \tag{2.25}$$

Oscillation probability depends upon the neutrino mixing matrix elements, neutrino mass squared differences Δm^2_{jk}, distance of propagation L and energy of neutrinos E.
Phase of oscillation in Eqn. (2.24) in natural unit can be written as

$$\frac{\Delta m^2_{jk} L}{4E} = 1.267 \left(\frac{\Delta m^2_{jk}}{\mathrm{eV}^2}\right) \left(\frac{L/E}{m/\mathrm{MeV}}\right). \tag{2.26}$$

For a distance L_{osc},

$$L_{\mathrm{osc}} = \frac{4\pi E}{|\Delta m^2_{jk}|}, \tag{2.27}$$

probability in Eqn. (2.24) will be simple product of matrix elements. Observation of a non-trivial value for probability indicates non-zero values for mixing matrix elements and mass squared differences Δm^2_{jk}. Consequently, atleast two of the three neutrinos must have non-zero masses. As mentioned earlier Majorana phases appear as overall phase and hence, don't appear in probability expression. This also indicates that in neutrino oscillation, the total lepton number is conserved. Depending upon the type of neutrino source used for experiments, the ratio of L/E plays a pivotal role to determine the range of Δm^2 to be within the sensitivity reach of experiments. In the next sections, we will present a detailed discussion on two and three flavor neutrino oscillation phenomena.

2.2.1 Two Flavor Oscillation

For a simple calculation for probability, one can consider two neutrino hypothesis. Here we consider two flavor of neutrinos for example ν_e and ν_μ and correspondingly two mass states ν_1 and ν_2. Flavor states will be related to mass states through a

2×2 unitary matrix as

$$\begin{pmatrix} \nu_e \\ \nu_\mu \end{pmatrix} = U \begin{pmatrix} \nu_1 \\ \nu_2 \end{pmatrix} = \begin{pmatrix} \cos\theta & \sin\theta \\ -\sin\theta & \cos\theta \end{pmatrix} \begin{pmatrix} \nu_1 \\ \nu_2 \end{pmatrix}, \tag{2.28}$$

where U is the unitary matrix, which can rotate the flavor states to mass states in 2-dimensional space. The parameter θ is known as "mixing angle" whose value can be determined from experiments.

Oscillation probability for ν_α to ν_β transition can be calculated using the Eqn. (2.23)

$$P_{\nu_\alpha \to \nu_\beta} = \sin^2 2\theta \sin^2 \left(\frac{\Delta m^2 L}{4E} \right) = \sin^2 2\theta \sin^2 \left(1.27 \frac{\Delta m^2 L}{E} \right), \tag{2.29}$$

where the notation $\Delta m^2 = m_2^2 - m_1^2$ and the energy of neutrinos are assumed to be same $E_1 = E_2 = E$. The survival probability i.e., the probability of detecting ν_α at the detector from a neutrino source of ν_α is given as

$$P(\nu_\alpha \to \nu_\alpha) = 1 - P(\nu_\alpha \to \nu_\beta). \tag{2.30}$$

In Figs. 2.2 and 2.3, we have shown both appearance and disappearance probabilities as a function of distance of propagation and energy of neutrino, respectively. Two flavor oscillation is important to explain the hidden facts in the observed neutrino oscillation. Using simple two flavor formulation, one can explore the mixing parameters and mass squared differences.

Mixing angle θ: It is the oscillation parameter, which describes that how much the flavor states deviate from the mass states. In other words, it describes the mixing between flavor states and mass states. Depending upon the value of mixing angle probability can change in between maximum and minimum oscillation probabilities.

Mass squared difference (Δm^2): Neutrino oscillation in two flavor implies for a non-zero Δm^2, which in turn indicates that neutrinos are massive. It is important to note that the oscillation probability will be same for both positive and negative values of Δm^2. Therefore, it is difficult to conclude which mass state is the heavier one.

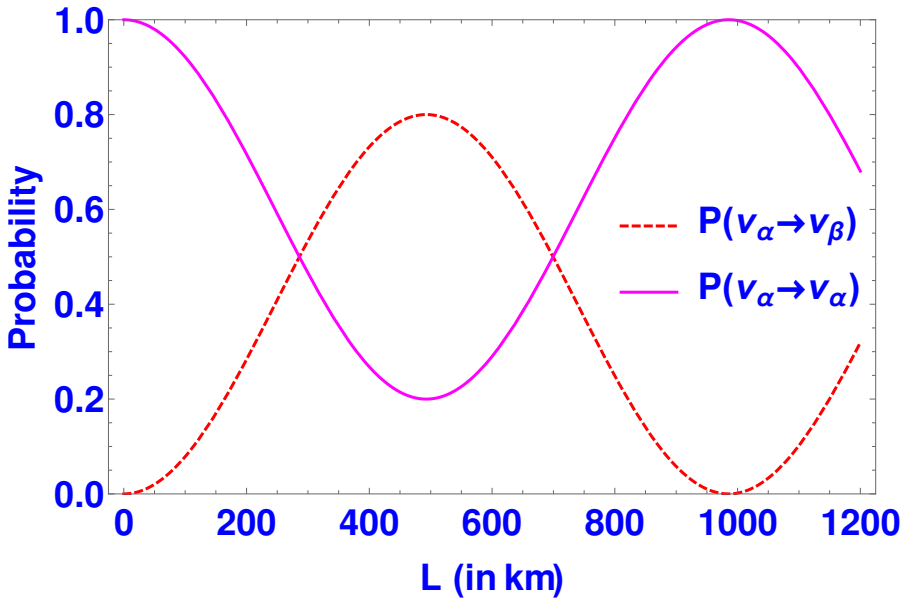

FIGURE 2.2: Appearance (Disappearance) probability as a function of distance of propagation in dashed red (solid magenta) curve with oscillation parameter $\sin^2 2\theta = 0.8$, $\Delta m^2 = 2.51 \times 10^{-3}$ eV^2 and $E = 1$ GeV.

Ratio of L to E (L/E): This ratio determines the oscillation probability for a given Δm^2. Some experiments are dedicated to explore Δm^2 in some particular ranges. In that case, the distance of propagation L and energy of neutrino E have to be chosen to maximize the probability.

2.2.2 Three Flavor Oscillation

In three flavor scenario, mixing angles are real parameters while CP violating phases are the imaginary parameters. There are three real parameters for both Dirac and Majorana cases, while only a single CP phase for Dirac neutrinos and three CP phases in case of Majorana neutrinos [34].

Hence, the PMNS matrix can be parametrized in terms of three mixing angles, i.e., solar mixing angle (θ_{12}), reactor mixing angle (θ_{13}) and the atmospheric mixing angle (θ_{23}), one Dirac-type CP violating phase δ_{CP} and two Majorana phases α_{21} and α_{31}. Thus, one can express the flavour eigenstates in terms of the mass

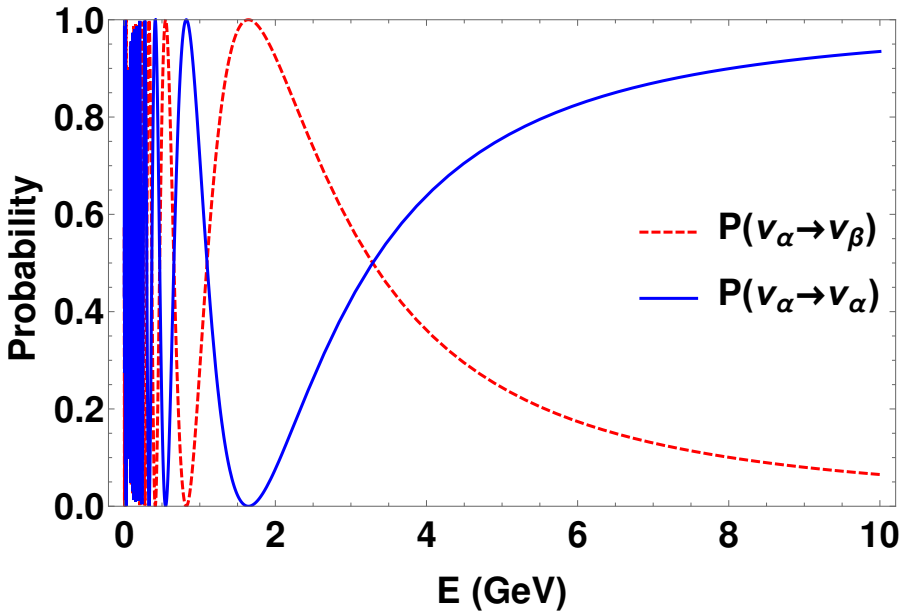

FIGURE 2.3: Appearance (Disappearance) probability as a function of Neutrino Energy in GeV with a distance of propagation $L = 810$ km, oscillation parameter $\theta = \frac{\pi}{4}$ and $\Delta m^2 = 2.51 \times 10^{-3}$ eV^2.

eigenstates as

$$\begin{pmatrix} \nu_e \\ \nu_\mu \\ \nu_\tau \end{pmatrix} = \begin{pmatrix} U_{e1} & U_{e2} & U_{e3} \\ U_{\mu 1} & U_{\mu 2} & U_{\mu 3} \\ U_{\tau 1} & U_{\tau 2} & U_{\tau 3} \end{pmatrix} \begin{pmatrix} \nu_1 \\ \nu_2 \\ \nu_3 \end{pmatrix}. \tag{2.31}$$

Here the mixing matrix U is called the PMNS matrix and it can be written by combination of three rotation matrices in "12", "13" and "23" planes

$$\begin{aligned} U_{\text{PMNS}} &= \begin{pmatrix} 1 & 0 & 0 \\ 0 & c_{23} & s_{23} \\ 0 & -s_{23} & c_{23} \end{pmatrix} \begin{pmatrix} c_{13} & 0 & s_{13}e^{-i\delta_{cp}} \\ 0 & 1 & 0 \\ -s_{13}e^{i\delta_{cp}} & 0 & c_{13} \end{pmatrix} \begin{pmatrix} c_{12} & s_{12} & 0 \\ -s_{12} & c_{12} & 0 \\ 0 & 0 & 1 \end{pmatrix} K \\ &= \begin{pmatrix} c_{12}c_{13} & s_{12}c_{13} & s_{13}e^{-i\delta_{CP}} \\ -s_{12}c_{23} - c_{12}s_{23}s_{13}e^{i\delta_{cp}} & c_{12}c_{23} - s_{12}s_{13}s_{23}e^{i\delta_{cp}} & c_{13}s_{23} \\ s_{12}s_{23} - c_{12}c_{23}s_{13}e^{i\delta_{cp}} & -c_{12}s_{23} - s_{12}s_{13}c_{23}e^{i\delta_{cp}} & c_{13}c_{23} \end{pmatrix} K, \end{aligned} \tag{2.32}$$

with $c_{ij} = \cos\theta_{ij}$, $s_{ij} = \sin\theta_{ij}$ and $K = \text{diag}(1, e^{i\alpha_{21}}, e^{i\alpha_{31}})$.

Using similar calculation as we discussed for n flavor scenario, one can get the oscillation probability for 3 neutrino case as given in Eqn. (2.24). For three flavor scenario there will be two independent mass squared differences Δm^2_{32} and Δm^2_{21}. Mass squared difference associated with "23" sector is known as atmospheric mass squared difference $\Delta m^2_{32} \sim 2.51 \times 10^{-3}$ eV^2 and solar mass squared difference $\Delta m^2_{21} \sim 7.42 \times 10^{-5}$ eV^2 is the mass splitting in "12" sector [35].

Let's assume for the time being that there is no CP violation, i.e., $\delta_{CP} = 0$. Hence, Eqn. (2.24) will reduce to

$$P_{\nu_\alpha \to \nu_\beta} = \delta_{\alpha\beta} - 4 \sum_{j>k}^{3} U_{\beta j} U^*_{\alpha j} U^*_{\beta k} U_{\alpha k} \sin^2 \left(\frac{\Delta m^2_{jk} L}{4E} \right). \tag{2.33}$$

So the expression for appearance oscillation probability ($\alpha \neq \beta$) is

$$P_{\nu_\alpha \to \nu_\beta} = -4 \sum_{j>k}^{3} U_{\beta j} U^*_{\alpha j} U^*_{\beta k} U_{\alpha k} \sin^2 \left(\frac{\Delta m^2_{jk} L}{4E} \right), \tag{2.34}$$

where $j, k = 1, 2, 3$. Assuming for an experiment with small L/E, the term $(\Delta m^2_{21} L)/E$ will be sufficiently small to write

$$\sin^2 \left(1.267 \Delta m^2_{21} \frac{L}{E} \right) \to 0. \tag{2.35}$$

With the approximation $\Delta m^2_{31} \simeq \Delta m^2_{32}$, Eqn. (2.34) can be written as

$$P_{\nu_\alpha \to \nu_\beta} = -4 \left(U_{\alpha 1} U_{\beta 1} U_{\alpha 3} U_{\beta 3} + U_{\alpha 2} U_{\beta 2} U_{\alpha 3} U_{\beta 3} \right) \sin^2 \left(1.267 \Delta m^2_{32} \frac{L}{E} \right). \tag{2.36}$$

Similarly for large L/E, the phase terms containing Δm^2_{31} and Δm^2_{32} will average out to 1/2. Then Eqn. (2.34) will reduce to

$$\begin{aligned} P_{\nu_\alpha \to \nu_\beta} = & - 4 \left[U_{\alpha 1} U_{\beta 1} U_{\alpha 2} U_{\beta 2} \sin^2 \left(1.267 \Delta m^2_{21} \frac{L}{E} \right) \right] \\ & + 4 \left[\frac{1}{2} \left(U_{\alpha 1} U_{\beta 1} U_{\alpha 3} U_{\beta 3} + U_{\alpha 2} U_{\beta 2} U_{\alpha 3} U_{\beta 3} \right) \right]. \end{aligned} \tag{2.37}$$

With an assumption $\theta_{13} = 0$, Eqns. (2.36) and (2.37) can be analysed based on the value of L/E.

- For small value of L/E

$$P(\nu_\mu \to \nu_\tau) = \sin^2 2\theta_{23} \sin^2 \left(1.267\ \Delta m^2_{23} \frac{L}{E}\right). \tag{2.38}$$

- For large value of L/E

$$P(\nu_e \to \nu_\mu) = \sin^2 2\theta_{12} \sin^2 \left(1.267\ \Delta m^2_{21} \frac{L}{E}\right). \tag{2.39}$$

Depending upon the value of L/E the above equations (2.38), (2.39) can be identified as the probability expressions for atmospheric and solar neutrino oscillations, respectively. In this way, one can explore solar and atmospheric neutrinos from three flavor scenario.

Also information regarding the measurement of θ_{13} can be extracted. For experiments with shorter baseline about few kilometre and neutrinos with energy of few MeV, solar oscillations are very slow compared to atmospheric oscillations. Only atmospheric oscillation terms will be observable at short baseline experiments. Survival oscillation probability for ν_e is

$$P_{\nu_e \to \nu_e} = 1 - \sin^2 2\theta_{13} \sin^2 \left(1.267\ \Delta m^2_{32} \frac{L}{E}\right). \tag{2.40}$$

This probability is independent of all other mixing angles except θ_{13}. Similarly disappearance probability for $\bar{\nu}_e$ can measure the reactor mixing angle θ_{13}.

Neutrino oscillation in presence of earth matter potential is really interesting, and will be discussed in next section.

2.3 Neutrino Oscillation in Matter

As mentioned earlier, neutrino oscillation is due to the phase difference between the mass states with evolution of time. The phase difference is due to the different velocities of mass states having different masses. In vacuum, potential energy is zero and the total energy decides the phase difference between the states. If there will be some potential V in the path of neutrinos, some additional phase will be introduced depending upon the total energy of neutrino $E+V$. Also the potential V is flavor dependent, differs from flavor to flavor and also medium dependent.

Scattering of neutrinos with electrons of earth matter in charge current process is

$$\nu_\ell(p) + e^- \rightarrow \nu_\ell(p) + e^-. \tag{2.41}$$

The momentum p of neutrino remains unchanged during this process. Maximum amplitude for this charge current process will be obtained with $l = e$. In contrast to other neutrinos, electron neutrino contributes an additional term to the Hamiltonian, which appears as an extra phase in neutrino oscillation. While in neutral current interaction of neutrinos with earth matter is given as

$$\nu_\ell(p) + X \rightarrow \nu_\ell(p) + X. \tag{2.42}$$

for any flavor of neutrinos interacting with any of the earth matter particles (e^-, p and n). This additional contribution to Hamiltonian is same for all flavor of neutrinos and appear as an overall phase, and hence, does not involve in neutrino oscillation.

The effective low-energy Hamiltonian for interaction of neutrinos with earth matter at any point x is given as

$$H = \frac{G_F}{\sqrt{2}} \left[\underbrace{J_\alpha^{(+)}(x) J^{(-)\alpha}(x)}_{\text{Charge Current}} + \underbrace{\frac{1}{4} J_\alpha^{(N)}(x) J^{(N)\alpha}(x)}_{\text{Neural Current}} \right], \tag{2.43}$$

where J^+ and J^- are the charge currents and J^N is the neutral current of neutrino interactions. Expression of these currents are

$$\begin{aligned} J_\alpha^{(+)}(x) &= \bar{\nu}_e(x)\gamma_\alpha(1-\gamma_5)e(x), \\ J_\alpha^{(-)}(x) &= \bar{e}(x)\gamma_\alpha(1-\gamma_5)\nu_e(x), \end{aligned} \tag{2.44}$$

and

$$\begin{aligned} J_\alpha^{(N)}(x) = \bar{\nu}_e(x)\gamma_\alpha(1-\gamma_5)\nu_e(x) - \bar{e}(x)\left(\gamma_\alpha(1-\gamma_5) - 4\sin^2\theta_W\gamma_\alpha\right)e(x) \\ +\bar{p}(x)\left(\gamma_\alpha(1-g_A^{(p)}\gamma_5) - 4\sin^2\theta_W\gamma_\alpha\right)p(x) - \bar{n}(x)\gamma_\alpha(1-g_A^{(n)}\gamma_5)n(x). \end{aligned} \tag{2.45}$$

Here $g_A^{(n)}$ and $g_A^{(p)}$ are the axial couplings for neutron and proton of matter. Effective Hamiltonian for charge current process after summing over all the electrons

of the medium is

$$H_{CC} = \sqrt{2} G_F n_e \bar{\nu}_{eL}(x) \gamma_0 \nu_{eL}(x), \tag{2.46}$$

where n_e is the number density for electrons. From the above expression, the potential energy for ν_e can be visualised as,

$$V_{CC} = \sqrt{2} G_F n_e \simeq 7.5 X_e \frac{\rho}{10^{14}\ (g/\mathrm{cm}^3)} \mathrm{eV}, \tag{2.47}$$

where relative electron number density

$$X_e = \frac{n_e}{n_p + n_n}, \tag{2.48}$$

with $n_p(n_n)$ is the number density for proton (neutron). For a neutral medium $X_e = 0.5$. For antineutrino the potential will change its sign to negative, $V_{CC} = -\sqrt{2} G_F n_e$. Similarly effective potential for neutral current interaction is

$$V_{NC} = \frac{1}{\sqrt{2}} G_F \left[-n_e (1 - 4 \sin^2 \theta_W) + n_p (1 - 4 \sin^2 \theta_W) - n_n \right]. \tag{2.49}$$

For a charge free medium the number density for electron should be same to proton i.e. $n_e = n_p$. Hence the potential is

$$V_{NC} = -\frac{1}{\sqrt{2}} G_F n_n. \tag{2.50}$$

However, neutral current potential plays a part of overall phase, so does not appear in neutrino oscillation. After including the charge current potential the Schrdinger equation for neutrino is given as

$$i \frac{d|\nu\rangle}{dt} = H|\nu\rangle, \quad H = H_m + U^\dagger V U, \tag{2.51}$$

where for a family of n generations of neutrino $|\nu\rangle = |\nu_1, \nu_2, \nu_3, ..., \nu_n\rangle^T$, H_m is the effective Hamiltonian and the kinetic energy part is $H_m = \frac{1}{2E} \mathrm{diag}(m_1^2, m_2^2, m_3^2, ..., m_n^2)$. The effective potential is denoted by V. For standard three flavor case the effective potential is

$$V = \mathrm{diag}(\pm \sqrt{2} G_F n_e, 0, 0). \tag{2.52}$$

Potential is positive for neutrinos while negative for antineutrinos. For a simple

understanding of matter effect in neutrino oscillation, we will focus on two flavor scenario. In two flavor case using the usual 2×2 mixing matrix Eqn. (2.51) will reduce to

$$H = \frac{1}{2E}\left[\begin{pmatrix} m_1^2 & 0 \\ 0 & m_2^2 \end{pmatrix} + \begin{pmatrix} \cos\theta & \sin\theta \\ -\sin\theta & \cos\theta \end{pmatrix}\begin{pmatrix} V_\alpha - V_\beta & 0 \\ 0 & 0 \end{pmatrix}\begin{pmatrix} \cos\theta & \sin\theta \\ -\sin\theta & \cos\theta \end{pmatrix}\right]. \tag{2.53}$$

Denoting $\Delta V = V_\alpha - V_\beta = 2\sqrt{2}G_F n_e E$, as the difference between the earth matter potential for neutrino flavor α and β, Eqn. (2.53) can be rewritten as,

$$\begin{aligned} H &= \frac{1}{2E}\begin{pmatrix} m_1^2 & 0 \\ 0 & m_2^2 \end{pmatrix} + \begin{pmatrix} \Delta V\cos^2\theta & \Delta V\cos\theta\sin\theta \\ \Delta V\cos\theta\sin\theta & \Delta V\sin^2\theta \end{pmatrix}, \\ &= \frac{1}{2E}\begin{pmatrix} m_1^2 + \Delta V\cos^2\theta & \Delta V\cos\theta\sin\theta \\ \Delta V\cos\theta\sin\theta & m_2^2 + \Delta V\sin^2\theta \end{pmatrix}. \end{aligned} \tag{2.54}$$

As noticed from Eqn. (2.54), the mass matrix is not diagonal which implies that the mass eigenstates of vacuum are not the actual eigenstates in matter. In order to get the mass of the physical states, the matrix should be diagonalised. The eigenvalues after diagonalising the matrix are m_{1m} and m_{2m},

$$m^2_{1m,2m} = \frac{1}{2}\left[(m_1^2 + m_2^2 + \Delta V) \pm \sqrt{(\Delta V - \Delta m^2\cos 2\theta)^2 + (\Delta m^2)^2\sin^2 2\theta}\right]. \tag{2.55}$$

The effective mass squared difference in matter is given as

$$\Delta m^2_m = m_1^2 - m_2^2 = \Delta m^2\sqrt{(\Delta V/\Delta m^2 - \cos 2\theta)^2 + \sin^2 2\theta}. \tag{2.56}$$

The new mass splitting is different from the vacuum mass squared difference and depends upon the matter potential. Similarly the effective mixing angle θ_m can be written as

$$\sin 2\theta_m = \frac{\sin 2\theta}{\sqrt{(\Delta V/\Delta m^2 - \cos 2\theta)^2 + \sin^2 2\theta}}. \tag{2.57}$$

Oscillation probability in terms of effective oscillation parameters in matter [36–39] is

$$P_m(\nu_\alpha \to \nu_\beta) = \sin^2 2\theta_m \sin^2\left(1.267\ \Delta m^2_m \frac{L}{E}\right). \tag{2.58}$$

Several important observations can be made from neutrino oscillation in matter.

- If $\Delta V = 0$, i.e., potential free earth matter or vacuum, then the effective oscillation parameters will be same as the oscillation parameters in vacuum.
- For a medium with very high density ($\Delta V \to \infty$), then $\sin 2\theta_m \to 0$, indicates that no oscillation for very highly dense matter.
- Also, no oscillation is possible if $\sin 2\theta \to 0$ implies to $\sin 2\theta_m \to 0$, that means neutrinos must have mixing in vacuum to observe neutrino oscillation in matter.
- If $\Delta V/\Delta m^2 = \cos 2\theta$ implies to $\sin 2\theta_m \to 1$, which results maximum oscillation in matter irrespective of neutrino mixing in vacuum. Hence, in some cases neutrinos have tiny mixing in vacuum, but for a certain electron number density, neutrino oscillation is possible with maximum probability. This condition is known as **Mikheyev-Smirnov-Wolfenstein (MSW)** resonance.
- Matter effect will be different, if the mass splitting changes its sign i.e., $\Delta m^2 \to -\Delta m^2$ in Eqn. (2.56). So, if there will be any hierarchy in mass squared difference, it can be explored using the matter effect which is not possible in vacuum.
- As mentioned earlier neutrinos and antineutrinos interact differently with the earth matter. So oscillation probabilities for neutrino and antineutrino will be differ from each other.

Matter effect in two flavor scenario plays a significant role to explain the solar neutrino oscillation. A large number of electron neutrinos are produced inside the core of sun and propagate towards the outer surface of sun. In between core and the outer surface, some of the ν_e's may satisfy the MSW resonance condition due to the high electron density of sun. These electron neutrinos will oscillate to ν_μ. Outside the sun, many solar neutrinos do not oscillate during their journey to

earth due to the vacuum. So, some of the solar neutrinos born as ν_e and oscillate to ν_μ by the time they leave the sun.

Similar to two flavor one can do the calculation for three flavour neutrino case. The effective Hamiltonian in the flavor basis using Eqns. (2.51) and (2.52) is

$$H = \frac{1}{2E}\text{diag}(0, \Delta m^2_{21}, \Delta m^2_{31})U^\dagger + \text{diag}(V, 0, 0). \tag{2.59}$$

Exact expression of probability can be calculated by taking the square of transition amplitude and the expression for the transition amplitude is given by

$$\mathcal{A}_{\alpha\beta} = \sum_{j=1}^{3} U'_{\beta j} e^{-iE_j t} U'^*_{\alpha j}, \quad \alpha, \beta = e, \mu, \tau\ , \tag{2.60}$$

where U' is the lepton mixing matrix which can diagonalise the Hamiltonian in Eqn. (2.59). It is quite tedious to get the exact expression of oscillation probabilities. However, in Ref. [40] exact expressions for oscillation probabilities have been calculated with the assumption of $\delta_{CP} = 0$. For a constant matter density, analytical expressions for probabilities considering only upto second order terms of θ_{13} and α have been calculate as [41–43]

$$\begin{aligned} P_{e\mu} &= \sin^2\theta_{23}\sin^2 2\theta_{13}\frac{\sin^2[(1-\hat{A})\Delta]}{(1-\hat{A})^2} + \alpha^2\cos^2\theta_{23}\sin^2 2\theta_{12}\frac{\sin^2(\hat{A}\Delta)}{\hat{A}^2} \\ &\mp \alpha\cos\theta_{13}\sin 2\theta_{13}\cos 2\theta_{12}\sin 2\theta_{23}\sin(\Delta)\frac{\sin(\hat{A}\Delta)}{\hat{A}}\frac{\sin[(1-\hat{A})\Delta]}{(1-\hat{A})}\sin\delta_{CP} \\ &+ \alpha\cos\theta_{13}\sin 2\theta_{13}\sin 2\theta_{12}\sin 2\theta_{23}\cos(\Delta)\frac{\sin(\hat{A}\Delta)}{\hat{A}}\frac{\sin[(1-\hat{A})\Delta]}{(1-\hat{A})}\cos\delta_{CP}, \end{aligned} \tag{2.61}$$

$$P_{ee} = 1 - \alpha^2\sin^2 2\theta_{12}\frac{\sin^2\hat{A}\Delta}{\hat{A}^2} - 4\sin^2\theta_{13}\frac{\sin^2(1-\hat{A})\Delta}{(1-\hat{A})^2}, \tag{2.62}$$

$$\begin{aligned} P_{e\tau} &= \alpha\sin^2 2\theta_{12}\sin^2\theta_{23}\frac{\sin^2\hat{A}\Delta}{\hat{A}^2} + 4\sin^2\theta_{13}\cos^2\theta_{23}\frac{\sin^2(1-\hat{A})\Delta}{(1-\hat{A})^2} \\ &- 2\alpha\sin\theta_{13}\sin 2\theta_{12}\sin 2\theta_{23}\cos(\Delta-\delta_{CP})\frac{\sin\hat{A}\Delta}{\hat{A}}\frac{\sin(1-\hat{A})\Delta}{1-\hat{A}}, \end{aligned} \tag{2.63}$$

where $\alpha = \Delta m^2_{21}/\Delta m^2_{31}$, $\Delta = \Delta m^2_{31}L/4E$, $\hat{A} = A/\Delta m^2_{31}$, with $A = \pm 2\sqrt{2}G_F n_e E$, G_F being the Fermi coupling constant while n_e represents the electron number density and " $+$ " sign refers to neutrinos while " $-$ " is for antineutrinos. The negative (positive) sign in the 3rd term of $P_{\mu e}$ is for neutrinos (antineutrinos).

Neutrino oscillation experiments will have advantages due to the matter effect and all the major unknowns can be determined by studying different oscillation channels in presence of earth matter. Appearance channels are important for the determination of the CP violation in long-baseline experiments. Also, one can calculate the hierarchy in mass splitting Δm^2_{31} and octant of θ_{23} by focusing on first two terms in expression (2.62). As matter potential is different for neutrino and antineutrino, by comparing neutrino and antineutrino results, information about CP phase (δ_{CP}) can be drawn [44]. Three flavor oscillation in matter can play decisive part in the determination of unknowns in neutrino sector.

2.4 Experimental Proof of Neutrino Oscillation

Neutrino flavor oscillation measurement has been performed by wide variety of experiments using different sources and techniques. Experiments require very intense source of neutrinos and large detectors due to their extremely feeble interaction. Prior to doing the experiment, one should have adequate knowledge and great measurement accuracy of neutrino flux. Details of neutrino oscillation experiments will be discussed in the next sections. There are several discrepancies observed between the experimental and expected results, which give the evidence for neutrino oscillation. These anomalies will be discussed briefly in the following subsections.

2.4.1 Solar Neutrino Anomaly

Neutrinos produced inside the sun are known as solar neutrinos. Mainly electron neutrinos produced inside the sun via two chain processes namely *pp* chain [45, 46] and CNO cycle [47]. The *pp* chain process is shown in the Fig. 2.4. In CNO cycle several neutrino producing processes are,

$$^{13}N \rightarrow {}^{13}C + e^+ + \nu_e, \quad \text{refereed as} \quad (^{13}N), \tag{2.64}$$

$$^{15}O \rightarrow {}^{15}N + e^+ + \nu_e, \quad \text{refereed as} \quad (^{15}O), \tag{2.65}$$

$$^{17}F \rightarrow {}^{17}O + e^+ + \nu_e, \quad \text{refereed as} \quad (^{17}F). \tag{2.66}$$

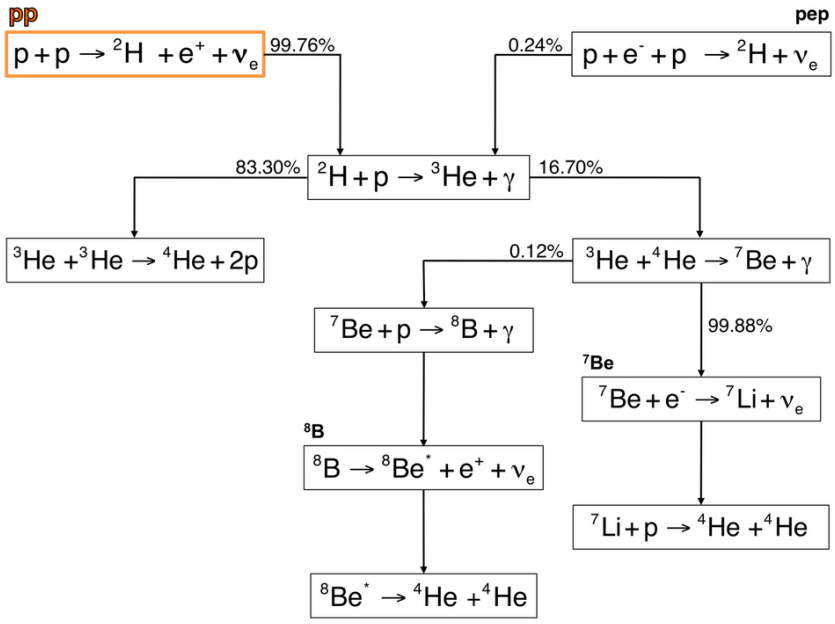

FIGURE 2.4: Solar neutrinos produce in *pp* chain processes. Figure adapted from Ref. [48, 49].

By calculating the ratio of solar luminosity to energy release for each neutrino, the total neutrino flux can be determined. The Standard Solar Model (SSM) predicts the neutrino fluxes at earth surface. In Fig. 2.5, neutrino flux spectra for different processes predicted by SSM and neutrino energy ranges of various solar experiments have shown. There are several solar experiments, such as Gallium experiments, Chlorine experiments, Super Kamiokande and Sudbury Neutrino Observatory (SNO).

Around the mid 90's, three well established experiments (Gallium, Chlorine and Kamiokande) reported that the observed solar ν_e flux is below the predicted data. Further Super Kamiokande clarified the deficit more precisely. The first ever solar neutrino experiment, Homestake observed the number of neutrino as $2.56 \pm 0.16 \pm 0.16$ SNU while the prediction by SSM was $8.46^{+0.87}_{-0.88}$ SNU [51, 52], where SNU is the unit to measure event rate, 1 SNU= 10^{-36} interactions/(atoms . second). Similarly combination of Gallium Experiment (GALLEX) and Gallium Neutrino Observatory (GNO) experiment observed the event rates as $69.3 \pm 4.1 \pm 3.6$ SNU [53], while Soviet-American Gallium Experiment (SAGE) observed $65.4^{+3.1+2.6}_{-3.0-2.8}$ SNU event rates [54]. At the same time SSM prediction for both experiment was $127.9^{+8.1}_{-8.2}$ SNU [52]. Super-Kamiokande experiment observed the neutrino flux as $(2.345 \pm 0.014 \pm 0.036) \times 10^6$ cm^{-2}s^{-1} [55], compared to SSM prediction

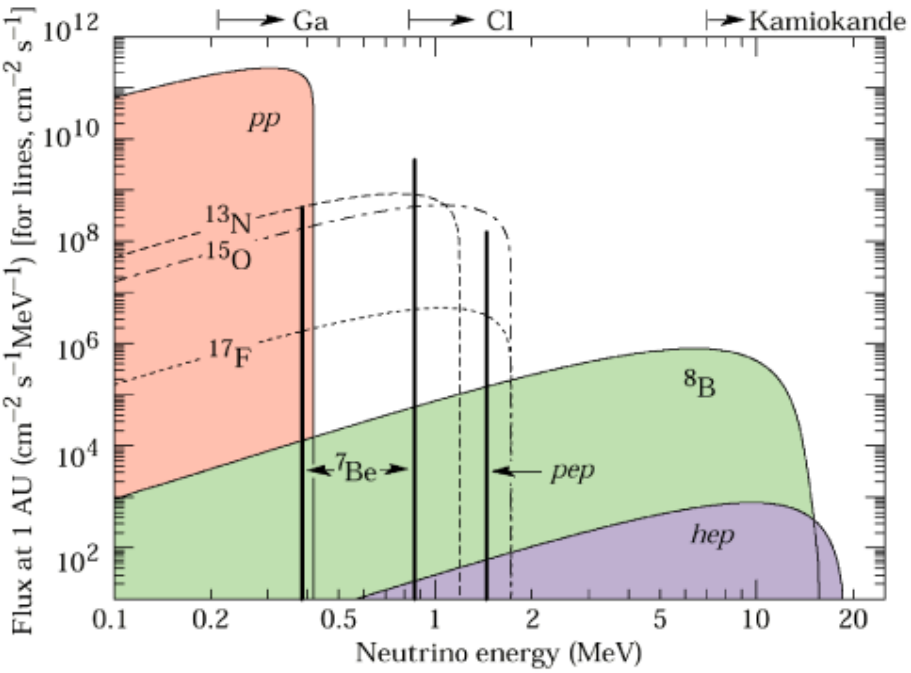

FIGURE 2.5: Spectrum for neutrino fluxes predicted by SSM and solar neutrino energy ranges of several experiments [50].

$(5.46 \pm 0.66) \times 10^6$ cm^{-2}s^{-1} [56]. These disparities between observed and predicted solar data is known as **Solar Neutrino Problem**.

Three anticipated solutions are there for this problem. Firstly there is something wrong with the experiments, causing the measurements to be below the predictions. Secondly the SSM might be defective, but the SSM is well enough to explain the other sectors of physics related to sun. Fortunately, the solution to the anomalous result can be the neutrino oscillation. Electron neutrinos produced inside the core and during their propagation to the earth might convert to ν_μ's and ν_τ's. This possible explanation widely accepted and latter proved by SNO experiment.

All the experiments except SNO were detecting the neutrinos through charge current processes in a flavor dependent way. As a result these experiments observed only ν_e's, no ν_μ and ν_τ components of the total flux. SNO experiment detected the neutrinos via three different interactions namely Elastic Scattering (ES), Charged Current (CC) and Neutral Current (NC). Total flux measured from NC processes by SNO experiment was $(5.25 \pm 0.16^{+0.11}_{-0.13})$ cm^{-2}s^{-1} [57], which is consistent with the SSM prediction. SNO measured all the three type of neutrinos in NC processes while in CC processes only measured the ν_e's. In ES interactions, SNO measured

flux of ν_e's along with 15% of the sum of ν_μ and ν_τ fluxes. By comparing the fluxes from the three different processes, SNO confirmed that, initially only ν_e's produced inside the sun and two third of solar ν_e's were converting into other flavor of neutrinos during the propagation to earth.

2.4.2 Atmospheric Neutrino Anomaly

Cosmic rays mainly consisting of protons ($\sim 95\%$), α particles ($\sim 5\%$), electrons ($\sim< 1\%$) and a small contribution from heavier nuclei. These particles continuously interact with the nucleons present in the atmosphere to produce pions and kaons. These particles decay dominantly in the process of

$$\begin{aligned} & \pi^+ \rightarrow \mu^+\nu_\mu, \quad \mu^+ \rightarrow e^+\nu_e\bar{\nu}_\mu \ , \\ \text{and} \quad & \pi^- \rightarrow \mu^-\bar{\nu}_\mu, \quad \mu^- \rightarrow e^-\bar{\nu}_e\nu_\mu \ . \end{aligned} \tag{2.67}$$

Decay of these hadrons produce atmospheric neutrinos in wide range of energies from sub GeV to multi GeV scales and these neutrinos can travel long distances $\sim$ 10 km to 13000 km before captured at detector.

In order to observe atmospheric neutrinos, large detector should be placed in underground. Kolar Gold Field experiment in India observed atmospheric neutrinos for the first time [58]. Experiments like Kamiokande [59] and IMB [60] observed neutrinos using water Cherenkov detectors, while Frejus [61], NUSEX [62] used iron tracking calorimeters for detection of neutrinos. Based on charge current interaction the flavor of neutrinos can be identified at the detector.

Observation from atmospheric experiments can be analysed by finding the ratio of sum neutrinos and antineutrinos of muon flavor to electron flavor. This ratio can be denoted as R,

$$R = \frac{\nu_\mu + \bar{\nu}_\mu}{\nu_e + \bar{\nu}_e} \sim 2 \ , \tag{2.68}$$

and is predicted to be 2 at energy around $\sim$ 1 GeV. At higher energies the ratio may increase. As neutrinos are produced randomly in atmosphere and can approach the detector from any direction, one can expect symmetry in number of upward and downward moving neutrinos. Zenith angle (Θ_{zen}) is measure of the travelled

Experiment	Experiment type	R
Super-Kamiokande	Water Cherenkov	0.675 ± 0.085
IMB	Water Cherenkov	0.54 ± 0.12
Kamiokande	Water Cherenkov	0.60 ± 0.07
Soudan2	Iron Calorimeter	0.69 ± 0.13
Frejus	Iron Calorimeter	1.0 ± 0.15

TABLE 2.1: Different atmospheric neutrino experiments and their measured double ratio values.

length of atmospheric neutrinos. In other word zenith angle describes the direction of detected neutrinos at detector.

The ratio R predicted to be ~ 2 with uncertainty around $< 5\%$. Further the uncertainty can be reduced by calculating the double ratio between observed and expected data. The double ratio of neutrino events is given by

$$R = \frac{(\nu_\mu/\nu_e)_{\text{obs}}}{(\nu_\mu/\nu_e)_{\text{exp}}} \,. \tag{2.69}$$

The predicted value for R is equal to 1, but Kamiokande experiment reported the value of R to be less than one [63, 64], also all other atmospheric experiments except Frejus experiment agree well with Kamiokande. Observed value of R from different experiments has been shown in Table 2.1. Small value of R indicates that either the number of ν_μ's are less compared to predicted data or ν_e's are more in number than the prediction or both cases are possible. This problem is known as Atmospheric Neutrino Anomaly.

Observation from Super-Kamiokande could solve the atmospheric anomaly [65]. Observed muon-like neutrino events are far below the predicted events for upward moving neutrinos. There is no such deficit for electron-like events. At higher energies, ν_μ's have a significant deviation for $\cos\Theta_{zen} < 0$, i.e., neutrinos coming from down, while at low energy clear deficit for all values of zenith angle i.e., for muon neutrinos coming from both up and down sides. This anomaly can be explained by neutrino oscillation with oscillation parameter as $\Delta m^2 \sim 2.5 \times 10^{-3}$ eV^2 and $\theta \sim 45°$. As mentioned earlier the distance of propagation may vary from 10 km to 13000 km depending upon the direction of neutrinos. For multi-GeV neutrinos, the probability of oscillation will be zero for neutrinos moving downward while for neutrinos moving upward can oscillate with probability $\frac{1}{2}\sin^2 2\theta \sim 0.5$.

This indicates that, ν_μ's are oscillating to ν_τ's not to ν_e's, because the electron like events are not increasing and matching with the prediction.

2.5 Neutrino Oscillation Experiments

Detection of neutrinos is extremely challenging due to their weakly interacting properties. To capture a neutrino, the detector should be large enough and have to wait for a long period of time. Also to reduce the backgrounds detector should be placed under ground. For precise measurement of oscillation parameters and neutrino oscillation, experiments should have extensive knowledge on neutrino source and flux (both natural and artificial). Neutrino interactions with the detectors play a crucial role in detecting neutrinos. Experiments are categorized depending upon the source of neutrinos and their energy ranges as shown in Fig. 2.6. This section will be dedicated to various types of oscillation experiments.

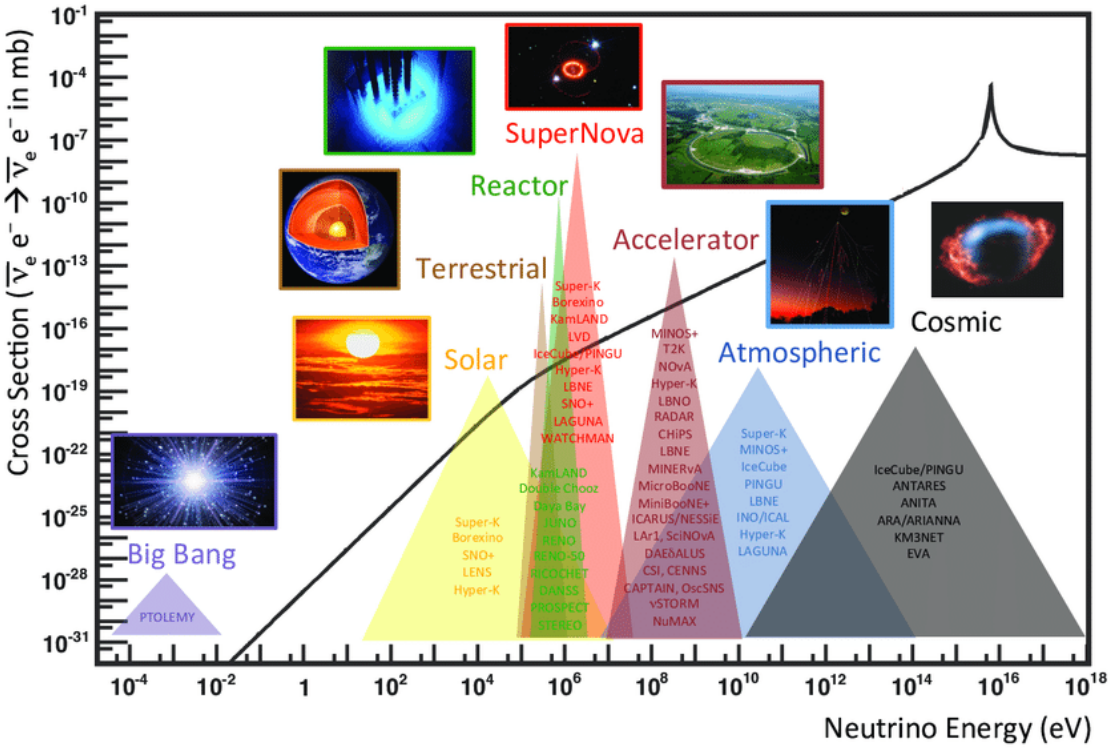

FIGURE 2.6: Various neutrino sources with different energy ranges and neutrino experiments. Figure used from Ref. [66, 67].

2.5.1 Solar Neutrino Experiments

In previous section 2.4.1, we have discussed in details about the solar neutrino flux. This section will be on solar neutrino experiments. In Table 2.2, various solar neutrino experiments have been shown.

Experiment	Detector	Threshold Energy (MeV)	Year of data taking
Homestake	C_2Cl_4	0.814	1970-94
SAGE	Ga	0.233	1989-
GALLEX	$GaCl_3$	0.233	1991-97
GNO	$GaCl_3$	0.233	1998-2003
Kamiokane	H_2O	6.5	1987-95
Super-Kamiokande	H_2O	3.5	1996-
SNO	D_2O	3.5	1999-2006
KamLAND	Liquid Scintillator	1.8	2001-07
Borexino	Liquid Scintillator	0.19	2007-

TABLE 2.2: Solar neutrino experiment with type of target material and threshold energy.

All the experiment prior to SNO, reported the solar neutrino anomaly. All these experiments detected neutrinos through charge current interactions. In general maximum energy for solar neutrinos is around 30 MeV. In charge current processes, interaction of earth matter with neutrinos should produce the leptons corresponds flavor of neutrinos ($\nu_l + X \rightarrow l + Y,\ l = e,\ \mu$ and τ). Mass of muon and tauon are $\sim$ 105 MeV and $\sim$ 1.78 GeV, respectively. As rest mass energy of muon and tauon are too large compared to maximum solar energy, it is difficult for solar neutrinos to produce μ's or τ's in charge current processes. These experiments are capturing only ν_e solar neutrinos. In order to observe ν_μ and ν_τ, the techniques to detect neutrino need to be changed. SNO experiment used heavy water (D_2O) as the target. Deuteron can easily break into parts around energy of 3.5 MeV. Hence, all the solar neutrinos (ν_e, ν_μ and ν_τ) can easily break the deuteron through neutral current processes. SNO can detect all the solar neutrinos via three different ways.

- Elastic Scattering : $\nu + e^- \rightarrow \nu + e^-$,
- Charged Current : $\nu_e + d \rightarrow p + p + e^-$,

- Neutral Current : $\nu + d \rightarrow n + p + \nu$.

Neutral current flux measured in SNO agrees well with SSM predicted flux, resolved the solar neutrino anomaly.

Borexino used liquid scintillator detector of 300 ton to detect solar neutrino. It has a very low threshold energy ~ 0.19 MeV and gave the real time detection of ^7Be solar neutrinos [68]. Also measured the *pp* and *pep* neutrinos, can explain the MSW effect in solar neutrinos. KamLAND experiment was ν_e disappearance experiment. Synergy of KamLAND and other solar experiments predicted the oscillation parameter as,

$$\Delta m^2_{21} = 7.9 \times 10^{-5}\ \text{eV}^2\ , \quad \sin^2 2\theta_{12} = 0.81. \tag{2.70}$$

2.5.2 Atmospheric Neutrino Experiments

Section 2.4.2 discussed about atmospheric neutrino flux, anomaly and several atmospheric neutrino experiments. Most of the atmospheric neutrino experiments are observing the deficit in ν_μ flux. This anomalous result is a consequence of neutrino oscillation in earth matter, already discussed in previous section. Muon neutrinos are not oscillating to electron neutrinos because the ν_e like events are not increasing and remains same as prediction. This indicates oscillation of $\nu_\mu \rightarrow \nu_\tau$. It is very difficult to observe ν_τ events in Super-Kamiokande even though it is able to explain the atmospheric neutrino anomaly. Threshold energy for the charge current interaction of ν_τ is very high (> 3.5 GeV) and also the τ is short lived which make it hard to observe ν_τ events. However, appearance of ν_τ events has been observed in long-baseline experiment OPERA [69] and in IceCube experiment [70] for atmospheric neutrinos.

2.5.3 Reactor Experiments

Electron anti-neutrinos are the by-product of nuclear fission process of heavy elements at nuclear reactor. Reactor neutrino flux depends upon the output thermal power.

Observation of appearance of $\bar{\nu}_\mu$ and $\bar{\nu}_\tau$ from electron type anti-neutrino is quite difficult as the energy of $\bar{\nu}_\mu$ ($\bar{\nu}_\tau$) is not sufficient to produce the charged μ (τ)

Experiment	Baseline (km)	Mass of detector (ton)
KamLAND	180	1000
Double Chooz	1.05	8.3
Daya Bay	1.65	20×4
RENO	1.38	16
JUNO	53	20000

TABLE 2.3: Different reactor experiments with their baselines and detector masses.

through charged current interaction. The only possibility to observe $\bar{\nu}_e$ disappearance events is through inverse beta decay processes

$$\bar{\nu}_e + p \rightarrow e^+ + n. \tag{2.71}$$

The neutron produced in the above process captured by the detector material to produce a photon. Observation of an instant e^+ signal and a delayed γ recognise the events and effectively reduce the backgrounds. In general, detectors are consist of a large volume of liquid scintillator material in a reactor neutrino experiment. Small amount of Gadolinium (Gd) added to liquid scintillator to enhance the neutron detection capability.

Baseline for neutrino propagation can be set according to the mass squared difference to be explored in that experiment. As atmospheric and solar neutrino experiments have already reported two types of mass splittings i.e., solar and atmospheric mass splittings. Reactor experiments with baseline about $\sim$ 100 km can investigate $\Delta m^2 \sim (10^{-4} - 10^{-5})$ eV^2 range, while an experiment of $\sim$ 1 km baseline can explore $\Delta m^2 \sim (10^{-2} - 10^{-3})$ eV^2 scale. Table 2.3 shows the different reactor neutrino experiments, their baselines and mass of detectors. Experiment like Double Chooz [71], Daya Bay [72] and RENO [73] can measure the angle θ_{13} precisely by observing $\bar{\nu}_e$ disappearance channel. NEOS experiment [74] observed excess $\bar{\nu}_e$ events around 5 MeV energy, hinting towards a new mass splitting $\Delta m^2 \sim 1$ eV^2. Other experiments focusing on the new $\Delta m^2 \sim 1$ eV^2 are DANSS, STEREO, PROSPECT, NEUTRINO-4 and SoLid.

2.5.4 Accelerator Based Experiments

In accelerator based neutrino experiments, the neutrino beam is produced in an artificial way. Usually high energetic protons collide with the target material to produce π's and K's. Decay of these particles in decay pipe produce neutrinos. Magnetic horns used to direct the neutrinos in the direction of detector. Direction of current in magnetic horn current decide the neutrino or anti-neutrino mode of running. Neutrinos have to propagate a long distance to reach detector and the distance is known as baseline of the experiment. During the propagation of neutrinos in the long-baseline, neutrinos interact with the earth's matter. The experiments will have advantages due to the matter effect and hence, all the major unknowns of neutrino sector can be determined by studying different oscillation channels in presence of earth matter. Matter effect has significant ramification on appearance channels ($\nu_\mu \to \nu_e$ and $\overline{\nu_\mu} \to \overline{\nu_e}$) compared to disappearance channels. In addition to this, appearance channels have crucial role in determination of the CP violation, hence all the long-baseline experiments are focussing on the appearance channels.

The ratio of baseline to energy of neutrino (L/E) should be chosen properly to observe maximum oscillation. In some of the experiments, detectors are placed off-axial i.e., detector placed at a small angle to the direction of propagation to get narrow neutrino flux at the desired energy and to reduce the background events. One can calculate the neutrino energy from π decay as

$$E_\nu = \frac{\left(1 - \left(\frac{m_\mu}{m_\pi}\right)^2\right) E_\pi}{1 + \gamma^2\theta^2}, \qquad \gamma = \frac{E_\pi}{m_\pi}, \tag{2.72}$$

where E_ν (E_π) is the energy of neutrino (pion) and θ is the angle between neutrino beam direction and pion. In on-axial case where $\theta = 0$ implies that $E_\nu \propto E_\pi$, while in off-axial case ($\theta \neq 0$), E_ν depends upon the angle θ. In this way, experiments can achieve a narrow monochromatic spectrum at a central value of energy [75]. Examples of such experiments are NOvA, T2K, T2HK and T2HKK.

Ratio of baseline to energy decide the range of Δm^2 the experiment will be sensitive. For a ratio of $L/E \sim 500$ km/GeV, the experiment can explore a mass squared difference of $\Delta m^2 \sim 2.5 \times 10^{-3}$ eV^2 at first oscillation maxima. Experiments with neutrino energy of order of GeV and baseline around $\sim (100 - 1000)$ km are called long-baseline experiments. Also, some long-baseline experiments

Experiment	Type of Far Detector	Baseline (km)	E_ν (GeV)
K2K	Water Cherenkov	250	1.3
MINOS	Iron Scintillator	735	3
MINOS+	Iron Scintillator	735	7
OPERA	Nuclear Emulsion	730	17
T2K	Water Cherenkov	295	0.6
NOvA	Liquid Scintillator Tracking Calorimeter	810	2
DUNE	Liquid Argon TPC	1300	2.5
ESSnuSB	Water Cherenkov	540 or 360	0.25
T2HK	Water Cherenkov	295	0.6
T2HKK	Water Cherenkov	1100	0.6
P2O	Sea Water	2595	3.5

TABLE 2.4: Several long-baseline experiments with type of detector, baseline and peak energy of neutrinos for the experiments.

like ESSnuSB and T2HKK focus on the second oscillation maxima. At second oscillation maxima the δ_{CP} dependence is more compared to the first oscillation maximum, so the experiment will be sensitive towards δ_{CP} and can explain CP violation in neutrino sector. While some experiments can describe oscillation at mass splitting ~ 1 eV^2 with baseline ~ 1 km, are called short-baseline experiments.

2.5.4.1 Long-Baseline Experiments

Long-baseline experiments usually have two detectors one at near and other at far distances, to decrease the uncertainties in neutrino beam. Near detector observes the unoscillated beam, can extract information about neutrino flux and spectrum. Far detector observes the oscillated beam.

First long-baseline experiment was K2K, where neutrinos propagate a distance of 250 km from KEK to Super-Kamiokande. Other long-baseline experiments are MINOS, MINOS+, OPERA, T2K and NOvA. Some other upcoming experiments are DUNE, ESSnuSB, T2HK, T2HKK and P2O. Table 2.4 shows several long baseline experiment with type of far detector, baseline and peak energy for neutrino beam.

Experiment	Type of Detector	Detector Mass (ton)	Baseline (m)
LSND	Liquid Scintillator	167	30
KARMEN	Liquid Scintillator	65 m^3	17.7
MiniBooNE+	Mineral and Oil	818	541
MicroBooNE	Liquid Argon TPC	85	470
ICARUS	Liquid Argon TPC	760	600
JSNS	Liquid Scintillator	17	24

TABLE 2.5: Several short-baseline experiments with types of detectors, fiducial masses, and baseline lengths.

2.5.4.2 Short-Baseline Experiments

The baseline of these experiments are of few meters with peak energy in the range of MeV. Such experiments are LSND, KARMEN, MiniBooNE, MicroBooNE and JSNS. Table 2.5 displays the list of short-baseline experiments with types of detectors, fiducial masses, and baseline of the experiments. These experiments can probe the mass splitting of the order of ~ 1 eV^2. Most of the short baseline experiments show excess ν_e and $\bar{\nu}_e$ appearance events. This aberrant result hints towards existence of sterile neutrinos. However, recently MicroBooNE experiment reported no such excess of events.

2.6 Current status of neutrino oscillation

This is the precision era for neutrino oscillation parameters. All the parameters except δ_{CP} have been measured with very high accuracy. Current best fit values and the 3σ uncertainties are shown in Table 2.6. However, the degeneracy in atmospheric mass square difference (Δm^2_{31}) is not yet resolved, which is known as Mass Hierarchy (MH) problem. The hierarchy is known as Normal Hierarchy (NH) for $\Delta m^2_{31} > 0$ or $m_1 < m_2 \ll m_3$, while $\Delta m^2_{31} < 0$ or $m_3 \ll m_1 < m_2$ refers to Inverted Hierarchy (IH) [76] as shown in Fig. 2.7. In addition to this, the value of the atmospheric mixing angle θ_{23} is also not known precisely. The Super-Kamiokande experiment observed the value of θ_{23} such that the value of $\sin^2\theta_{23}$ will be maximum i.e. $\theta_{23} = \pi/4$, while the oscillation result from MINOS experiment with beam and atmospherics neutrinos prefers non-maximal mixing [79]. This deviation creates two degenerate solutions; the value of $\theta_{23} < 45°$ is

Parameters	Best fit values values	3σ Ranges
$\sin^2\theta_{12}$	0.304	0.269→0.343
$\sin^2\theta_{13}$	0.02220	0.02034→0.02430
$\sin^2\theta_{23}$	0.573	$0.405 \rightarrow 0.620$
δ_{CP}	194°	$105° \rightarrow 405°$
Δm^2_{12}	7.42×10^{-5} eV^2	$(6.82 \rightarrow 8.04) \times 10^{-5}$ eV^2
Δm^2_{31}	2.515×10^{-3} eV^2	$(2.431 \rightarrow 2.599) \times 10^{-3}$ eV^2

TABLE 2.6: Values of neutrino oscillation parameters from Ref. [35].

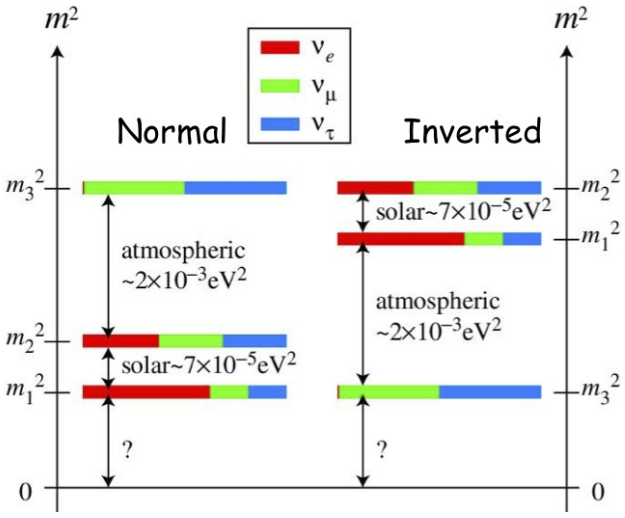

FIGURE 2.7: Normal and Inverted mass hierarchy in different flavor combination of mass states. Figure adapted from Ref. [77, 78].

called Lower Octant (LO) while Higher Octant (HO) corresponds to $\theta_{23} > 45°$, known as octant degeneracy. This degeneracy in θ_{23} consequently affect the measurement of neutrino oscillation parameters [80, 81]. One of the most important issues in neutrino sector is the measurement of CP violation. CP violation from neutrino sector can give rise to the phenomenon of leptogenesis which subsequently can explain the observed baryon asymmetry of the universe through Baryogenesis [82, 83]. However, we do not have any concrete evidence regarding CP violation in neutrino sector so far, i.e., the exact value of the Dirac CP phase δ_{CP} is still unknown. The most recent measurements from the currently running long-baseline experiments NOvA and T2K in the measurement of δ_{CP} show some discrepancies. NOvA experiment prefers the CP conserving value for $\delta_{CP} \sim \pi$ while T2K prefers maximal CP violation $\delta_{CP} \sim 3\pi/2$ [84]. Apart from these unknowns, there are

some open questions like what are the absolute mass scales of neutrinos, the nature of neutrinos, i.e., whether they are Dirac or Majorana particles (Neutrinoless double beta decay to explain the Majorana nature of neutrinos), why neutrino mixing differs from quark mixing and so on. Additionally, existence of Sterile neutrino [85, 86], CPT violation [87, 88], Non-Standard Interaction (NSI) [36, 37], Lorentz Invariance Violation (LIV) [89], etc., are some of the current open questions in this sector. All these open questions make Neutrino Physics extensive and wide area for scientific research. The effort of many dedicated neutrino oscillation experiments [90–105] over the last two decades, provide us a splendid understanding about the main features of these tiny and elusive particles. Many dedicated experiments have been planned to shed light on the unknowns of neutrino sector.

2.7 Conclusion

In this chapter, we made an effort to enlighten the concept of neutrino oscillation. Neutrino oscillation in two and three flavors are discussed in detail. Then we discussed the oscillation in matter when neutrinos interact with the matter during their propagation. Later evidences of neutrino oscillation and different neutrino oscillation experiments discussed thoroughly. At the end of this chapter current status of neutrino oscillation parameters and unknowns in neutrino sector are discussed briefly. Experimental study of these unknowns is quite important in neutrino sector. Next chapters will be on the effect of various BSM physics on the measurement of oscillation parameters at various long-baseline experiments.

Chapter 3

Implication of sterile neutrino on currently running long-baseline and neutrino less double beta decay experiment

3.1 Introduction

Neutrinos being unique in nature, posses various distinct features. One of the interesting aspects is related to its mass, although it is massless in the SM, neutrino oscillation demands neutrinos to have tiny but non-zero mass as already discussed in chapter 1 and 2. In this regard, tremendous attempts are being made to understand the origin of their masses and mixing phenomena, mass scale, whether they are Dirac or Majorana in nature, neutrino mass orderings, etc.

Besides these, another major unsolved issue in this sector is the possible existence of additional eV-scale sterile neutrino (ν_s) species, which has attracted a lot of attention in recent times, following some anomalies reported by various experiments. Initially such type of peculiar result was report by the LSND experiment [106], in the measurement of anti-neutrino flux in $\overline{\nu}_\mu \to \overline{\nu}_e$ oscillation. The short-baseline experiment LSND with a baseline of 30 m was detecting oscillation with a 167 ton liquid scintillator detector. An excess of $87.9 \pm 22.4 \pm 6.0$ events in the electron

anti-neutrino ($\overline{\nu}_e$) appearance data has been observed after extracting the background. This could be explained by introducing a new mass splitting $\Delta m^2 \sim 1\text{eV}^2$. This result was further supported by the $\bar{\nu}_e$ appearance results at the MiniBooNE experiment [107]. MiniBooNE experiment detects the neutrinos produced from decay of Pions and Kaons generated by using 8 GeV protons from the Fermilab Booster. A detector of 818 tons mineral oil at a distance of 541 m detects ν_e and $\bar{\nu}_e$ through charge current quasi elastic (CCQE) process. The observed 460.5 ± 99.0 excess events corresponds to 4.7σ significance [108]. Another hint for existence of a new mass splitting has emerged from the deficit in the estimated anti-neutrino flux from reactor experiments [109, 110]. Recent measurements of the ratios of inverse beta-decay energy spectra by the short-baseline experiments NEOS [111] and DANSS [112], at different distances also appear to exhibit some preference for new mass splitting, while other recent short-baseline measurements, PROSPECT [113] and STEREO [114], don't show any such evidence. Similar anomalies have also been observed at GALLEX [115–117] and SAGE [118] Gallium experiments for solar neutrino observation. These experiments detect electron neutrinos produced through electron capture using radioactive sources ^{51}Cr and ^{37}Ar inside the detectors. Finally the produced neutrino captured by ^{71}Ga for identification of solar neutrinos. A deficit of 2.8σ between predicted and observed events, is known as the Gallium anomaly, which indicates the existence of additional mass squared difference [116, 119–122]. Recently MiniBooNE collaboration [108], reported their new analysis with twice the data sample size used earlier, confirming the anomaly at the level of 4.8σ, which becomes $> 6\sigma$, if combined with LSND data.

This distinct mass squared difference is different from the two well-known mass splittings and it demands the number of neutrino has to be more than three. CERN based Large Electron Positron (LEP) collider experimental result from invisible decay of Z boson shows that the number of neutrinos below half of the mass of Z boson is three, which can couple to Z boson [123]. If the number of neutrino species increased to four to accommodate the new mass splitting, the fourth neutrino cannot have gauge interactions with the SM gauge bosons, thus safeguarding the precision measurement of Z boson decay width by LEP experiment. Hence, such a neutrino is known as sterile neutrino, while the usual standard model neutrinos are known as active neutrinos.

However, no evidence of active-sterile neutrino mixing is observed by the MINOS and MINOS+ collaborations [124], and the joint analysis of these experiments sets

stringent limits on the active-sterile mixing angles for values $\Delta m^2_{41} > 10^{-2}$ eV^2, through the study of ν_μ disappearance. More importantly, the entire MiniBooNE 90% CL allowed region is excluded by MINOS/MINOS+ at 90% CL. This in turn implies a tension between MiniBooNE and MINOS/MINOS+ results. Recently, NOνA [125] has also performed the search for active-sterile neutrino mixing using neutral current interactions, though no evidence of $\nu_\mu \to \nu_s$ has been found. Also the MicroBooNE experiment designed to verify the result of MiniBooNE, recently reported no excess of ν_e appearance events [126]. Interestingly, in a recent work by Denton et al. [127], suggested that there will be hints for $\Delta m^2 \sim 1.42$eV^2 from ν_e disappearance channel of MicroBooNE, which agrees well with the other experimental results for the existence of eV scale sterile neutrino. The long-standing anomalous results related to sterile neutrinos are expected to be resolved by the Fermilab's short-baseline neutrino program, SBND and ICARUS experiments and also by SoLid experiment.

Though the possible existence of an eV-scale neutrino could explain the above mentioned reactor as well as the LSND and MiniBooNE anomalies, sterile neutrinos are blind to weak interactions. However, they can mix with active neutrinos and affect the oscillation phenomenology. Therefore, in this work, we explore the effect of such active-sterile mixing on the determination of neutrino oscillation parameters by currently running long-baseline neutrino experiments. We, further investigate its effect on neutrinoless double beta decay process. The implications of light sterile neutrino on the physics potential of various long-baseline experiments, such as T2K, T2HK, NOνA and DUNE have been explored by several authors [128–141] for various possible combinations of run-period. However, in this work we focus our attention on the following aspects. First, we would like to see whether the determination of mass-ordering by the currently running long-baseline experiments NOνA and T2K would be affected by the presence of light sterile neutrinos. Next, as the recent global fit hints towards the possibility of maximal CP violation in the neutrino sector, i.e., $\delta_{\rm CP} \approx 3\pi/2$ [142], we therefore, investigate the sensitivity of these experiments for the exclusion of maximal CP-violation scenario. We also briefly demonstrate the implications of light sterile neutrinos on neutrinoless double beta decay.The impact of one sterile neutrino in the sensitivity studies of these two experiments towards neutrino mass hierarchy and CP violation discovery has been performed in a recent work [132]. However, our work differs from their analysis in the following ways. Firstly, we have considered all the three new mixing angles as well as the additional two CP violating

phases to be non-zero, whereas they have assumed $\sin^2\theta_{34} = 0$ and $\delta_{34} = 0$. Secondly, concerning the CP violation studies, we have performed the analysis for the exclusion of maximal CP-violation scenario, which has been done for the first time to the best of our knowledge.

The chapter is organised as follows. In section 3.2, we discuss the theoretical framework for (3+1) flavor oscillation scheme. Section 3.3 covers the experimental set-up and details about the analysis adopted in this work. The effect of light sterile-neutrino on oscillation parameters is discussed in section 3.4. Section 3.5 deals with mass hierarchy (MH) sensitivity, while the maximal CP violation sensitivity is discussed in section 3.6. Section 3.7 focused on the impact of sterile neutrino on neutrinoless double beta decay, prior to conclusion in section 3.8.

3.2 Brief Discussion about 3+1 Oscillation Model

In the presence of one sterile neutrino in addition to three light standard neutrino is referred as 3+1 scenario. There will be mixing between the three active neutrinos with the sterile one and hence, the neutrino mixing matrix can be represented by a 4×4 unitary matrix. Consequently, the parametrization of the neutrino mixing matrix requires some additional parameters as mentioned in Chapter 2, which includes three mixing angles $(\theta_{14}, \theta_{24}, \theta_{34})$ and two phases $(\delta_{14}, \delta_{34})$. Thus, analogous to the standard PMNS matrix, the four dimensional mixing matrix will have the form

$$U^{3+1} = O(\theta_{34}, \delta_{34})R(\theta_{24})O(\theta_{14}, \delta_{14})R(\theta_{23})O(\theta_{13}, \delta_{13})R(\theta_{12}) \ , \tag{3.1}$$

where $R(\theta_{ij})$ $(O(\theta_{ij}, \delta_{ij}))$ are the real (complex) 4×4 rotation matrices in the ij plane, which contain the 2×2 sub-matrices

$$R^{2\times2}(\theta_{ij}) = \begin{pmatrix} \cos\theta_{ij} & \sin\theta_{ij} \\ -\sin\theta_{ij} & \cos\theta_{ij} \end{pmatrix}, \tag{3.2}$$

$$O^{2\times2}(\theta_{ij}, \delta_{ij}) = \begin{pmatrix} \cos\theta_{ij} & \sin\theta_{ij}e^{-i\delta_{ij}} \\ -\sin\theta_{ij}e^{i\delta_{ij}} & \cos\theta_{ij} \end{pmatrix}, \tag{3.3}$$

as the ij sub-block. Incorporating the 4×4 mixing matrix (3.1), the oscillation probability for $\nu_\mu \to \nu_e$ transition in the 3+1 framework can be expressed in terms of the effective mixing matrix elements ($\tilde{U}_{\alpha i}$) and effective mass square differences $\Delta\tilde{m}^2_{ij}$, in presence of matter as [143]

$$P(\nu_\mu \to \nu_e) = \sum_i |\tilde{U}_{\mu i}|^2 |\tilde{U}_{ei}|^2 + 2\sum_{i<j} \left[\mathrm{Re}(\tilde{U}_{\mu i}\tilde{U}_{ej}\tilde{U}^*_{\mu j}\tilde{U}^*_{ei}) \cos\Delta_{ij} - \mathrm{Im}(\tilde{U}_{\mu i}\tilde{U}_{ej}\tilde{U}^*_{\mu j}\tilde{U}^*_{ei}) \sin\Delta_{ij} \right], \quad (3.4)$$

where $\Delta_{ij} = \Delta\tilde{m}^2_{ij} L/2E$, L and E are baseline and energy of neutrino beam, respectively. The effective mass squared difference $\Delta\tilde{m}^2_{ij}$ can be written in terms of two arbitrary mass squared differences as

$$\Delta\tilde{m}^2_{ij} = \hat{\Delta}m^2_{i1} - \hat{\Delta}m^2_{j1} \, . \quad (3.5)$$

The exact analytical expressions for $\hat{\Delta}m^2_{i1} (i = 1, 2, 3, 4)$ can be found in [143]. The effective mixing elements can be related to the 4×4 mixing matrix elements ($U_{\alpha i}$, $\alpha = e, \mu, \tau, s$) as

$$\tilde{U}_{ei}\tilde{U}^*_{\mu j} = \frac{1}{\prod_{k\neq i} \Delta\tilde{m}^2_{ik}} \left[\sum_j F^{ij}_{e\mu} U_{ej} U^*_{\mu j} + C_{e\mu} \right] , \quad (3.6)$$

where

$$\begin{aligned} F^{ij}_{e\mu} &= A^2\Delta m^2_{j1} + A\Delta m^2_{j1}(\Delta m^2_{j1} - \sum_{k\neq i} \hat{\Delta}m^2_{k1}) + (\Delta m^2_{j1})^3 - \sum_{k\neq i} (\Delta m^2_{j1})^2 \hat{\Delta}m^2_{k1} \\ &\quad + \sum_{k,l;k\neq l\neq i} \Delta m^2_{j1}\hat{\Delta}m^2_{k1}\hat{\Delta}m^2_{l1} \, , \\ C_{e\mu} &= A' \sum_{kl} \Delta m^2_{k1}\Delta m^2_{l1} U_{ek} U^*_{\mu l} U_{sk} U^*_{sl} + A \sum_{k,l} \Delta m^2_{k1}\Delta m^2_{l1} |U_{ek}|^2 U_{el} U^*_{\mu l} \, , \end{aligned} \quad (3.7)$$

with $A = 2\sqrt{2} G_F N_e E$, $A' = -\sqrt{2} G_F N_n E$ and $N_e (N_n)$ is the electron (neutron) density. One can get back the oscillation probability for three neutrino scenario in the presence of matter, from the 3+1 case by assuming $U_{\alpha 4} = 0$, $U_{si} = 0$, and $A' = 0$.

Now, we would like to see the impact of a sterile neutrino on the physics potentials of accelerator based long-baseline neutrino oscillation experiments, which are primarily designed to study $\nu_\mu \to \nu_e$ and $\overline{\nu}_\mu \to \overline{\nu}_e$ oscillation channels. The first and

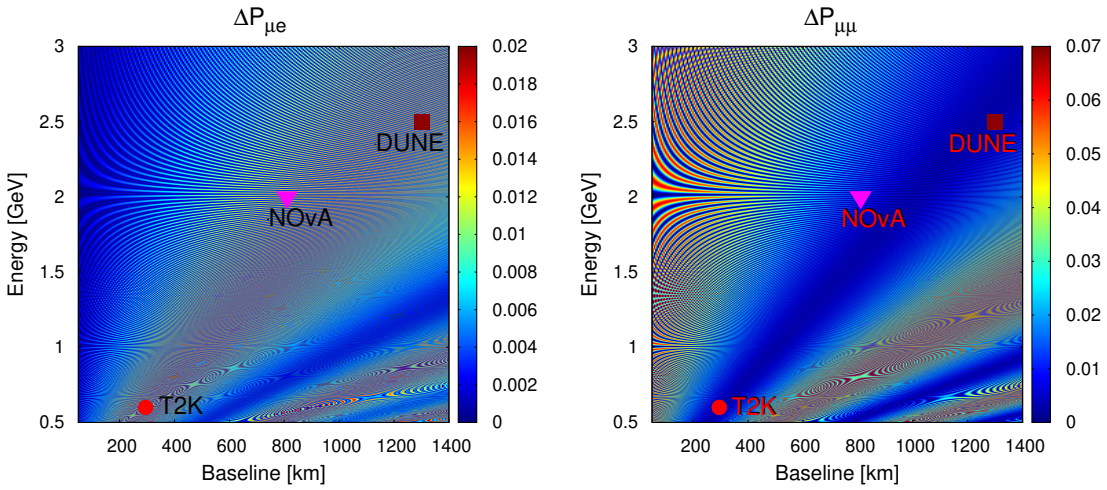

FIGURE 3.1: Graphical representation of $\Delta P_{\mu e}$ ($\Delta P_{\mu\mu}$) in the $L - E$ plane in left (right) panel.

foremost implication can be demonstrated by defining a quantity $\Delta P_{\alpha\beta}$, which is the absolute difference between the oscillation probabilities in the presence of a sterile neutrino and the standard three flavor interaction (SI) scenario in presence of matter, i.e., $\left(\Delta P_{\alpha\beta} = |P^{\text{sterile}}_{\alpha\beta} - P^{\text{SI}}_{\alpha\beta}|\right)$. Analogously, one can also construe the corresponding parameter for anti-neutrino case as $\overline{\Delta P}_{\alpha\beta}$. In Fig.3.1, we show the graphical representation of oscillograms for $\Delta P_{\mu e}$ ($\Delta P_{\mu\mu}$) in left (right) panel, as function of baseline (L) and energy (E) for neutrino beam. For obtaining these oscillograms, we have used the best-fit oscillation parameters as given in the Table 3.1. In the plots 3.1, dark red regions represent large deviation between the oscillation probabilities. Moreover, it is clear from $\Delta P_{\mu e}$ plot that, one can probe sterile neutrino in long-baseline experiments like T2K ($L = 295$ km, $E = 0.6$ GeV), NOνA ($L = 810$ km, $E = 2$ GeV) and DUNE ($L = 1300$ km, $E = 2.5$ GeV). Hence, sterile neutrinos may play a crucial role in the determination of the oscillation parameters in long-baseline neutrino oscillation experiments. Similarly, the sensitivity of $\Delta P_{\mu\mu}$ towards the presence of sterile neutrino for these experiments is also non-negligible ($\sim 1\%$), as seen from the right panel of Fig.3.1.

Parameters	True values	Test value Range
$\sin^2\theta_{12}$	0.310	NA
$\sin^2\theta_{13}$	0.0224	NA
$\sin^2\theta_{23}$	0.58	$0.4 \to 0.62$
	(LO 0.42)	$0.4 \to 0.5$
	(HO 0.58)	$0.5 \to 0.62$
$\delta_{\rm CP}$	$-90°$	$-180° \to 180°$
Δm^2_{21}	7.39×10^{-5} eV^2	NA
Δm^2_{31}	$+2.525 \times 10^{-3}$ eV^2 (NH)	$+(2.43 \to 2.63) \times 10^{-3}$eV^2
	-2.512×10^{-3} eV^2 (IH)	$(-2.61 \to -2.41) \times 10^{-3}$ eV^2
Δm^2_{14}	1 eV^2	NA
$\sin^2\theta_{14}$	0.0204	$(0.0098 \to 0.031)$
$\sin^2\theta_{24}$	0.0163	$(0.006 \to 0.0268)$
$\sin^2\theta_{34}$	0.0197	$(0 \to 0.0413)$
δ_{14}	$-90°$	$-180° \to 180°$
δ_{34}	$-90°$	$-180° \to 180°$

TABLE 3.1: Values of oscillation parameters considered in our analysis are taken from the latest NuFIT results [144]. Values for the sterile mixing angles and their allowed ranges are calculated from the 3σ ranges of the matrix elements $|U_{\alpha 4}|$ as discussed in [145].

3.3 Simulation details

As we are interested in exploring the impact of an eV-scale sterile neutrino on currently running long baseline experiments NOνA and T2K, we simulate these experiments using GLoBES software package [146, 147]. GLoBES "General Long Baseline Experiment Simulator" is a highly competent software package to study neutrino oscillation at long baseline and reactor experiments. In GLoBES, informations of long baseline experiments described in a compact way through "Abstract Experiment Definition Language" (AEDL) and it use a C-library to execute the long baseline experiments. One can calculate oscillation probabilities, event rates and $\Delta\chi^2$ using GLoBES. Additionally we have used snu plugin [148] to incorporate sterile neutrino. The auxiliary files and experimental specification of these experiments that we use in our analysis are taken from [149].

T2K and NOνA are complementary accelerator-based experiments with similar

capabilities and goals, but differ only on their baselines. NOνA experiment is optimised to study the appearance of $\nu_e(\overline{\nu}_e)$ from a beam of $\nu_\mu(\overline{\nu}_\mu)$, consists of two functionally identical detectors, each located 14.6 mrad off the central-axis of Fermilab's neutrino beam, to receive a narrow band neutrino beam with peak energy near 2 GeV, corresponding to $\nu_\mu \to \nu_e$ oscillation maximum. Its near detector (ND) of mass 280 ton is located about 1 km downstream (100 m underground) from the source to measure un-oscillated beam of muon-neutrinos and estimate backgrounds at the far detector (FD). Oscillated neutrino beam is observed by 14 kton far detector, situated in Ash River, 810 km away from Fermilab. In order to simulate NOνA, we consider 120 GeV proton beam energy with 6×10^{20} protons on target (POT) per year. We assume signal efficiencies for both electron (muon) neutrino and anti-neutrino as 45% (100%). The background efficiencies for misidentified muons (anti-muons) at the detector are considered as 0.83% (0.22%). The neutral current background efficiency for ν_μ ($\overline{\nu}_\mu$) is assumed to be 2% (3%). We further assume the intrinsic beam contamination, i.e., the background contribution coming from the existence of electron neutrino (anti-neutrino) in the beam to be about 26% (18%). Apart from these, we also consider 5% uncertainty on signal normalization and 10% on background normalization.

The muon neutrino beam of T2K experiment is produced at Tokai and is directed towards the water Cherenkov detector of fiducial mass 22.5 kt kept 295 km far away at Kamioka [150]. The neutrino flux peaks around 0.6 GeV as the detector is kept 2.5° off-axial to the neutrino beam direction. In order to simulate T2K experiment, we consider a proton beam power of 750 kW and with a proton energy of 30 GeV which corresponds to a total exposure of 7.8×10^{21} POT with 1:1 ratio of neutrino to anti-neutrino modes. We match the signal and back-ground event spectra and rates as given in the recent publication of the T2K collaboration [151]. We consider an uncorrelated 5% normalization error on signal and 10% normalization error on background for both the appearance and disappearance channels as given in Ref. [151] to analyse the prospective data from the T2K experiment. We assume that the set of systematics for both the neutrino and anti-neutrino channels are uncorrelated.

We simulate the true ($N^{\rm true}$) and test ($N^{\rm test}$) event rates and compare them by using binned χ^2 method defined in GLoBES, i.e.,

$$\chi^2_{\rm stat}(\vec{p}_{\rm true},\vec{p}_{\rm test}) = \sum_{i\in{\rm bins}} 2\left[N_i^{\rm test} - N_i^{\rm true} - N_i^{\rm true}\ln\left(\frac{N_i^{\rm test}}{N_i^{\rm true}}\right)\right], \qquad (3.8)$$

where $\vec{p}$ stands for the array of standard neutrino oscillation parameters. However, for numerical evaluation of χ^2, we also incorporate the systematic errors using pull method, which is generally done with the help of nuisance parameters as discussed in the GLoBES manual. Detail calculation of χ^2 analysis mentioned in Appendix A. Suppose $\vec{q}$ denotes the oscillation parameter in presence of sterile neutrino, then the Mass Hierarchy (MH) sensitivity is given by

$$\begin{aligned} \chi^2_{\rm MH}(\vec{q}) &= \chi^2_{\rm IH}(\vec{q}) - \chi^2_{\rm NH}(\vec{q}), \quad \text{(for true Normal Hierarchy (NH))}, \\ \chi^2_{\rm MH}(\vec{q}) &= \chi^2_{\rm NH}(\vec{q}) - \chi^2_{\rm IH}(\vec{q}), \quad \text{(for true Inverted Hierarchy (IH))}. \end{aligned} \tag{3.9}$$

Further, we obtain minimum $\chi^2_{\rm min}$ by doing marginalization over all oscillation parameters. In our analysis, we do not explicitly simulate the near detector for these experiments which may provide some information about the active-sterile mixing angles θ_{i4}, but certainly, the near detector data is blind to the CP phases, whose implications are mainly explored in this work.

3.4 Degeneracies among oscillation parameters

In this section, we discuss the degeneracies among the oscillation parameters in presence of an eV-scale sterile neutrino. Here, we focus only on NOνA experiment.

In order to analyse degeneracies among the oscillation parameters at probability level, we show ν_e ($\overline{\nu}_e$) appearance probability as a function of $\delta_{\rm CP}$ in the left (right) panel of Fig. 3.2. The upper panel of the figure corresponds to oscillation probability in standard paradigm and that for 3+1 case is given in lower panel. The green, orange, blue and red bands in the figure represent the oscillation probabilities for possible hierarchy-octant combinations: NH-HO, NH-LO, IH-HO and IH-LO, respectively, where HO and LO stand for higher octant and lower octant of θ_{23}. From the upper panel of the figure, it can be seen that the bands for NH-HO and IH-LO are very well separated in neutrino channel, whereas the NH-LO and IH-HO bands are overlapped with each other, which results degeneracies among the oscillation parameters. Also it should be noted that, in the anti-neutrino channel, the case is just opposite. Therefore, a combined analysis of neutrino and anti-neutrino data helps in the resolution of degeneracies and also improves the sensitivity of long-baseline experiments to precisely determine the

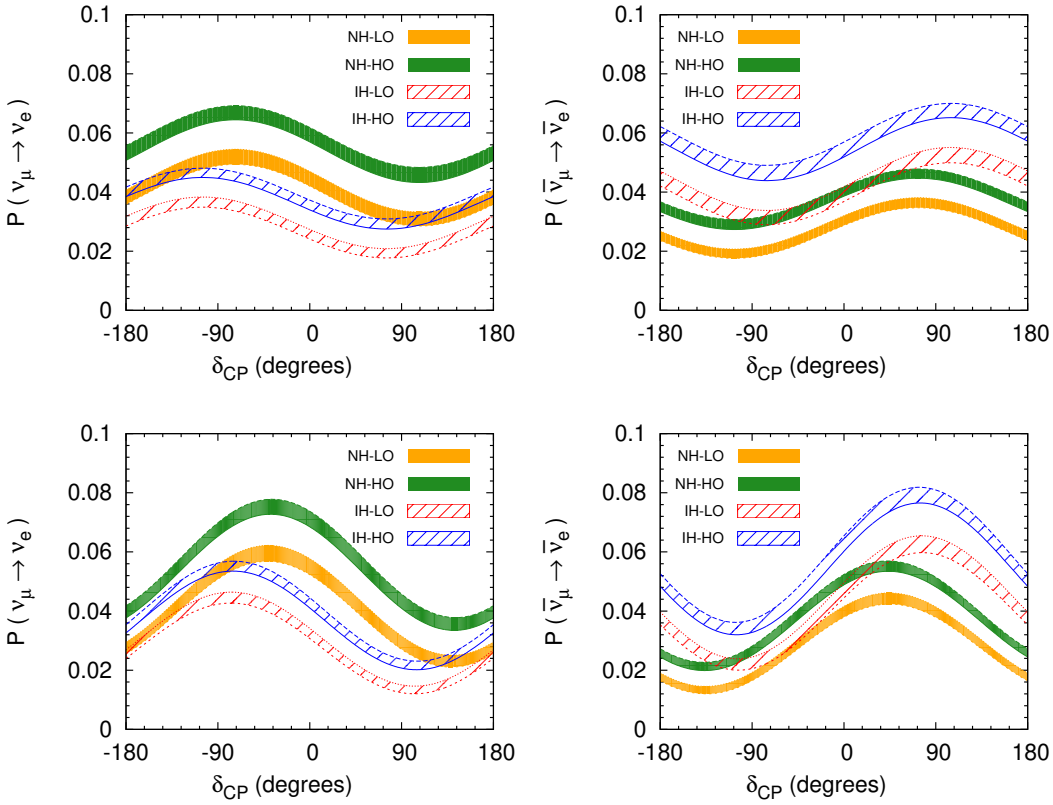

FIGURE 3.2: The neutrino (anti-neutrino) oscillation probability as a function of δ_{CP} is shown in the left (right) panel. The upper panel is for 3-flavor case, while the lower panel is for 3+1 case with $\delta_{14} = -90°$ and $\delta_{34} = -90°$.

unknowns of standard oscillation paradigm. From the bottom panel of the figure, it can be seen that new types of degeneracies among the oscillation parameters have emerged, in the presence of sterile neutrino even for single values of the new CP phases δ_{14} ($= -90°$) and δ_{34} ($= -90°$), which can worsen the sensitivity of the unknowns.

Another way of representing these degeneracies among oscillation parameters is by using the bi-probability plot. In this case, we calculate the oscillation probabilities for neutrino and anti-neutrino for a fixed hierarchy-octant combination for all possible values of δ_{CP} and display them in a neutrino-antineutrino probability plane in Fig. 3.3. The ellipses in the figure correspond to 3-flavor case, whereas the bands represent the oscillation probabilities in presence of sterile neutrino with all possible values of new phases δ_{14} and δ_{34}. From the figure, it can be seen that the ellipses for LO and HO are very well separated for both hierarchies, whereas the ellipses for NH and IH for both LO and HO are overlapped with each other

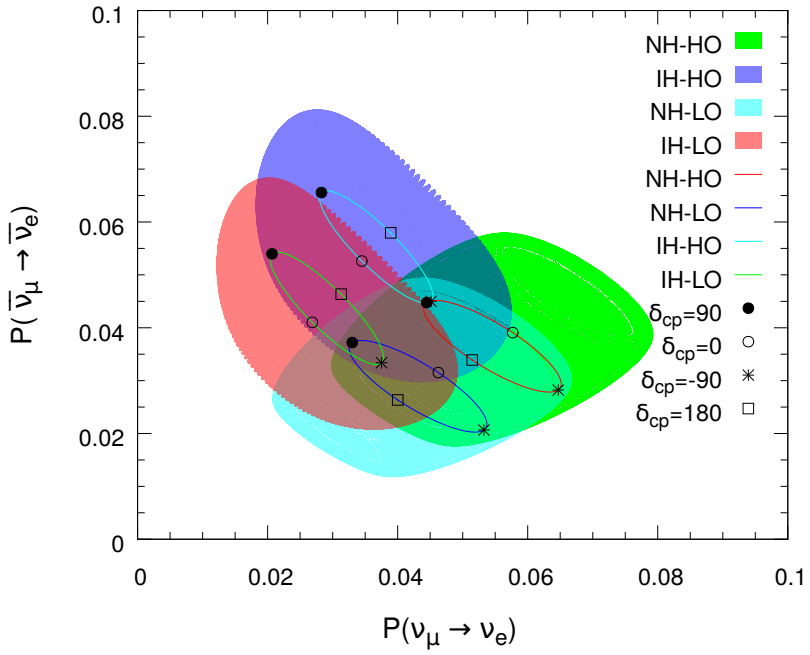

FIGURE 3.3: Bi-probability plots for NOνA in 3 years in neutrino and 3 years in anti-neutrino mode for different hierarchy and octant combinations.

and give rise to degeneracies. Therefore, NOνA experiment is more sensitive to octant of θ_{23} than that of mass hierarchy. While in $3+1$ paradigm, the bands are overlapped with each other for all combinations, which gives rise to new degeneracies. The additional degeneracies between lower and higher octants along with the standard ones, indicates that experiment is loosing its sensitivity in presence of sterile neutrino.

Next, we show the allowed parameter space in $\theta_{23} - \delta_{\rm CP}$ plane for each hierarchy-octant combination as given in Fig. 3.4. In order to obtain the allowed parameter space, we simulate the true event spectrum with oscillation parameters given in Table 3.1 and compare it with test event spectrum by varying test values of θ_{23}, $\delta_{\rm CP}$ in their allowed ranges and doing marginalization over $|\Delta m_{31}|^2$ for standard paradigm. In the $3+1$ case, we also do marginalization over new phases δ_{14} and δ_{34}. The solid blue (red) curve in the figure is for standard paradigm (3+1 case) for NOνA experiment, whereas the dashed curves are for the combined analysis of T2K and NOνA experiments. The plots in the left (right) panel correspond to lower (higher) octant. From the top panel of the figure, it can be seen that the allowed parameter space in the presence of sterile neutrino is enlarged which indicates

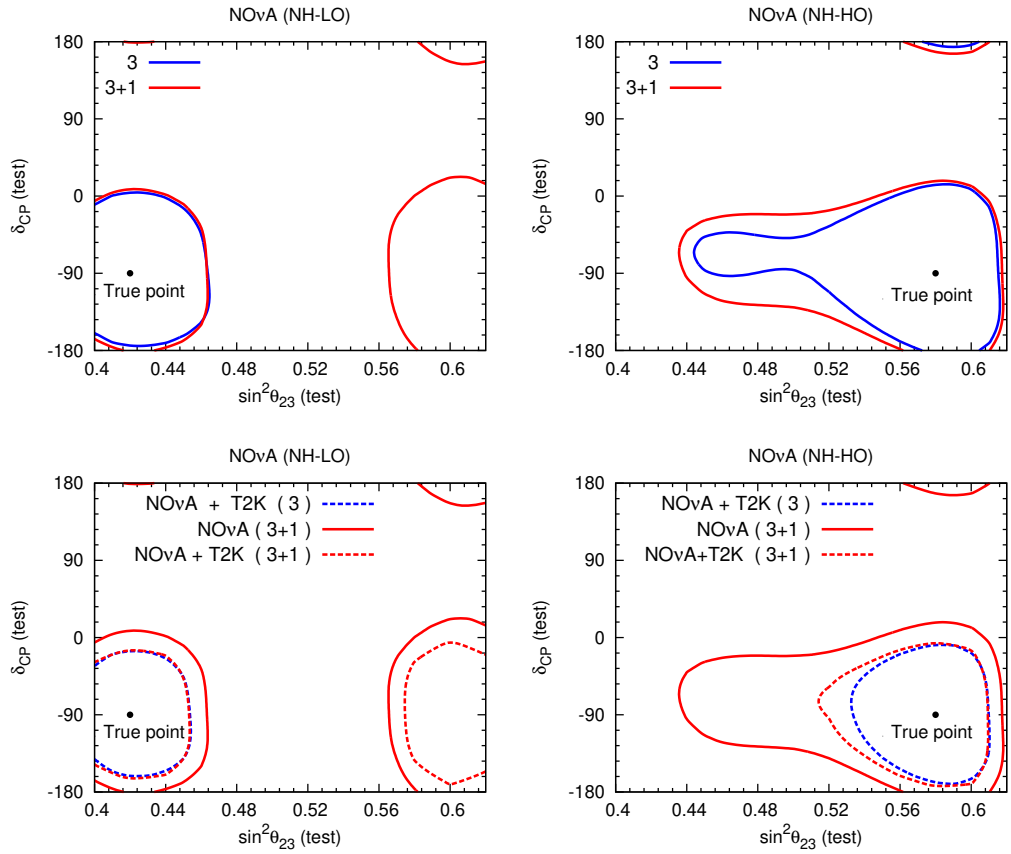

FIGURE 3.4: The allowed parameter space in $\theta_{23} - \delta_{\rm CP}$ plane for the long-baseline experiments T2K and NOνA. Oscillation parameter used for the analysis are given in Table 3.1. True value for the $\sin^2\theta_{23}$ for LO (HO) considered as 0.42 (0.58). The true point is shown as the black point in each plot.

that the degeneracy resolution capability is deteriorated significantly. However, the synergy of T2K and NOνA improves the degeneracy resolution capability.

3.5 Mass Hierarchy Sensitivity

In this section, we discuss how mass hierarchy sensitivity of NOνA experiment gets modified in presence of sterile neutrino. In order to obtain the MH sensitivity, we simulate the event spectrum by assuming true hierarchy as normal (inverted) and test hierarchy as inverted (normal). We obtain χ^2 by comparing true and test event spectra as discussed in Eqns.(3.8-3.9). While doing the calculation, we do marginalisation over $\delta_{\rm CP}$, θ_{23} and $|\Delta m^2_{31}|$ for standard paradigm, and in

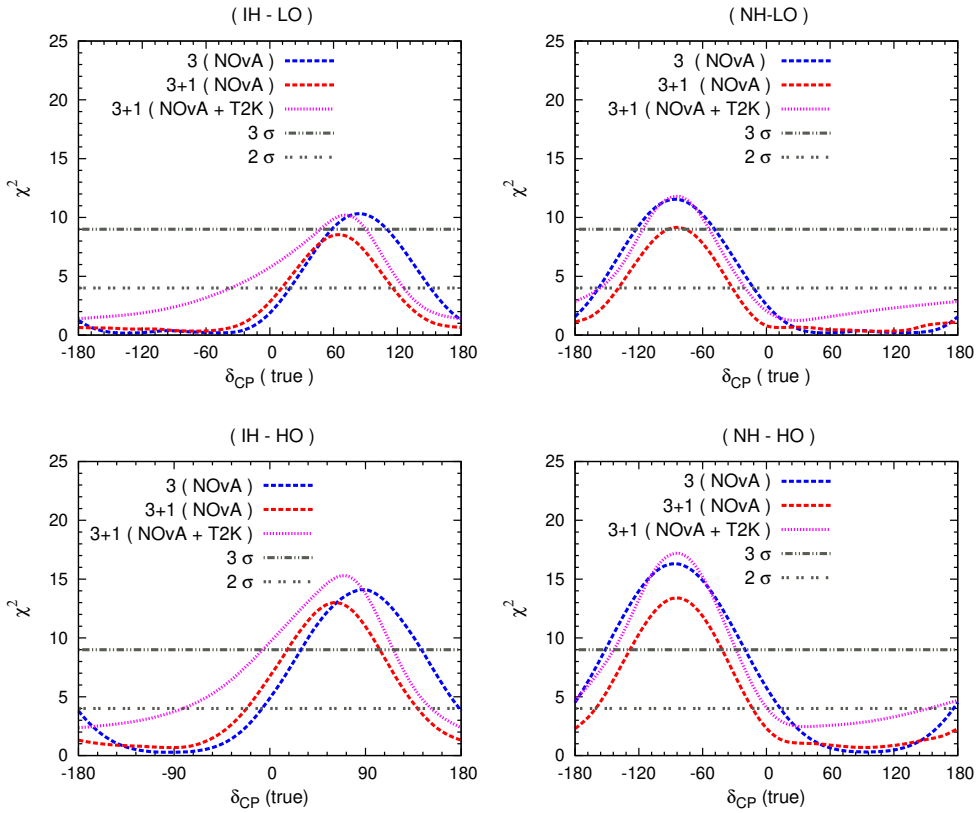

FIGURE 3.5: MH sensitivity as a function of true values of $\delta_{\rm CP}$. The left (right) panel is for inverted (normal) hierarchy and the upper (bottom) panel is for LO (HO).

addition to this, we also do marginalisation over δ_{14} and δ_{34} for (3+1) case, in their corresponding ranges as shown in Table 3.1. In Fig. 3.5, we present the hierarchy determination sensitivity of NOνA. The left (right) panel corresponds to inverted (normal) hierarchy as true hierarchy, while lower (upper) panel corresponds to lower (higher) octant. From the figure, one can see that the wrong mass hierarchy can be ruled out significantly above 2σ in the favourable regions, i.e., lower half-plane (upper half-plane) for NH (IH) in the standard paradigm as shown by dotted blue curves. Whereas, in presence of sterile neutrino the $\delta_{\rm CP}$ coverage for the mass hierarchy sensitivity is significantly reduced shown by dotted red curves. At the same time the combined analysis of T2K with NOνA shows a significant increase in MH sensitivity due to increase of $\delta_{\rm CP}$ coverage as shown in Fig. 3.5 by magenta curves.

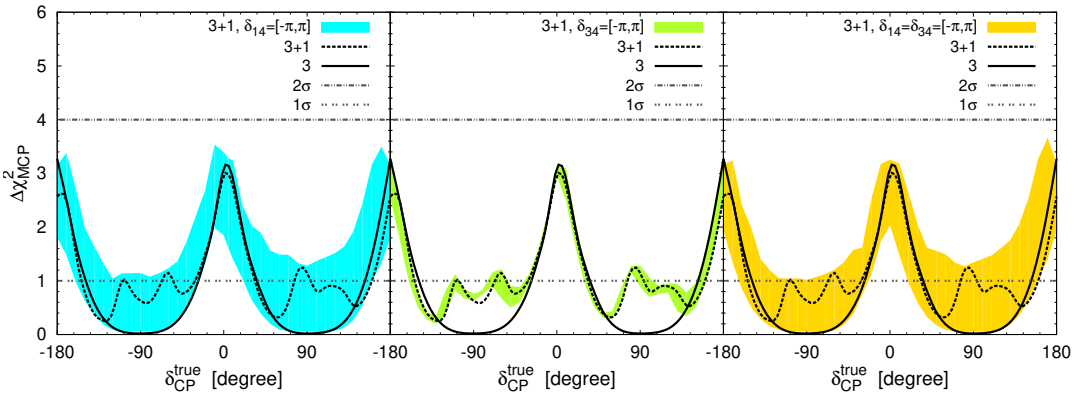

FIGURE 3.6: Maximal CP-violation exclusion sensitivity as a function of true value of $\delta_{\rm CP}$ for NOνA experiment. We assume the true hierarchy as NH and use the values of the oscillation parameters as given in Table 3.1.

3.6 Effect on maximal CP-violation exclusion sensitivity

One of the main objectives of long-baseline experiments is to look for non-zero CP-violation in leptonic sector. Further, the recent global-fit data provide us hint for maximal CP-violation with $\delta_{\rm CP} \approx -90^\circ$ [142]. Therefore, in this section, we check the compatibility of observed data with the maximal CP-violation hypothesis in presence of sterile neutrino. In order to quantify our analysis, we define the parameter,

$$\Delta\chi^2_{\rm MCP} = \min_{\delta^{\rm test}_{\rm CP}=\{90^\circ,-90^\circ\}} \left[\chi^2(\delta^{\rm test}_{\rm CP}) - \chi^2(\delta^{\rm true}_{\rm CP})\right]. \tag{3.10}$$

We show the sensitivities of excluding the maximal CP-violation ($\Delta\chi^2_{\rm MCP}$) for NOνA as a function of true values of $\delta_{\rm CP}$ for both standard 3 flavor and 3+1 flavor paradigms in Fig. 3.6. In each panel the black solid curve corresponds to the sensitivity in 3-neutrino scenario, while the black dashed curve is for 3+1 paradigm with the additional new phases $(\delta_{14}, \delta_{34})$ set to zero. In the left (middle) panel, we show the effect of additional phase δ_{14} (δ_{34}) in 3+1 scenario, whereas in the right panel, we show the effect of both phases. While doing the analysis, we use the true values of oscillation parameters as given in the Table I. For each true choice of $\delta_{\rm CP}$ ($=\delta_{13}$), we do marginalization over the phases: $\delta_{13}, \delta_{14}, \delta_{34}$, for 90° and -90°. In addition to this, we do marginalisation over the θ_{23} and Δm^2_{31}. Here, we assume the mass hierarchy to be normal. It can be seen from the figure that, for 3 flavor scenario the maximal CP violation hypothesis can be excluded

by $> 1\sigma$ CL. for values of $\delta_{\rm CP}$ near to the region of 0, $\pm\pi$ for NOνA experiment. The dashed black curve corresponds to the 3+1 scenario which is showing an oscillatory behaviour due to the additional mixing angles $(\theta_{14}, \theta_{24}, \theta_{34})$. From the figure, it should be noted that the CP-phase δ_{14} has large impact on the sensitivity compared to the δ_{34}.

3.7 Implications on Neutrinoless double beta decay

In this section, we would like to see the implication of the eV scale sterile neutrino on some low-energy phenomena, like neutrinoless double beta decay ($0\nu\beta\beta$). One of the important features of $0\nu\beta\beta$ process is that it violates the lepton number by two units and hence, its experimental observation would not only ascertain the Majorana nature of light neutrinos, but also can provide the absolute scale of lightest active neutrino mass. Various neutrinoless double beta decay experiments like KamLAND-Zen [24], GERDA [30], EXO-200 [31] etc., have provided bounds on the half-life ($\mathcal{T}_{1/2}$) of this process on various isotopes, which can be translated as a bound on effective Majorana mass parameter $|M_{ee}|$ [28, 29] as in Equation 1.70,

$$(\mathcal{T}_{1/2})^{-1} = Q \left| \frac{\mathcal{M}_\nu}{m_e} \right|^2 |M_{ee}|^2 \,, \tag{3.11}$$

where Q is the phase space factor, $\mathcal{M}_\nu$ is the nuclear matrix element (NME) and m_e is the electron mass. Recently $0\nu\beta\beta$ experiments involving ^{76}Ge, GERDA [30], ^{136}Xe EXO-200 [31] provided the upper limit on $|M_{ee}|$ as $\sim (0.2-0.4)$ eV, using the available results on nuclear matrix elements (NME) from literature. The current best upper limit on $|M_{ee}|$ has been reported by KamLAND-Zen Collaboration [24] as $|M_{ee}| < (0.061 - 0.165)$ eV at 90% CL. The next generation experiments are planning to probe towards $|M_{ee}| < (10^{-3} - 10^{-2})$ eV regime, and hopefully, they can cover the inverted mass hierarchy region of parameter space. The impact of an eV-scale sterile neutrino on neutrinoless double-beta decays is studied in [152] following the Bayesian statistical approach, where it has been shown that a null signal from the future $0\nu\beta\beta$ decay experiments with a sensitivity to $|M_{ee}| \approx \mathcal{O}(10^{-2})$ would be able to set stringent constraints on the mass of the sterile neutrino as well as the active-sterile mixing angle.

The effective Majorana mass, which is the key parameter of $0\nu\beta\beta$ decay process is defined in the standard three neutrino formalism as in Equation 1.71,

$$|M_{ee}| = \left| U_{e1}^2\, m_1 + U_{e2}^2\, m_2 e^{i\alpha} + U_{e3}^2\, m_3 e^{i\beta} \right| , \tag{3.12}$$

where U_{ei} are the PMNS matrix elements and α, β are the Majorana phases. In terms of the lightest neutrino mass m_l and the atmospheric and solar mass-squared differences, it can be expressed for NH and IH as

$$|M_{ee}|_{\rm NH} = \left| U_{e1}^2\, m_l + U_{e2}^2 \sqrt{\Delta m^2_{\rm sol} + m_l^2}\; e^{i\alpha} + U_{e3}^2 \sqrt{\Delta m^2_{\rm atm} + m_l^2}\, e^{i\beta} \right|, \tag{3.13}$$

and

$$|M_{ee}|_{\rm IH} = \left| U_{e1}^2 \sqrt{\Delta m^2_{\rm atm} - \Delta m^2_{\rm sol} + m_l^2} + U_{e2}^2 \sqrt{\Delta m^2_{\rm atm} + m_l^2}\; e^{i\alpha} + U_{e3}^2\, m_l\, e^{i\beta} \right|. \tag{3.14}$$

Analogously, one can obtain the expression for $|M_{ee}|$ in the presence of an additional sterile neutrino as

$$|M_{ee}| = \left| U_{e1}^2\, m_1 + U_{e2}^2\, m_2 e^{i\alpha} + U_{e3}^2\, m_3 e^{i\beta} + U_{e4}^2\, m_4 e^{i\gamma} \right|. \tag{3.15}$$

Now varying the PMNS matrix elements as well as the Dirac CP phase within their 3σ range [142] and the Majorana phases α, β and γ between $[0, 2\pi]$, we show the variation of $|M_{ee}|$ for three generation of neutrinos in the top panel of Fig. 3.7. Including the contributions from the eV scale sterile neutrino the corresponding plots are shown in the bottom panel, where the left panel is for NH and the right one for IH. In all these plots, the horizontal regions represent the bounds on effective Majorana mass from various $0\nu\beta\beta$ experiments, while the vertical shaded regions are disfavoured from Planck data on the sum of light neutrinos, where the current bound is $\Sigma_i m_i < 0.12$ eV from Planck+WP+highL+BAO data at 95% C.L. [153]. It should be noted that with the inclusion of an eV-scale sterile neutrino, part of the parameter space of $|M_{ee}|$ (for IH) is within the sensitivity reach of KamLAND-Zen experiment. Furthermore, there is also some overlap regions between NH and IH cases. Thus, the future $0\nu\beta\beta$ decay experiments may shed light on several issues related the nature of neutrinos.

Comment on sensitivity reach of future experiments:

Here, we present a brief discussion on the sensitivity of eV-scale sterile neutrino

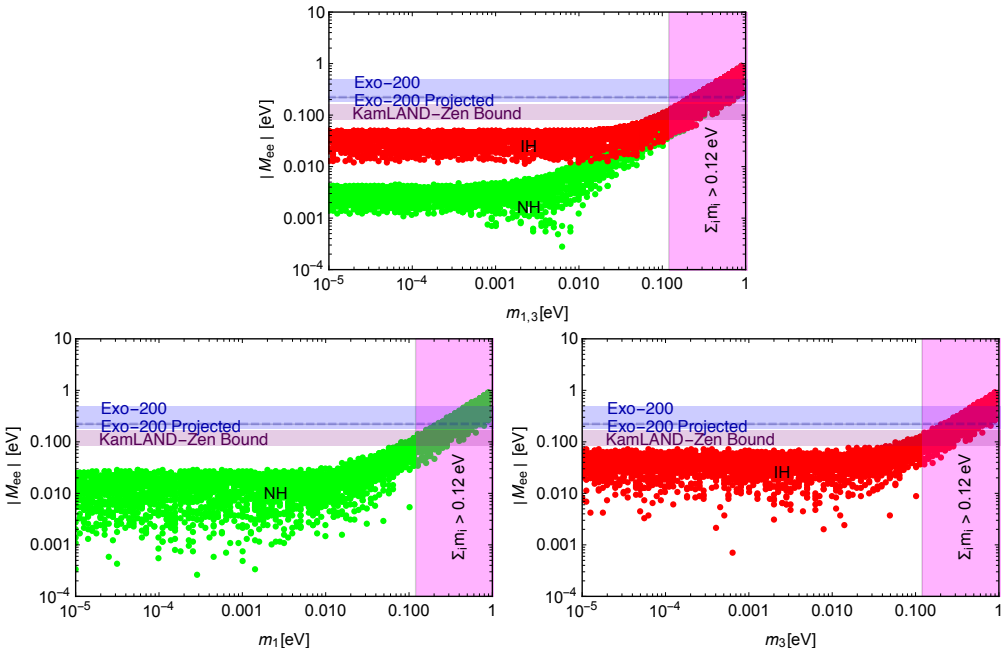

FIGURE 3.7: Variation of the effective Majorana mass parameter $|M_{ee}|$ with the lightest neutrino mass, where the top panel is for the standard three generation of neutrinos, whereas the bottom panels are due to the presence of an additional eV scale neutrino.

in the future ^{136}Xe experiment. The discovery sensitivity of an experiment is characterized by the value of half-life ($\mathcal{T}_{1/2}$) for which it has 50% probability of measuring a 3σ signal, above the background, defined as [154, 155]

$$\mathcal{T}_{1/2} = \frac{\ln 2 N_A \varepsilon}{m_a S_{3\sigma}(B)} , \tag{3.16}$$

where N_A is the Avogadro's number, m_a denotes the atomic mass of the Xe isotope, $B = \beta\varepsilon$ (β and ε stand for the background and exposure sensitivity), and $S_{3\sigma}$ signifies the value for which 50% of the measurements would give a signal above B, which can be calculated assuming a Poisson distribution

$$1 - CDF_{\text{Poisson}}(C_{3\sigma}|S_{3\sigma} + B) = 50\%. \tag{3.17}$$

Here $C_{3\sigma}$ indicates the number of counts for which $CDF_{\text{Poisson}}(C_{3\sigma}|B) = 3\sigma$ and the continuous Poisson distribution can be defined in terms of incomplete gamma

function as

$$CDF_{\text{Poisson}}(C|\mu) = \frac{\Gamma(C+1,\mu)}{\Gamma(C+1)} \ . \tag{3.18}$$

Thus, with Eqns. (3.16) and (3.18), we show in Fig. 3.8, the discovery sensitivity of $\mathcal{T}_{1/2}$ for ^{136}Xe as a function of ε for various values of β. The red band corresponds to a representative value of $|M_{ee}| = 10^{-2}$ eV in the presence of a sterile neutrino (expressed in terms of the half-life $\mathcal{T}_{1/2}$ using Eqn. 3.16), and varying the parameters in the PMNS matrix within their 3σ allowed ranges and also taking into account the uncertainty in the nuclear matrix element ($\mathcal{M}_\nu$). In Fig. 3.8, the dotted black line represents the future 3σ sensitivity of nEXO [156], which is $\mathcal{T}_{1/2} = 5.7 \times 10^{27}$ years. The black, blue, red, and magenta lines correspond to different values of the sensitive background levels of 0, $10^{-5}, 10^{-4}$ and 10^{-3} cts/(kg$_{\text{iso}}$yr), respectively. From the figure, we can see that for a sensitive background level of 10^{-4} cts/(kg$_{\text{iso}}$yr), the 10^{-2}eV region could be probed with a sensitive exposure of $\sim 10^4$ kg$_{\text{iso}}$yr.

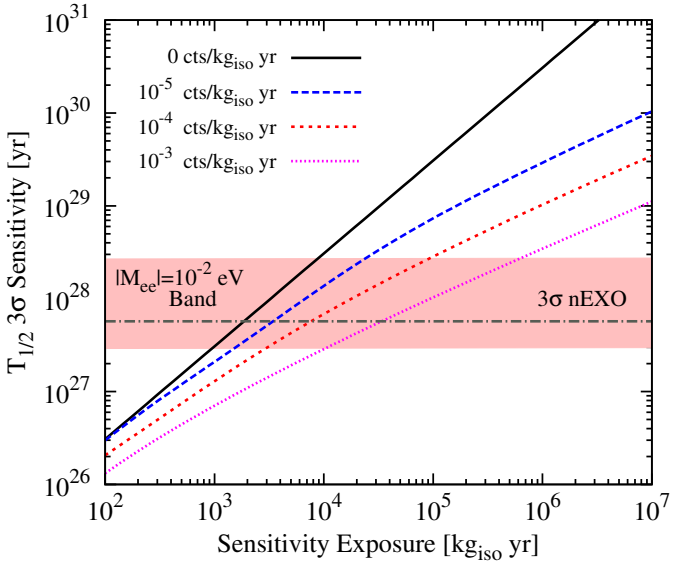

FIGURE 3.8: ^{136}Xe discovery sensitivity as a function of sensitivity exposure for a representative set of sensitive background levels. The black, blue, red and magenta lines correspond to the values of sensitive background levels of $0, 10^{-5}, 10^{-4}$ and 10^{-3} cts/(kg$_{\text{iso}}$yr), respectively.

3.8 Conclusion

The various short baseline anomalies hint towards existence of an eV scale sterile neutrino. If such neutrino exists, it can mix with active neutrinos and affect the sensitivities of long-baseline experiments. As one of the main objectives of currently running long-baseline experiments is to determine mass hierarchy of neutrinos, in this chapter, we discussed the effect of active-sterile mixing on the degeneracy resolution capability and MH sensitivity of NOνA experiment. We found that introduction of sterile neutrino gives rise to new kind of degeneracies among the oscillation parameters which results in reduction of $\delta_{\rm CP}$ coverage for MH sensitivity of NOνA experiment. We also found that the addition of T2K data helps in resolving the degeneracies among the oscillation parameters and for MH sensitivity analysis, results a significant increase in $\delta_{\rm CP}$ coverage for one additional sterile neutrino. We further scrutinized the compatibility of the observed data with the maximal CP-violation hypothesis in presence of sterile neutrino. We have also studied the effect sterile neutrino on neutrinoless double beta decay process and shown that the inclusion of an eV-scale sterile neutrino can enhance the value of the effective mass parameter $|M_{ee}|$, and for IH it could be within the sensitivity reach of KamLAND-Zen experiment. We also comment on the sensitivity reach of future ^{136}Xe experiments for exploring the presence of eV-scale sterile neutrino and found that for a sensitive background level of 10^{-4} cts/(kg$_{\rm iso}$yr), the 10^{-2}eV region of effective Majorana mass parameter ($|M_{ee}|$) could be probed with a sensitive exposure of $\sim 10^4$ kg$_{\rm iso}$yr.

Chapter 4

Study of CPT Violation with Hyper-Kamiokande and ESSnuSB

4.1 Introduction

Understanding the physics beyond Standard Model (BSM) is one of the prime objectives of present-day particle physics research. With the non-observation of any new heavy BSM particle through direct detection at LHC, the focus has been shifted to other frontiers, e.g., Intensity and Cosmic. In the Intensity frontier, neutrinos provide a promising avenue for revealing new physics. The compelling evidence of neutrino oscillations from various experiments already indicates that the minimal SM of particle physics is not exhaustive and requires modification. In general, SM is considered as a low-energy effective theory originating from the unified theory of Quantum Gravity at the Planck scale. Hence, understanding the true nature of the Planck scale physics through experimental signatures is of great importance, albeit extremely challenging to identify. It is expected that the long-baseline experiments will provide the ideal platform to look for tiny violations of Lorentz invariance or CPT symmetry that may exist as the low-energy remnants of Planck scale physics.

It is well-established that local relativistic quantum field theories, including the Standard Model, are invariant under Lorentz and CPT transformations. CPT theorem [157] states that "*Any quantum theory formulated on flat space time is symmetric under the combined action of CPT transformations, provided the theory respects (i) Locality (ii) Unitarity and (iii) Lorentz invariance*". One of the

phenomenological consequences of CPT symmetry is that particles and antiparticles will have the same masses and lifetimes. If any discrepancy is found either in their masses or lifetimes, it would be a clear sign of CPT violation. The results from numerous experiments are consistent with the predictions of this symmetry. Although no conclusive evidence of CPT violation has been observed so far, there are many reasons to perform a careful investigation of possible mechanisms and descriptions of Lorentz and CPT violations. One of the ambitious motivations is that the Lorentz and CPT violations might arise from a fundamental theory at the Planck scale, but nonetheless may leave their footprints in some low-energy observables which can be detected in the current or upcoming experiments of exceptional sensitivity.

Studies related to CPT violation are not new, see e.g., Refs. [87–89, 158–170]. There are several theories by which Quantum Gravity induced CPT violation can occur. Especially neutrinos, in addition to neutral kaons [171], make potential candidates to provide good insight into CPT violation, if it exists. For instance, some interesting aspects of Quantum gravity decoherence (non-local) in neutrinos introduce CPT violation and account for the smallness of neutrino mass [172].

There exist experimental limits on CPT violating parameters from kaon and the lepton sectors. However, the current neutrino oscillation data provides the most stringent constraints on various oscillation parameters [88]:

$$\begin{aligned} &|\Delta m^2_{21} - \Delta \overline{m}^2_{21}| < 4.7 \times 10^{-5}\ \text{eV}^2, \\ &|\Delta m^2_{31} - \Delta \overline{m}^2_{31}| < 2.5 \times 10^{-4}\ \text{eV}^2, \\ &|\sin^2\theta_{12} - \sin^2\overline{\theta}_{12}| < 0.14, \\ &|\sin^2\theta_{13} - \sin^2\overline{\theta}_{13}| < 0.029, \\ &|\sin^2\theta_{23} - \sin^2\overline{\theta}_{23}| < 0.19. \end{aligned} \tag{4.1}$$

Further, in Ref. [87] it has been shown that DUNE will test the CPT violation in atmospheric mass difference to an unprecedented level and provide the most stringent limit as $\left|\Delta m^2_{31} - \Delta \overline{m}^2_{31}\right| < 8.1 \times 10^{-5}\ \text{eV}^2$ at 3σ C.L.

Without delving into the specifications of any model, in this work we would like to test the predictions of CPT conservation in the light of future neutrino oscillation experiments Hyper-Kamiokande (T2HK and T2HKK), the European Spallation Source ν-Beam (ESSnuSB) project and Deep Underground Neutrino Experiment

(DUNE). Since neutrino oscillation experiments are only sensitive to mass-squared differences and mixing angles, one can test the CPT symmetry by measuring the differences in the oscillation parameters of neutrinos and antineutrinos. If the fundamental CPT invariance is not assumed, neutrinos and anti-neutrinos need to be parametrized by different 3×3 unitary mixing matrices. In the case of neutrinos, the flavor eigenstates $|\nu_\alpha\rangle$ and the mass eigenstates $|\nu_i\rangle$ are related by a 3×3 unitary leptonic mixing matrix [173],

$$|\nu_\alpha\rangle = \sum_{i=1}^{3} U_{\alpha i}(\theta_{12}, \theta_{13}, \theta_{23}, \delta_{CP})|\nu_i\rangle \ . \tag{4.2}$$

Analogously, the corresponding states for the antineutrinos are related as

$$|\overline{\nu}_\alpha\rangle = \sum_{i=1}^{3} U^*_{\alpha i}(\overline{\theta}_{12}, \overline{\theta}_{13}, \overline{\theta}_{23}, \overline{\delta}_{CP})|\overline{\nu}_i\rangle \ . \tag{4.3}$$

Denoting the neutrino and antineutrino masses by m_i and $\overline{m}_i$ $(i = 1, 2, 3)$, the mass-squared differences of neutrinos are represented as $\Delta m^2_{ij} \equiv m^2_i - m^2_j$ and that of anti-neutrinos as $\Delta\overline{m}^2_{ij} \equiv \overline{m}^2_i - \overline{m}^2_j$. Consequently the oscillation probabilities of neutrinos and antineutrinos are functions of the oscillation parameters $(\theta_{12}, \theta_{13}, \theta_{23}, \Delta m^2_{21}, \Delta m^2_{31}, \delta_{CP})$ and $(\overline{\theta}_{12}, \overline{\theta}_{13}, \overline{\theta}_{23}, \Delta\overline{m}^2_{21}, \Delta\overline{m}^2_{31}, \overline{\delta}_{CP})$, respectively. In principle, neutrino oscillation experiments will be able to place bounds on the predictions of CPT symmetry violation. In this work, we investigate the ability of the future long-baseline experiments: T2HK, T2HKK, ESSnuSB and DUNE to constrain the CPT violating parameters, such as $\left|\delta_{CP} - \overline{\delta}_{CP}\right|$, $|\Delta m^2_{31} - \Delta\overline{m}^2_{31}|$ and $\left|\sin^2\theta_{23} - \sin^2\overline{\theta}_{23}\right|$. We further, analyse neutrino and antineutrino data independently and constrain the oscillation parameters by considering the combination of the experiments DUNE+T2HKK and DUNE+ESSnuSB. In addition, assuming CPT symmetry is violated in nature, we study the individual ability of T2HK, T2HKK, DUNE and ESSnuSB experiments to establish CPT violation.

The outline of the chapter is as follows. In section 4.2, we give a brief overview of the experimental and simulation details of T2HK, T2HKK, ESSnuSB and DUNE. In section 4.3, we determine the bounds placed by these experiments on the parameters $\Delta(\delta_{CP})$, $\Delta(\Delta m^2_{31})$ and $\Delta(\sin^2\theta_{23})$ by assuming CPT symmetry exists in nature. Further, in section 4.3.1 we analyse the combined data of DUNE+T2HKK, DUNE+ESSnuSB and how well they can measure neutrino and antineutrino oscillation parameters independently. Additionally, in section 4.4 we assume that CPT

symmetry is violated in nature and estimate the sensitivity of T2HK, T2HKK, ESSnuSB and DUNE to establish CPT invariance violation individually. Finally, our results are summarized in section 4.5.

4.2 Experimental and Simulation Details

In this section, we discuss the detailed experimental features of the long-baseline experiments T2HK, T2HKK, ESSnuSB and DUNE.

T2HK: Tokai to Hyper Kamiokande (T2HK) is an up-gradation proposed to the existing T2K facility in Japan. In this plan, the JPARC beam will produce a 1.3 MW powered beam and the far detector (FD) will have two identical water Cherenkov detectors of 187 kt ($2 \times 187 = 374$ kt) fiducial volume to be placed at 295 km baseline, 2.5° off from the beam axis.

T2HKK: T2HKK is an alternative choice to T2HK, where the proposed FD is placed in Korea, which is 1100 km away from the JPARC facility. One of the two tanks (187 kt) proposed in the T2HK experiment will be placed at 1100 km with an off-axis angle (OAA) of 1.5° or 2° or 2.5°. Basing on the study in [174, 175], we consider the OAA 1.5° as it provides maximum sensitivity to the oscillation parameters. We consider the proposed run time ratio of $(1\nu : 3\bar{\nu})$ years corresponding to a total exposure of 27×10^{21} protons on target (POT). The detector systematics are taken as per the [174–176].

ESSnuSB: The major objective of the European Spallation Source ν-Beam (ESSnuSB) project [177] is to measure the leptonic CP violation. A neutrino beam with a peak energy of 0.25 GeV is produced at the ESS facility in Lund, Sweden. This beam is made to travel 540 km to encounter a water Cherenkov detector of 500 kt to be placed at a mine in Garpenberg. The proposed runtime is $(2\nu + 8\bar{\nu})$ years with a total POT of 27×10^{22} corresponding to a 5 MW proton beam.

DUNE: The Deep Underground Neutrino Experiment (DUNE) [178] comprises of a broad band neutrino beam of 0.5-8 GeV energy, a near detector (ND) at Fermilab and a liquid argon time projection chamber (LArTPC) of fiducial volume 40 kt located at 1300 km in South Dakota. We have considered $(5\nu + 5\bar{\nu})$ year run-time, beam power of 1.2 MW corresponding to 10×10^{21} POT.

We have performed the numerical analysis using the GLoBES package [146, 147]. The experimental specifications along with the signal and background normalisation errors, are listed in Table 4.1.

The statistical χ^2 is obtained using

$$\chi^2_{\text{stat}} = 2\sum_i \left\{ N_i^{\text{test}} - N_i^{\text{true}} + N_i^{\text{true}} \ln \frac{N_i^{\text{true}}}{N_i^{\text{test}}} \right\}, \tag{4.4}$$

where N_i^{test} corresponds to the number of events predicted by the model while N_i^{true} denotes the total number of simulated events (signal and background) in i^{th} bin. Details can be found in Appendix A. The systematic uncertainties are incorporated into the simulation using the Pull method. The pull variables being the signal and background normalisation uncertainties of ν_e, $\bar{\nu}_e$ appearance and ν_μ, $\bar{\nu}_\mu$ disappearance channels. The values of the normalisation errors on signals and backgrounds (bkg) corresponding to different channels of the experiments are listed in Table 4.1. Here, χ^2_{pull} accounts for these errors and acts as a penalty term to the total χ^2 (χ^2_{tot}).

Experiment	T2HK	T2HKK	ESSnuSB	DUNE
Baseline	295 km	295 km; 1100 km	540 km	1300 km
Fiducial Volume	374 kt	187 kt (@ 295 km) + 187 kt (@ 1100 km)	500 kt	40 kt
Normalisation Uncertainty				
ν_e signal (bkg)	3.2% (5%)	3.8% (5%)	3.2% (5%)	2% (5%)
$\bar{\nu}_e$ signal (bkg)	3.9% (5%)	4.1% (5%)	3.9% (5%)	2% (5%)
ν_μ signal (bkg)	3.6% (5%)	3.8% (5%)	3.6% (5%)	5% (5%)
$\bar{\nu}_\mu$ signal (bkg)	3.6% (5%)	3.8% (5%)	3.6% (5%)	5% (5%)

TABLE 4.1: The experimental specifications and systematic uncertainties of T2HK, T2HKK, ESSnuSB and DUNE.

Parameters	True values	Test value Range
$\sin^2\theta_{12}$	0.304	NA
$\sin^2\theta_{13}$	0.02221	$0.02034 \rightarrow 0.02430$
$\sin^2\theta_{23}$	0.57	$0.4 \rightarrow 0.62$
δ_{CP}	195°	$0^\circ \rightarrow 360^\circ$
Δm^2_{12}	7.42×10^{-5} eV^2	NA
Δm^2_{31}	2.514×10^{-3} eV^2 (NH)	$(2.431 \rightarrow 2.598) \times 10^{-3}$ eV^2

TABLE 4.2: The values of oscillation parameters that we considered in our analysis are taken from Ref. [35].

4.3 Sensitivity of the experiments T2HK, T2HKK, ESSnuSB to CPT violation

In this section, we calculate the CPT violation sensitivity of the long-baseline experiments T2HK, T2HKK, ESSnuSB and DUNE. At first, we assume that there is no intrinsic CPT violation in nature i.e., both neutrino and antineutrino parameters are equal. That is for a given oscillation parameter, we simulate the data for each of these experiments with $\Delta x = |x - \bar{x}| = 0$, where x ($\bar{x}$) is the oscillation parameter for neutrinos (antineutrinos). Then we evaluate the sensitivity of each of the experiments to non-zero Δx. The true values for oscillation parameters used are given in Table 4.2. In each case, we choose three values for θ_{23}: lower octant ($\sin^2\theta_{23} = 0.43$), maximal ($\sin^2\theta_{23} = 0.5$) and higher octant ($\sin^2\theta_{23} = 0.57$) to study the correlation between the CPT sensitivity and the octant of θ_{23}. In the test values, we marginalize over all the oscillation parameters for both neutrinos and antineutrinos except x, $\bar{x}$ and the solar parameters (since T2HK, T2HKK, ESSnuSB and DUNE have no sensitivity to these parameters). After marginalization, we calculate the χ^2 value for the CPT violating observable through the relation

$$\chi^2(\Delta x) = \chi^2(|x - \bar{x}|) = \chi^2(x) + \chi^2(\bar{x}) \ , \tag{4.5}$$

and the minimum $\chi^2(\Delta x)$ has been calculated over all possible combinations of $|x - \bar{x}|$.

In Figs. 4.1, 4.2 and 4.3, we show the CPT violation sensitivity of these experiments to oscillation parameters $\Delta(\Delta m^2_{31}) \equiv \Delta m^2_{31} - \Delta\overline{m}^2_{31}$, $\Delta(\sin^2\theta_{23}) \equiv \sin^2\theta_{23} - \sin^2\overline{\theta}_{23}$ and $\Delta(\delta_{CP}) \equiv \delta_{CP} - \bar{\delta}_{CP}$, respectively. The results in left, middle and right

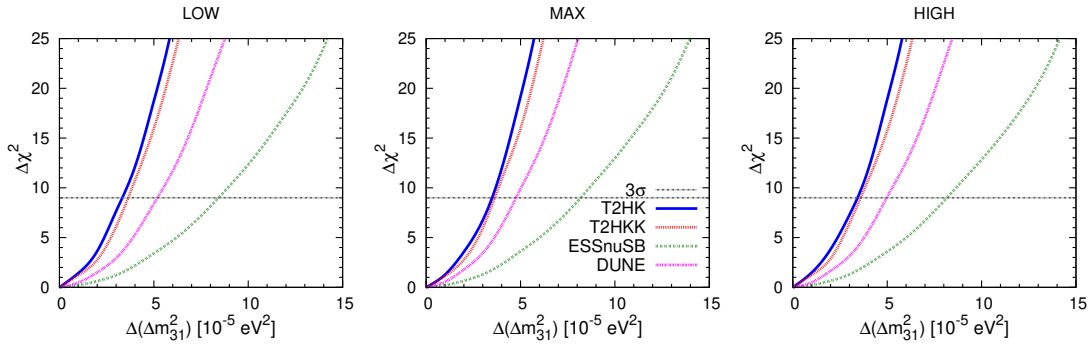

FIGURE 4.1: The sensitivity of the experiments T2HK (blue curve), T2HKK (red curve), ESSnuSB (green curve) and DUNE (magenta curve) to $\Delta(\Delta m^2_{31})$.

columns of these figures are obtained by assuming the octant of θ_{23} as low, maximal and high, respectively. The coloured curves blue, red, green and magenta show the sensitivities of T2HK, T2HKK, ESSnuSB and DUNE, respectively. The black dash-dot line represents 3σ confidence limit. The sensitivity for $\Delta(\sin^2\theta_{13})$ is not very significant, for which we have not shown the corresponding result here.

From Fig. 4.1, one can estimate the best bound on the parameter $\Delta(\Delta m^2_{31})$ at 3σ C.L. by T2HK experiment (blue curve) as $\Delta(\Delta m^2_{31}) < 3.32 \times 10^{-5}$ eV^2. It can be seen from all the columns of Fig. 4.1 that T2HK provides a better bound compared to T2HKK, ESSnuSB and DUNE, for all the three values of θ_{23} considered. The alternative choice of the Hyper-Kamiokande experiment, i.e., T2HKK (red curve) provides better bound on $\Delta(\Delta m^2_{31}) < 3.62 \times 10^{-5}$ eV^2 at 3σ C.L. than the bound from DUNE (magenta curve) experiment obtained in Ref.[87] and ESSnuSB. The list of the bounds at 3σ C.L. on $\Delta(\Delta m^2_{31})$ for $\theta_{23} < 45°$, $\theta_{23} = 45°$ and $\theta_{23} > 45°$ are given in the first column of Table-4.3. Here it is important to note that these experiments will highly improve upon the existing bounds posed by neutral kaon system.

It can be noted from the three plots of Fig. 4.2 that different sensitivities to $\Delta(\sin^2\theta_{23})$ are obtained for different true values of θ_{23}. Firstly, when the true value of θ_{23} is in higher and lower octants, degenerate solutions are obtained for $\Delta(\sin^2\theta_{23})$ at 3σ C.L. in the complementary octant for all the four experiments. However, for lower octant of θ_{23}, this degeneracy doesn't exist in the case of T2HKK (red) and DUNE (magenta) at 2σ C.L.. For true maximal θ_{23}, the sensitivity of the experiments increase with the increasing values of $\Delta(\sin^2\theta_{23})$.

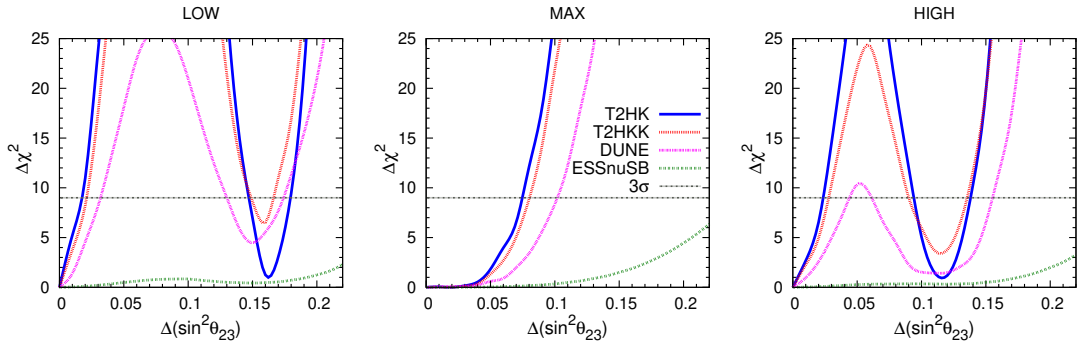

FIGURE 4.2: The sensitivity of the experiments T2HK (blue curve), T2HKK (red curve), ESSnuSB (green curve) and DUNE (magenta curve) to $\Delta(\sin^2\theta_{23})$.

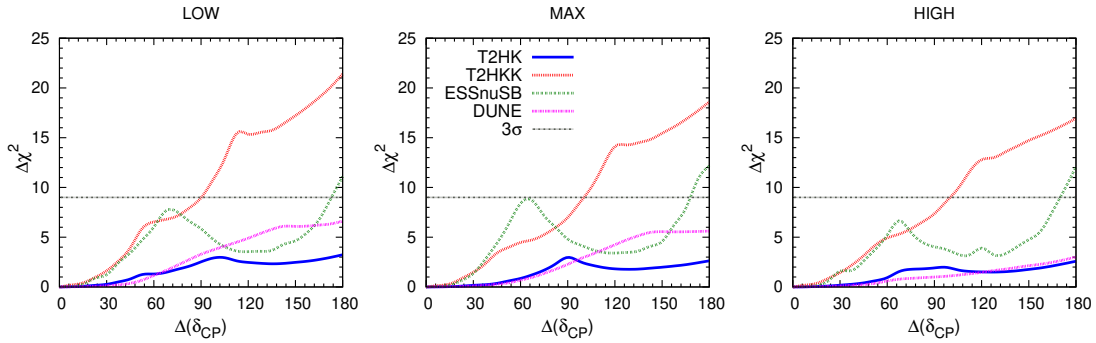

FIGURE 4.3: The sensitivity of the experiments T2HK (blue curve), T2HKK (red curve), ESSnuSB (green curve) and DUNE (magenta curve) to $\Delta(\delta_{CP})$.

Furthermore, ESSnuSB provides comparatively very low CPT violation sensitivity to $\Delta(\sin^2\theta_{23})$ for all values of true θ_{23}. The list of the bounds at 3σ C.L. on $\Delta(\sin^2\theta_{23})$ are given in second column of Table-4.3.

From Fig. 4.3, the best ever bounds on $\Delta(\delta_{CP})$ can be extracted from T2HKK (red curve) for CPT violation which is $\Delta(\delta_{CP}) < 100^0$ at 3σ confidence level. The next best bound on $\Delta(\delta_{CP})$ is obtained by ESSnuSB experiments. This is because both T2HKK and ESSnuSB experiments are planned at the second oscillation maxima to meet their primary goal of measuring the CP phase δ_{CP}. The list of the bounds at 3σ C.L. on $\Delta(\delta_{CP})$ are given in the third column of Table-4.3.

Bounds on CPT Violating Parameters			
Experiment	$\Delta(\Delta m^2_{31})$ [10^{-5} eV^2]	$\Delta(\sin^2\theta_{23})$	$\Delta(\delta_{CP})$
T2HK	[3.32, 3.45, 3.4]	[0.180, 0.075, 0.139]	–
T2HKK	[3.62, 3.62, 3.59]	[0.167, 0.08, 0.135]	[90, 100, 100]°
ESSnuSB	[8.43, 8.18, 8.14]	–	[173, 168, 170]°
DUNE	[5.2, 4.77, 4.96]	[0.173, 0.102, 0.155]	–

TABLE 4.3: Bounds on the CPT violating parameters at 3σ C.L. from T2HK, T2HKK, ESSnuSB and DUNE experiments. The set of three values in the brackets correspond to the results for θ_{23} value as $\theta_{23} < 45°$, $\theta_{23} = 45°$ and $\theta_{23} > 45°$.

4.3.1 Constraining CPT violation with combination of DUNE+T2HKK and DUNE+ESSnuSB

In this subsection, we continue to assume that CPT is a conserved symmetry in nature. We analyse the neutrino and antineutrino data independently and determine whether the corresponding oscillation parameters in both cases are the same as predicted by CPT symmetry. The true oscillation parameters are considered in the analysis are provided in Table-4.2 and for the test scenario, we take the six oscillation parameters for both neutrino (Δm^2_{31}, θ_{23} ,δ_{CP}) and antineutrino ($\Delta\overline{m}^2_{31}$, $\overline{\theta}_{23}$, $\overline{\delta}_{CP}$) in their allowed ranges as given in Table 4.2. Marginalisation is done over the remaining four parameters while showing the effect of the rest two oscillation parameters. The results are shown in Fig. 4.4, where the axes can be visualised for both neutrino and antineutrino parameters. It is shown in Ref. [179] that, while DUNE and T2HK can resolve the octant degeneracy assuming CPT conservation, the combination of DUNE+T2HK cannot resolve this degeneracy while treating neutrino and antineutrino parameters individually. In this subsection, we explore the same by considering the combination of DUNE+T2HKK and DUNE+ESSnuSB experiments. The blue and red contours in all the plots in Fig. 4.4 represent the allowed contours with 99% C.L. for neutrino and antineutrino data, respectively. The left (right) panel shows the allowed regions of the neutrino and antineutrino oscillation parameters of DUNE+T2HKK (DUNE+ESSnuSB) experiments. From all the left panel plots, it can be seen that DUNE+T2HKK

resolve octant degeneracy in θ_{23}, and $\bar{\theta}_{23}$ at 99% C.L. when CPT conservation is assumed in nature. Besides, when we combined the simulated data from the antineutrino beams of DUNE and ESSnuSB (red curves of right side panel) degenerate solutions to δ_{CP} and θ_{23} are obtained. However, this degeneracy disappears when we considered the neutrino beams of DUNE and ESSnuSB. Overall, from all the plots of Fig. 4.4, we can observe that neutrino oscillation data constrains the parameters better than the antineutrino data.

4.4 Discovering CPT violation

In this section, we assume that CPT is violated in nature. We generate the simulated data for the experiments T2HK, T2HKK, ESSnuSB and DUNE by assuming different neutrino and antineutrino oscillation parameters. In particular, we only consider the case where the CP-violating phases δ_{CP} and $\bar{\delta}_{CP}$ are not equal[1]. We further consider $\theta_{23} = \overline{\theta}_{23}$, $\Delta m^2_{31} = \Delta\overline{m}^2_{31}$, $\theta_{13} = \overline{\theta}_{13}$ and their true values are taken from Table-4.2. In Fig. 4.5, we plot the allowed regions of δ_{CP}(test) and $\bar{\delta}_{CP}$(test) as obtained from the experiments T2HK (blue), T2HKK (red), ESSnuSB (green) and DUNE (magenta). The solid and dotted contours in all the figures correspond to 68% and 99% C.L. and the dashed black lines correspond to CPT conserving values. Top panel of Figure 4.5 shows that both the configurations of Hyper-Kamiokande experiment - T2HK (blue) and T2HKK (red) will be able to establish CPT violation with 99% C.L. by showing that $\delta_{CP} \neq \bar{\delta}_{CP}$ in their proposed run-time. This can be inferred from the fact that there are no degenerate solutions obtained in the figure. However, T2HKK provides tighter constraints on the parameter space of δ_{CP}-$\bar{\delta}_{CP}$, compared with T2HK, as seen from the red and blue contours of the top panel. This can be attributed to the higher sensitivity of T2HKK experiment to the CP violating phase δ_{CP} as its far detector (Korea) is going to be placed at second oscillation maxima ($\nu_\mu \rightarrow \nu_e$ channel) unlike in the case of T2HK experiment which focuses on first oscillation maxima. The bottom panel of Fig. 4.5 shows that ESSnuSB and DUNE can establish CPT violation with 99% C.L. on their own. Additionally, since ESSnuSB experiment has higher sensitivity to CP phase when compared to DUNE, it can be seen that the green contours (ESSnuSB) in the bottom left panel are tighter than the magenta contours (DUNE) of the bottom right panel. In conclusion, if nature has

[1]We consider the variation in δ_{CP} and $\bar{\delta}_{CP}$ as these parameters are poorly constrained.

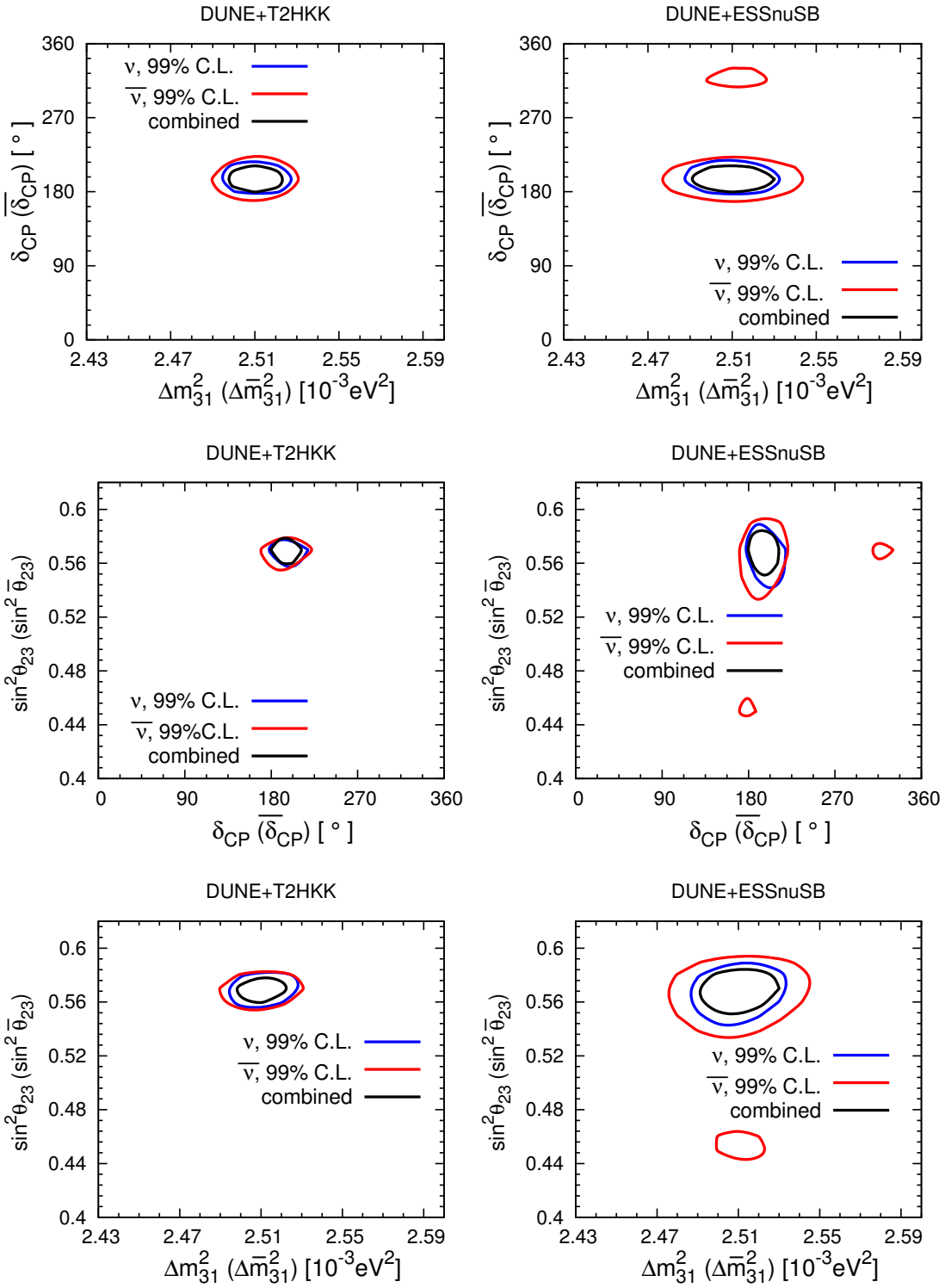

FIGURE 4.4: Allowed parameter space between different neutrino and antineutrino oscillation parameters at 99% C.L. for combination of DUNE and T2HKK as well as DUNE and ESSnuSB experiments. In each plot, the blue (red) curve is for neutrino (antineutrino) parameters and the black curve is the combined result of neutrino and antineutrino parameters.

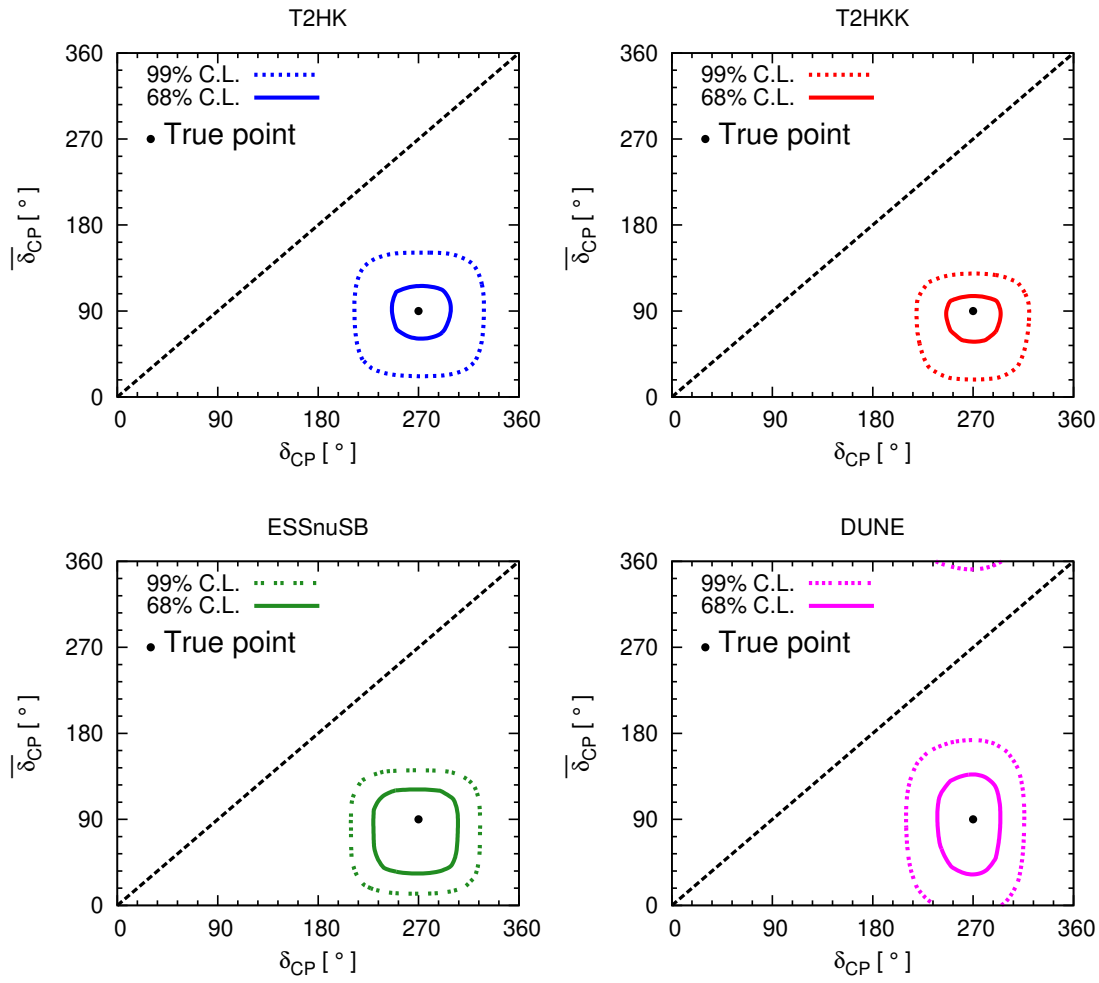

FIGURE 4.5: Allowed regions between δ_{CP} and $\overline{\delta}_{CP}$ in the CPT violating scenario. Solid (Dotted) curve shows the parameter space at 68% and 99% C.L..

CPT violation, then the forthcoming experiments Hyper-K, ESSnuSB and DUNE will be able to establish CPT violation individually in their proposed run-times.

4.5 Summary

CPT symmetry is one of the fundamental symmetries of nature and its breaking is related to Planck scale physics. However, CPT violation has not been observed unambiguously so far, and it is an exciting challenge to search for its implications. It is expected that some of the CPT violating observables might be observed at low-energy scales. So far, the most stringent bound on CPT violation comes from the neutral kaon sector. Remarkably, the current evidence for neutrino oscillations

lies at levels where Planck-suppressed effects might be expected to appear. Hence, the neutrino sector can provide a better opportunity to explore CPT violation.

In this paper, we have studied the sensitivity reach of the upcoming long-baseline experiments, T2HK, T2HKK, ESSnuSB and DUNE to explore the CPT violation in the neutrino sector. Our findings are summarized below:

• We obtained the sensitivity limits on the CPT violating parameters $\Delta(\Delta m^2_{31})$, $\Delta(\sin^2\theta_{23})$ and $\Delta(\delta_{CP})$. We found that the T2HKK and ESSnuSB experiments are quite sensitive to the CP violating phase δ_{CP}, whereas T2HK, T2HKK and DUNE are sensitive to the atmospheric mixing parameters. The most stringent limits on $\Delta(\Delta m^2_{31})$ and $\Delta(\sin^2\theta_{23})$ come from T2HK experiment whereas T2HKK will provide the best bound on $\Delta(\delta_{CP})$.

• Next, we obtained the constraint on CPT violation with the combination DUNE+T2HKK and DUNE+ESSnuSB experiments. Assuming that nature is invariant under CPT, we analysed the neutrino and antineutrino data independently for these combinations of experiments and scrutinized whether they provide the same oscillation parameters as predicted by CPT symmetry. We found that these experiments are sensitive to CPT violation and DUNE+T2HKK can even resolve the octant degeneracy in θ_{23} and $\bar{\theta}_{23}$ at 99% C.L..

• Finally, we have shown that if CPT violation exists in nature, the upcoming long-baseline experiments T2HK, T2HKK, ESSnuSB and DUNE will be able to establish CPT violation individually at 99% C.L. in their proposed run-times by demonstrating $\delta_{CP} \neq \bar{\delta}_{CP}$.

In conclusion, we found that the upcoming experiments T2HK, T2HKK, ESSnuSB and DUNE have great potential to establish CPT violation in neutrino oscillation and provide stringent limits on the CPT violating parameters $\Delta(\Delta m^2_{31})$ and $\Delta(\sin^2\theta_{23})$.

Chapter 5

Exploring the effect of Lorentz invariance violation with the currently running long-baseline experiments

5.1 Introduction

Neutrino oscillation, bestows the first experimental evidence of physics beyond the SM. Without the loss of generality, SM is considered as a low-energy effective theory, emanating from a fundamental unified picture of gravity and quantum physics at the Planck scale. To understand the nature of the Plank scale physics through experimental signatures is therefore of great importance, though extremely challenging to identify. Lorentz symmetry violation constitutes one of such signals, basically associated with tiny deviation from relativity. In recent times, the search for Lorentz violating and related CPT violating signals have been explored over a wide range of systems and at remarkable sensitivities [159, 180–190]. One of the phenomenological consequences of CPT invariance is that a particle and its anti-particle will have exactly the same mass and lifetime and if any difference observed either in their mass or lifetime, would be a clear hint for CPT violation. There exists stringent experimental bounds on Lorentz and CPT violating parameters from kaon and the lepton sectors. For the kaon system, the observed mass difference provides the upper limit on CPT violation as $\left|m_{K^0} - m_{\overline{K^0}}\right|/m_K < 6 \times 10^{-18}$ [191],

which is quite stringent. However, parametrizing in terms of m_K^2 rather than m_K, as kaon is a boson and the natural mass parameter appears in the Lagrangian is the squared mass, the kaon constraint turns out to be $\left|m_{K^0}^2 - m_{\overline{K^0}}^2\right| < 0.25$ eV^2, which is comparable to the bounds obtained from neutrino sector, though relatively weak. Furthermore, neutrinos are fundamental particles, unlike the kaons hence, the neutrino system can be regarded as a better probe to search for CPT violation. For example, the current neutrino oscillation data provides the most stringent bounds: $\left|\Delta m_{21}^2 - \Delta\overline{m}_{21}^2\right| < 5.9 \times 10^{-5}$ eV^2 and $\left|\Delta m_{31}^2 - \Delta\overline{m}_{31}^2\right| < 1.1 \times 10^{-3}$ eV^2 [192]. Recently, MINOS experiment [79] has also provided the bound on the atmospheric mass splitting for the neutrino and antineutrino modes at 3σ C.L. as $|\Delta m_{31}^2 - \Delta\bar{m}_{31}^2| < 0.8 \times 10^{-3}$ eV^2. If these differences are due to the interplay of some kind of CPT violating new physics effects, they would influence the oscillation phenomena for neutrinos and antineutrinos as well as have other phenomenological consequences, such as neutrino-antineutrino oscillation, baryogenesis [193] etc.

It is well known that the local relativistic quantum field theories are based on three main ingredients: Lorentz invariance, locality and hermiticity. The CPT violation is intimately related to Lorentz violation, as possible CPT violation can arise from Lorentz violation, non-locality, non-commutative geometry etc. So if CPT violation exists in nature and is related to quantum gravity, which is supposedly non-local and expected to be highly suppressed, long-baseline experiments have the capability to probe such effects. Here, we present a brief illustration about, how the violation of Lorentz symmetry can affect the neutrino propagation. In general, Lorentz symmetry breaking and quantum gravity are interrelated, which requires the existence of an universal length scale for all frames. However, such universal scale is in conflict with general relativity, as length contraction is one of the consequences of Lorentz transformation. Such contradiction can be avoided by the modification of Lorentz transformations (or in other words modifying dispersion relations). The effects of perturbative Lorentz and CPT violation on neutrino oscillations has been studied in [89]. Moreover, it has been shown explicitly in Ref. [194], how the oscillation probability gets affected by the modified dispersion relation, however, for the sake of completeness we will present a brief discussion about it. The modified energy-momentum relation for the neutrinos can be expressed as

$$E_i^2 = p_i^2 + \frac{1}{2}m_i^2\left(1 + e^{2A_iE_i/m_i^2}\right), \tag{5.1}$$

where m_i, E_i and p_i are the mass, energy and momentum of the ith neutrino in the

mass basis, and A_i is the dimensionful and Lorentz symmetry breaking parameter. Assuming that all the neutrinos have the same energy (E), the probability of transition from a given flavour α to another flavour β for two neutrino case is given as

$$P(\nu_\alpha \to \nu_\beta) = 1 - \sin^2 2\theta \sin^2 \left(\frac{\Delta p L}{2}\right) , \tag{5.2}$$

where θ represents the mixing angle and

$$\Delta p \approx \frac{\Delta m^2}{2E} + \frac{1}{2}(A_i - A_j), \tag{5.3}$$

with $\Delta m^2 = m_i^2 - m_j^2$. Hence, the neutrino oscillation experiments might provide the opportunity to test this kind of new physics. The limits on Lorentz and CPT violating parameters from MINOS experiment are presented in [195]. The possible effect of Lorentz violation in neutrino oscillation phenomena has been intensely investigated in recent years [87, 89, 162, 183, 194, 196–213].

In this chapter, we are interested to study the phenomenological consequences introduced in the neutrino sector due to the presence of Lorentz invariance violation terms. In particular, we investigate the impact of such new contributions on the neutrino oscillation probabilities for NOνA experiment. Further, we obtain the sensitivity limits on the LIV parameters from the currently running long-baseline experiments T2K and NOνA. We also investigate the implications of LIV effects on the determination of mass ordering as well as the CP violation discovery potential of NOνA experiment.

5.2 Theoretical Framework

The Lorentz invariance violation effect can be introduced as a small perturbation to the standard physics descriptions of neutrino oscillations. Thus, the effective Lagrangian that describes Lorentz violating neutrinos and anti-neutrinos [159, 163] is given as

$$\mathcal{L} = \frac{1}{2}\bar{\Psi}_A(i\gamma^\mu \partial_\mu \delta_{AB} - M_{AB} + \hat{\mathcal{Q}}_{AB})\Psi_B + \text{h.c.} , \tag{5.4}$$

where $\Psi_{A(B)}$ is a $2N$ dimensional spinor containing the spinor field $\psi_{\alpha(\beta)}$ with $\alpha(\beta)$ ranges over N spinor flavours and their charge conjugates $\psi^C_{\alpha(\beta)} = C\bar{\psi}^T_{\alpha(\beta)}$, expressed as $\Psi_{A(B)} = (\psi_{\alpha(\beta)}, \psi^C_{\alpha(\beta)})^T$ and the Lorentz violating operator is characterized by $\hat{\mathcal{Q}}$. Restricting ourselves to only a renormalizable theory (incorporating terms with mass dimension $\leq$4), one can symbolically write the Lagrangian density for neutrinos as [163]

$$\mathcal{L}_{\rm LIV} = -\frac{1}{2}\left[p^{\mu}_{\alpha\beta}\bar{\psi}_{\alpha}\gamma_{\mu}\psi_{\beta} + q^{\mu}_{\alpha\beta}\bar{\psi}_{\alpha}\gamma_5\gamma_{\mu}\psi_{\beta} - ir^{\mu\nu}_{\alpha\beta}\bar{\psi}_{\alpha}\gamma_{\mu}\partial_{\nu}\psi_{\beta} - is^{\mu\nu}_{\alpha\beta}\bar{\psi}_{\alpha}\gamma_5\gamma_{\mu}\partial_{\nu}\psi_{\beta}\right] + \text{h.c.}\,, \tag{5.5}$$

where $p^{\mu}_{\alpha\beta}$, $q^{\mu}_{\alpha\beta}$, $r^{\mu\nu}_{\alpha\beta}$ and $s^{\mu\nu}_{\alpha\beta}$ are the Lorentz violating parameters, in the flavor basis. More about the LIV parameters can be found in Appendix B. Since, only left-handed neutrinos are present in the SM, the observable effects which can be explored in the neutrino oscillation experiments can be parametrized as

$$(a_L)^{\mu}_{\alpha\beta} = (p+q)^{\mu}_{\alpha\beta}\,, \qquad (c_L)^{\mu\nu}_{\alpha\beta} = (r+s)^{\mu\nu}_{\alpha\beta}\,. \tag{5.6}$$

These parameters are hermitian matrices in the flavour space and can affect the standard vacuum Hamiltonian. The parameter $(a_L)^{\mu}_{\alpha\beta}$ is related to CPT violating neutrinos and $(c_L)^{\mu\nu}_{\alpha\beta}$ is associated with CPT-even, Lorentz violating neutrinos. Here, we consider the isotropic model (direction-independent) for simplicity, which appears when only the time-components of the coefficients are non-zero i.e., terms with $\mu = \nu = 0$ [159]. The sun-centred isotropic model is a popular choice and in this frame, the Lorentz-violating isotropic terms are considered as $(a)^0_{\alpha\beta}$ and $(c)^{00}_{\alpha\beta}$. Here onwards we change the notation $(a_L)^0_{\alpha\beta}$ to $a_{\alpha\beta}$ and $(c_L)^{00}_{\alpha\beta}$ to $c_{\alpha\beta}$ for convenience. Taking into account only these isotropic terms of Lorentz violation parameters, the Hamiltonian for neutrinos, including LIV contributions becomes

$$H = H_{\rm vac} + H_{\rm mat} + H_{\rm LIV}\,, \tag{5.7}$$

where $H_{\rm vac}$ and $H_{\rm mat}$ correspond to the Hamiltonians in vacuum and in the presence of matter effects and $H_{\rm LIV}$ refers to the LIV Hamiltonian. These are expressed

as

$$H_{\rm vac} = \frac{1}{2E} U \begin{pmatrix} m_1^2 & 0 & 0 \\ 0 & m_2^2 & 0 \\ 0 & 0 & m_3^2 \end{pmatrix} U^\dagger, \qquad H_{\rm mat} = \sqrt{2} G_F N_e \begin{pmatrix} 1 & 0 & 0 \\ 0 & 0 & 0 \\ 0 & 0 & 0 \end{pmatrix}, \tag{5.8}$$

$$H_{\rm LIV} = \begin{pmatrix} a_{ee} & a_{e\mu} & a_{e\tau} \\ a_{e\mu}^* & a_{\mu\mu} & a_{\mu\tau} \\ a_{e\tau}^* & a_{\mu\tau}^* & a_{\tau\tau} \end{pmatrix} - \frac{4}{3} E \begin{pmatrix} c_{ee} & c_{e\mu} & c_{e\tau} \\ c_{e\mu}^* & c_{\mu\mu} & c_{\mu\tau} \\ c_{e\tau}^* & c_{\mu\tau}^* & c_{\tau\tau} \end{pmatrix}, \tag{5.9}$$

where U is the neutrino mixing matrix, G_F is the Fermi constant and N_e is the number density of electrons. The factor $-4/3$ in $H_{\rm LIV}$ arises from the non-observability of the Minkowski trace of the CPT-even LIV parameter c_L, which forces the xx, yy, and zz components to be related to the 00 component [159]. Since the mass dimensions of $a_{\alpha\beta}$ and $c_{\alpha\beta}$ LIV parameters are different, the effect of $a_{\alpha\beta}$ is proportional to the baseline L, whereas $c_{\alpha\beta}$ is proportional to LE and in this work we focus only on the impact of $a_{\alpha\beta}$ parameters on the physics potential of currently running long-baseline experiments NOνA and T2K. Another possible way to introduce an isotropic Lorentz invariance violation is by considering the modified dispersion relation (MDR) preserving rotational symmetry [197], which can be expressed as

$$E^2 - \left(1 - f\left(\frac{|\vec{p}|}{E}\right)\right) |\vec{p}|^2 = m^2, \tag{5.10}$$

where the perturbative function f preserves the rotational invariance. However, this approach is not adopted in this work.

It should be noted that, the Hamiltonian in the presence of LIV (5.7), is analogous to that in the presence of NSI in propagation, which is expressed as [214]

$$H = H_{\rm vac} + H_{\rm mat} + H_{\rm NSI}\ , \tag{5.11}$$

with

$$H_{\rm NSI} = \sqrt{2} G_F N_e \begin{pmatrix} \epsilon_{ee}^m & \epsilon_{e\mu}^m & \epsilon_{e\tau}^m \\ \epsilon_{\mu e}^m & \epsilon_{\mu\mu}^m & \epsilon_{\mu\tau}^m \\ \epsilon_{\tau e}^m & \epsilon_{\tau\mu}^m & \epsilon_{\tau\tau}^m \end{pmatrix}, \tag{5.12}$$

where $\epsilon^m_{\alpha\beta}$ characterizes the relative strength between the matter effect due to NSI and the standard scenario. Thus, one obtains a correlation between the NSI and CPT violating scenarios through

$$a_{\alpha\beta} = \sqrt{2} G_F N_e \epsilon^m_{\alpha\beta} \equiv V_{CC} \epsilon^m_{\alpha\beta} \,, \tag{5.13}$$

where $V_{CC} = \sqrt{2} G_F N_e$. The off-diagonal elements of the CPT violating LIV Hamiltonian ($a_{e\mu}$, $a_{e\tau}$ and $a_{\mu\tau}$) are the lepton flavor violating LIV parameters, which can affect the neutrino flavour transition, are our subject of interest. These parameters are expected to be highly suppressed and the current limits on their values (in GeV), which are constrained by Super-Kamiokande atmospheric neutrinos data at 95% C.L. [204] as

$$|a_{e\mu}| < 2.5 \times 10^{-23} \,, \quad |a_{e\tau}| < 5 \times 10^{-23} \,, \quad |a_{\mu\tau}| < 8.3 \times 10^{-24} \,. \tag{5.14}$$

5.3 Simulation Details

We have consider the experimental features of T2K and NOνA experiments as discussed in Sec. 3.3 of chapter-3, for our analysis.

We use the Preliminary Earth Reference Matter (PREM) profile to calculate line-averaged constant Earth matter density (ρ_{avg}=2.8 g/cm^3) for both NOνA and T2K experiments.

GLoBES software package along with snu plugin [146, 147]are used to simulate the experiments. The implementation of LIV in neutrino oscillation scenario has been done by modifying the snu code [148] in accordance with the Lorentz violating Hamiltonian (5.7). We use the values of standard three flavor oscillation parameters as given in Table 5.1 and consider one LIV parameter at a time, while setting all other parameters to zero unless otherwise mentioned. As mentioned before, we have considered only the isotropic CPT violating parameters ($a_{\alpha\beta}$) for our analysis. The values of the LIV parameters considered in our analysis are: $|a_{e\mu}| = |a_{\mu\tau}| = |a_{e\tau}| = 2 \times 10^{-23}$ GeV and $|a_{ee}| = |a_{\mu\mu}| = |a_{\tau\tau}| = 1 \times 10^{-22}$ GeV.

Parameter	True value	Marginalization Range
$\sin^2\theta_{12}$	0.310	Not marginalized
$\sin^2\theta_{13}$	0.0224	Not marginalized
$\sin^2\theta_{23}$	0.5	$[0.4, 0.6]$
δ_{CP}	$-\pi/2$	$[-\pi, \pi]$
Δm^2_{21}	$7.39 \times 10^{-5}\text{eV}^2$	Not marginalized
Δm^2_{31}	$2.5 \times 10^{-3}\text{eV}^2$	$[2.36, 2.64] \times 10^{-3}\text{eV}^2$

TABLE 5.1: The values of oscillation parameters that we consider in our analysis [144].

5.4 Effect of Lorentz Invariance Violating parameters on $\nu_\mu \to \nu_e$ and $\nu_\mu \to \nu_\mu$ Oscillation Channels

In this section, we discuss the effect of LIV parameters $a_{\alpha\beta} = |a_{\alpha\beta}|e^{i\phi_{\alpha\beta}}$, ($\phi_{\alpha\beta} = 0$, for $\alpha = \beta$), on $\nu_\mu \to \nu_e$ oscillation channel, as the long-baseline experiments are mainly looking at this oscillation channel. The evolution equation for a neutrino state $|\nu\rangle = (|\nu_e\rangle, |\nu_\mu\rangle, |\nu_\tau\rangle)^T$, travelling a distance x, can be expressed as

$$i\frac{d}{dx}|\nu\rangle = H|\nu\rangle, \tag{5.15}$$

where H is the effective Hamiltonian given in Eq. (5.7). Then the oscillation probability for the transition $\nu_\alpha \to \nu_\beta$, after travelling a distance L can be obtained as

$$P_{\alpha\beta} = |\langle\nu_\beta|\nu_\alpha(L)\rangle|^2 = \left|\langle\nu_\beta|e^{-iHL}|\nu_\alpha\rangle\right|^2. \tag{5.16}$$

Neglecting higher order terms, the oscillation probability for $\nu_\mu \to \nu_e$ channel in the presence of LIV for NH can be expressed, which is analogous to the NSI case as [215–225],

$$
\begin{aligned}
P^{\rm LIV}_{\mu e} \;\simeq\;& x^2 f^2 + 2xyfg\cos(\Delta+\delta_{CP}) + y^2 g^2 + 4r_A|a_{e\mu}|\Big\{xf\Big[fs^2_{23}\cos(\phi_{e\mu}+\delta_{CP}) \\
+\;& gc^2_{23}\cos(\Delta+\delta_{CP}+\phi_{e\mu})\Big] + yg\Big[gc^2_{23}\cos\phi_{e\mu} + fs^2_{23}\cos(\Delta-\phi_{e\mu})\Big]\Big\} \\
+\;& 4r_A|a_{e\tau}|s_{23}c_{23}\Big\{xf\Big[f\cos(\phi_{e\tau}+\delta_{CP}) - g\cos(\Delta+\delta_{CP}+\phi_{e\tau})\Big] \\
-\;& yg[g\cos\phi_{e\tau} - f\cos(\Delta-\phi_{e\tau})]\Big\} + 4r^2_A g^2 c^2_{23}\Big|c_{23}|a_{e\mu}| - s_{23}|a_{e\tau}|\Big|^2 \\
+\;& 4r^2_A f^2 s^2_{23}\Big|s_{23}|a_{e\mu}| + c_{23}|a_{e\tau}|\Big|^2 + 8r^2_A fgs_{23}c_{23}\Big\{c_{23}\cos\Delta\Big[s_{23}(|a_{e\mu}|^2 - |a_{e\tau}|^2) \\
+\;& 2c_{23}|a_{e\mu}||a_{e\tau}|\cos(\phi_{e\mu}-\phi_{e\tau})\Big] - |a_{e\mu}||a_{e\tau}|\cos(\Delta-\phi_{e\mu}+\phi_{e\tau})\Big\} \\
+\;& \mathcal{O}(s^2_{13}a, s_{13}a^2, a^3)\ ,
\end{aligned}
\tag{5.17}
$$

where

$$
\begin{aligned}
& x = 2s_{13}s_{23}\ ,\quad y = 2rs_{12}c_{12}c_{23}\ ,\quad r = |\Delta m^2_{21}/\Delta m^2_{31}|\ , \\
& \Delta = \frac{\Delta m^2_{31}L}{4E}\ ,\quad V_{CC} = \sqrt{2}G_F N_e,\quad r_A = \frac{2E}{\Delta m^2_{31}} \\
& f = \frac{\sin\left[\Delta(1 - r_A(V_{CC}+a_{ee}))\right]}{1 - r_A(V_{CC}+a_{ee})}\ ,\qquad g = \frac{\sin\left[\Delta r_A(V_{CC}+a_{ee})\right]}{r_A(V_{CC}+a_{ee})}
\end{aligned}
\tag{5.18}
$$

and $s_{ij} = \sin\theta_{ij}$, $c_{ij} = \cos\theta_{ij}$. The antineutrino probability $P^{\rm LIV}_{\bar{\mu}\bar{e}}$ can be obtained from Eq. (5.17) by replacing $V_{CC} \to -V_{CC}$, $\delta_{CP} \to -\delta_{CP}$ and $a_{\alpha\beta} \to -a^*_{\alpha\beta}$. Similar expression for inverse hierarchy can be obtained by substituting $\Delta m^2_{31} \to -\Delta m^2_{31}$, i,e., $\Delta \to -\Delta$ and $r_A \to -r_A$. One can notice from Eq. (5.17), that only the LIV parameters a_{ee}, $a_{e\mu}$ and $a_{e\tau}$ contribute to appearance probability expression at leading order and the rest of the parameters appear only on sub-leading terms. Since Eq. (5.17) is valid only for small non-diagonal LIV parameter $a_{\alpha\beta}$, in our simulations the oscillation probabilities are evaluated using Eq. (5.16) without any such approximation, by modifying the neutrino oscillation probability function inside snu.c implementing the Lorentz violating Hamiltonian (5.7).

The expression for the survival probability for the transition $\nu_\mu \to \nu_\mu$, up to $\mathcal{O}(r, s_{13}, a_{\alpha\beta})$ is [217],

$$
\begin{aligned}
P^{\rm LIV}_{\mu\mu} \simeq\;& 1 - \sin^2 2\theta_{23}\sin^2\Delta \\
& - |a_{\mu\tau}|\cos\phi_{\mu\tau}\sin 2\theta_{23}\Big[(2r_A\Delta)\sin^2 2\theta_{23}\sin 2\Delta + 4\cos^2 2\theta_{23} r_A \sin^2\Delta\Big] \\
& + (|a_{\mu\mu}| - |a_{\tau\tau}|)\sin^2 2\theta_{23}\cos 2\theta_{23}\Big[(r_A\Delta)\sin 2\Delta - 2r_A\sin^2\Delta\Big].
\end{aligned}
\tag{5.19}
$$

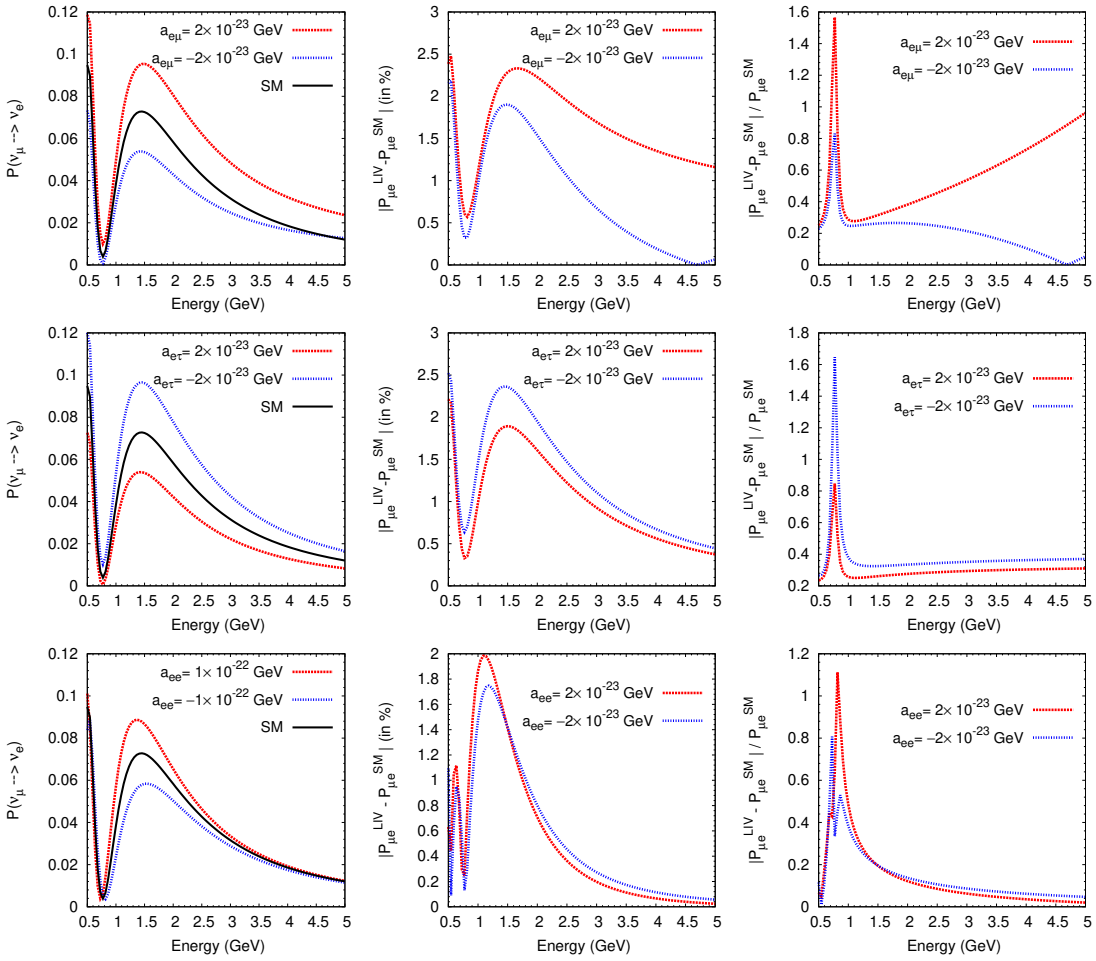

FIGURE 5.1: The ν_e appearance oscillation probabilities as a function of neutrino energy in presence of Lorentz violating parameters $a_{e\mu}$, $a_{e\tau}$ and a_{ee} in the left panel. The difference in the oscillation probability (in %) with and without LIV is shown in the middle panel whereas the relative change in probability is in the right panel.

It is important to observe from the survival probability expression (5.19) that, the LIV parameters involved in $\nu_\mu \to \nu_e$ transitions do not take part in $\nu_\mu \to \nu_\mu$ channel. This probability depends only on the new parameters $a_{\mu\mu}$, $|a_{\mu\tau}|$, $\phi_{\mu\tau}$ and $a_{\tau\tau}$.

The effect of LIV parameters on $\nu_\mu \to \nu_e$ channel for NOνA experiment is displayed in Fig. 5.1. The left panel of the figure shows how the oscillation probability gets modified in presence of LIV, the absolute difference of standard case from Lorentz violating case (in %) is shown in the middle panel and the relative change of the probability $\frac{|P^{\rm LIV}_{\alpha\beta} - P^{\rm SM}_{\alpha\beta}|}{P^{\rm SM}_{\alpha\beta}}$ is shown in the right panel of the figure. In each plot, the black curve corresponds to oscillation probability in the standard three

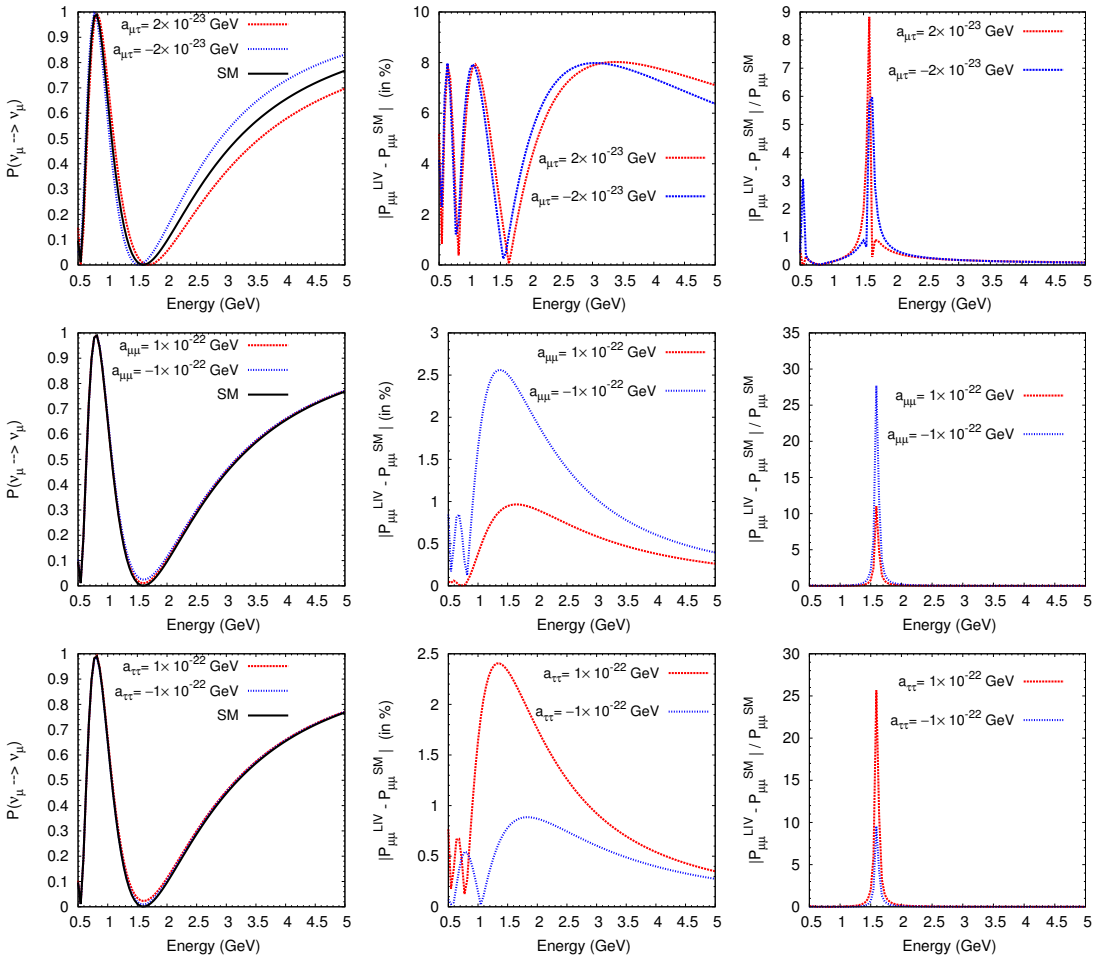

FIGURE 5.2: Same as Fig.1 for the ν_μ survival probability as a function of neutrino energy in presence of $a_{\mu\mu}$, $a_{\mu\tau}$, and $a_{\tau\tau}$ LIV parameters.

flavor oscillation paradigm and red (blue) dotted curve corresponds to the oscillation probability in presence of LIV parameters with positive (negative) value. From Fig. 5.1, it is clear that all the three $a_{e\mu}$, $a_{e\tau}$ and a_{ee} LIV parameters have significant impact on the oscillation probability. It should be further noted that the parameters $a_{e\tau}$ and $a_{e\mu}$ have impact on the amplitude of oscillation and a_{ee} is affecting to phase of the oscillation, which can be seen from the Eq. (5.17). It should be noted from the figure that positive and negative values for LIV parameter $a_{e\tau}$, shift the probabilities in opposite direction of the standard probability curve, while the case of $a_{e\mu}$ is just opposite to that of $a_{e\tau}$ and it also creates a distortion on the probability. Also as seen from the right panel of the Fig.5.1, the relative change of the probability for LIV case with respect to the standard case, becomes significant towards lower energy. Furthermore, it should be inferred from the left panel of the figure that the positive and negative values of LIV parameters

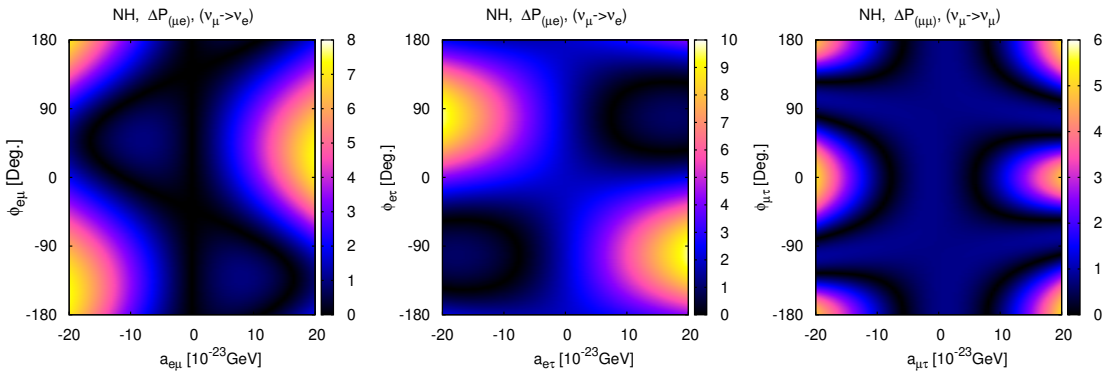

FIGURE 5.3: Representation of $\Delta P_{\mu e}$ and $\Delta P_{\mu\mu}$ in $a_{\alpha\beta} - \phi_{\alpha\beta}$ LIV parameter space for NOνA experiment. The left (middle) panel is for the sensitivities of $\Delta P_{\mu e}$ in $a_{e\mu} - \phi_{e\mu}$ ($a_{e\tau} - \phi_{e\tau}$) plane and right panel is for $\Delta P_{\mu\mu}$ in the $a_{\mu\tau} - \phi_{\mu\tau}$ plane. The color bars in right side of each plot represent the relative change of the $\Delta P_{\alpha\beta}$ in the corresponding plane.

affect the oscillation probabilities differently. However, the result is qualitatively independent of the actual sign of LIV parameters, i.e., the spectral form of the probability is same as the standard case both for positive and negative values of LIV parameters, either it is enhanced or reduced with respect to the standard oscillation probability. Hence, one can take the $|a_{\alpha\beta}|$ for sensitivity study of the experiment in presence of LIV parameters. In Fig. 5.2, the effect of LIV parameters $a_{\mu\mu}$, $a_{\mu\tau}$, and $a_{\tau\tau}$ on ν_μ survival probability is displayed. Analogous to the previous case, here also the effects of the parameters are noticeable; the parameter $|a_{\mu\tau}|$ significantly modifies the probability, whereas the changes due to $a_{\mu\mu}$ and $a_{\tau\tau}$ are negligibly small. In all cases, the positive or negative values of the LIV parameters are responsible for the decrease or enhancement of the oscillation probabilities. In the middle (right) panel of Fig. 5.2, we show the change (relative change) in oscillation probability due to the effect of LIV parameters.

5.5 Sensitivity limits on the Lorentz Invariance Violating parameters

In this section, we analyse the potential of T2K, NOνA, and the synergy of T2K and NOνA to constrain the LIV parameters. From Eqns. (16) and (18) or from Fig. 5.1 and Fig. 5.2, it can be seen that the LIV parameters $|a_{e\mu}|$ and $|a_{e\tau}|$ along

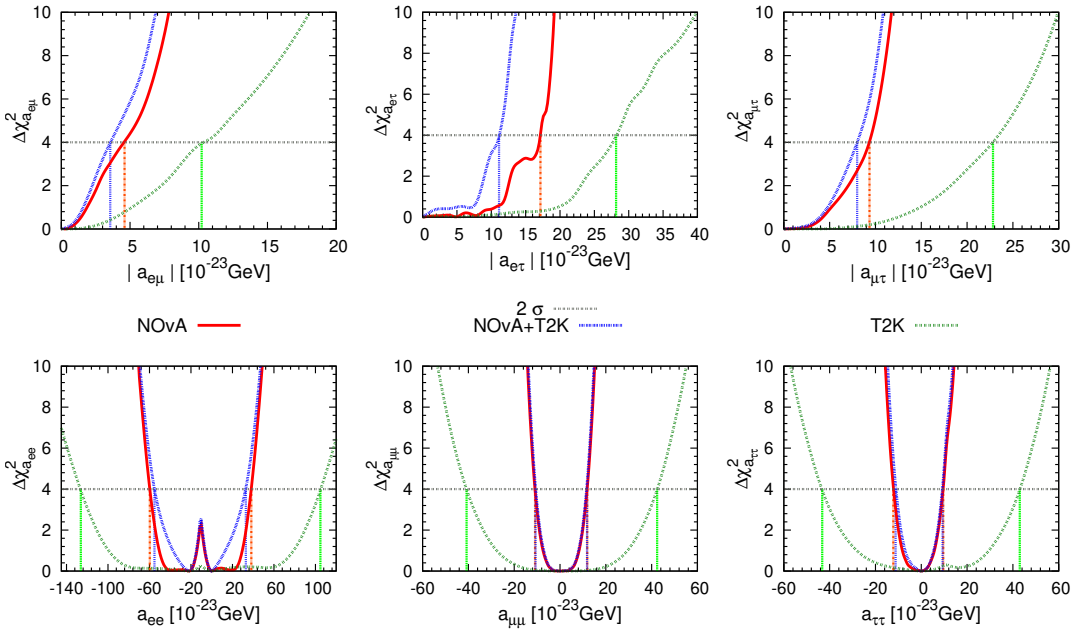

FIGURE 5.4: The sensitivities on LIV parameters from NOνA and T2K experiments.

with LIV phases $\phi_{e\mu}$ and $\phi_{e\tau}$ play major role in appearance channel ($\nu_\mu \to \nu_e$), whereas $|a_{\mu\tau}|$ and $\phi_{\mu\tau}$ influence the survival channel ($\nu_\mu \to \nu_\mu$). In order to see their sensitivities at probability level, we define two quantities, $\Delta P_{\mu e} = \frac{|P^{\rm LIV}_{\mu e} - P^{\rm SM}_{\mu e}|}{P^{\rm SM}_{\mu e}}$ and $\Delta P_{\mu\mu} = \frac{|P^{\rm LIV}_{\mu\mu} - P^{\rm SM}_{\mu\mu}|}{P^{\rm SM}_{\mu\mu}}$, which provide the information about the relative change in probability due to the presence of LIV term from the standard case. We evaluate their values for various LIV parameters and display them in $a_{\alpha\beta} - \phi_{\alpha\beta}$ plane in Fig. 5.3. From the left panel of the figure, one can see that the observable $\Delta P_{\mu e}$ has maximum value at the yellow region, for $\phi_{e\mu} \approx 45°$, if $a_{e\mu}$ is positive, whereas for negative value of $a_{e\mu}$, $\Delta P_{\mu e}$ is maximum for $\phi_{e\mu} \approx -135°$. This nature of $\Delta P_{\mu e}$ can be easily understood from Eqn. (5.17), as the appearance probability depends on sine and cosine functions of $\phi_{e\mu}$. However, the nature of $\Delta P_{\mu e}$ for $e\tau$ sector is quite different from that of $e\mu$ sector, even-though the appearance probability depends upon sine and cosine functions of $\phi_{e\tau}$. This is due to the opposite sign on $|a_{e\mu}|$ and $|a_{e\tau}|$ dependent terms in oscillation probability. As the LIV parameter $|a_{\mu\tau}|$ mainly appears on the survival channel, we calculate $\Delta P_{\mu\mu}$ which has cosine dependence on $\phi_{\mu\tau}$ and display it in the right panel of the figure.

Next, we analyse the potential of T2K, NOνA, and the synergy of T2K and NOνA to constrain the various LIV parameters, which are shown in Fig. 5.4. In order to

LIV parameter	Sensitivity limits on LIV parameters		
	T2K [$\times 10^{-22}$]	NOνA [$\times 10^{-22}$]	T2K+NOνA [$\times 10^{-22}$]
$\lvert a_{e\mu}\rvert$	< 1.02	< 0.46	< 0.36
$\lvert a_{e\tau}\rvert$	< 2.82	< 1.71	< 1.08
$\lvert a_{\mu\tau}\rvert$	< 2.28	< 0.93	< 0.8
a_{ee}	$[-12.62 : 10.47]$	$[-5.97 : 3.82]$	$[-5.52 : 3.29]$
$a_{\mu\mu}$	$[-4.09 : 4.24]$	$[-1.09 : 1.19]$	$[-1.07 : 1.18]$
$a_{\tau\tau}$	$[-4.33 : 4.3]$	$[-1.22 : 0.96]$	$[-1.12 : 0.93]$

TABLE 5.2: The sensitivity limits on each LIV parameters (in GeV) at 2σ C.L. from T2K, NOνA, and synergy between T2K and NOνA.

obtain these values, we compare the true event spectra which are generated in the standard three flavor oscillation paradigm with the test event spectra which are simulated by including one LIV parameter at a time and show the marginalized sensitivities as a function of the LIV parameters, $|a_{\alpha\beta}|$. The values of $\Delta\chi^2_{\alpha\beta}$ are evaluated using the standard rules as described in GLoBES and the details are presented in the Appendix A. From the figure, we can see that the sensitivities on LIV parameters obtained from T2K are much weaker than NOνA and the synergy of T2K and NOνA can improve the sensitivities on these parameters. For a direct comparison, we give the sensitivity limits on each LIV parameter (in GeV) at 2σ C.L. in Table 5.2. All these limits are slightly weaker than the bounds obtained from Super-Kamiokande Collaboration (5.14).

5.6 Effect of Lorentz Invariance Violation on various sensitivities of NOνA

In this section, we discuss the effect of LIV on the sensitivities of long-baseline experiment to determine neutrino mass ordering and CP-violation by taking NOνA as a case of study. In addition to this, we also present the correlations between the LIV parameters and the standard oscillation parameters θ_{23} and δ_{CP}.

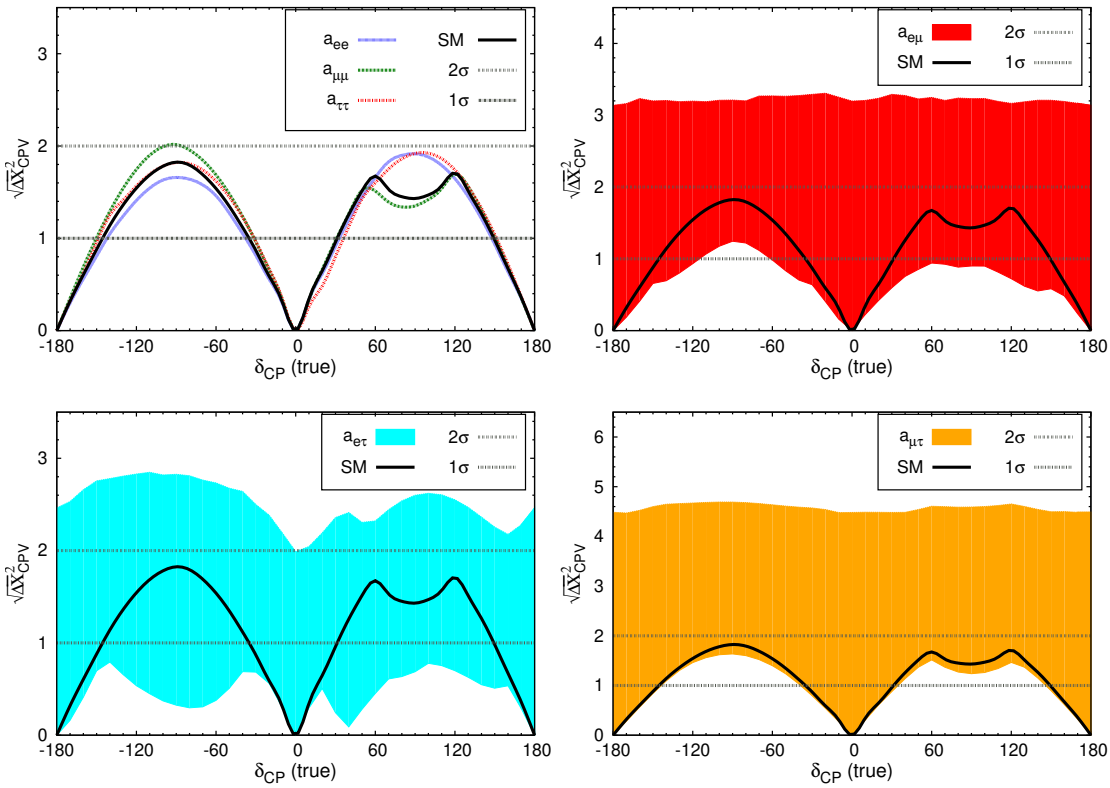

FIGURE 5.5: CP Violation sensitivity as a function of true values of δ_{CP} for NOνA experiment. Standard case is represented by black curve in each plot. The top-left panel is for diagonal Lorentz violating parameters and non-diagonal LIV parameters in $e\mu$, $e\tau$ and $\mu\tau$ sectors shown in top-right, bottom-left and bottom-right panels, respectively.

5.6.1 CP violation discovery potential

It is well known that the determination of the CP violating phase δ_{CP} is one of the most challenging issues in neutrino physics today. CP violation in the leptonic sector may provide the key ingredient to explain the observed baryon asymmetry of the Universe through leptogenesis. In this section, we discuss how the CP violation sensitivity of NOνA experiment gets affected due to impact of LIV parameters. Fig. 5.5 shows the significance with which CP violation, i.e. $\delta_{CP} \neq 0, \pm\pi$ can be determined for different true values of δ_{CP}. For the calculation of sensitivities, we have used the oscillation parameters as mentioned in Table 5.1. Also, the amplitude of all the diagonal LIV parameters considered as 1×10^{-22} GeV and non-diagonal elements as 2×10^{-23} GeV. The expression for the test statistics $\Delta\chi^2_{CPV}$, which quantifies the CP violation sensitivity is provided in the Appendix A. We consider here the true hierarchy as normal, true parameters as given in

Table 5.1, and vary the true value for δ_{CP} in the allowed range $[-\pi, \pi]$. Also the possibility of exclusion of CP conserving phases has been shown by taking the test spectrum δ_{CP} value as 0, $\pm\pi$. This exclusion sensitivity is obtained by calculating the minimum $\Delta\chi^2_{\text{min}}$ after doing marginalization over both hierarchies NH and IH, as well as Δm^2_{31} and $\sin^2\theta_{23}$ in their 3σ ranges. The CPV sensitivity for standard case and in presence of diagonal LIV parameters is shown in the top left panel of Fig. 5.5. The black curve depicts the standard case, and for diagonal elements a_{ee}, $a_{\mu\mu}$ and $a_{\tau\tau}$, the corresponding plots are displayed by blue, green and red, respectively. Further, we show the sensitivity in presence of non-diagonal LIV parameters in $e\mu$, $e\tau$, and $\mu\tau$ sectors respectively in the top right, bottom left, and bottom right panels of the same figure. As the extra phases of the non-diagonal parameters can affect the CPV sensitivity, we calculate the value of $\Delta\chi^2_{\text{min}}$ for a particular value of δ_{CP} by varying the phase $\phi_{\alpha\beta}$ in its allowed range $[-\pi, \pi]$, which results in a band structure. It can be seen from the figure that LIV can significantly affect the CPV discovery potential of the NOνA experiment. All the three non-diagonal LIV parameters have significant impact on CPV sensitivity. It can be seen from the figure that CPV sensitivity spans on both sides of standard case in presence of non-diagonal LIV parameters. Although there is a possibility that the sensitivity can be deteriorated in presence of LIV for some particular true value of the phase of the non-diagonal parameter ($\phi_{\alpha\beta}$), for most of the case the CP violation sensitivity is significantly get enhanced. Moreover, one can expect some sensitivity where there is less or no such significance for δ_{CP} regions in standard case. Further, the parameters $a_{e\mu}$ and $a_{e\tau}$ have comparatively large effect on the sensitivity with respect to $a_{\mu\tau}$. Similar observation can also be found by considering inverted hierarchy.

5.6.2 MH Sensitivity

Mass hierarchy determination is one of the main objectives of the long baseline experiments. It is determined by considering true hierarchy as NH (IH) and comparing it with the test hierarchy, assumed to be opposite to the true case, i.e., IH (NH). Fig. 5.6 shows the effect of LIV parameters on MH sensitivity at oscillation probability level. We obtain the bands by varying the δ_{CP} within its allowed range $[-\pi, \pi]$ and considering the other parameters as given in the Table 5.1, and the

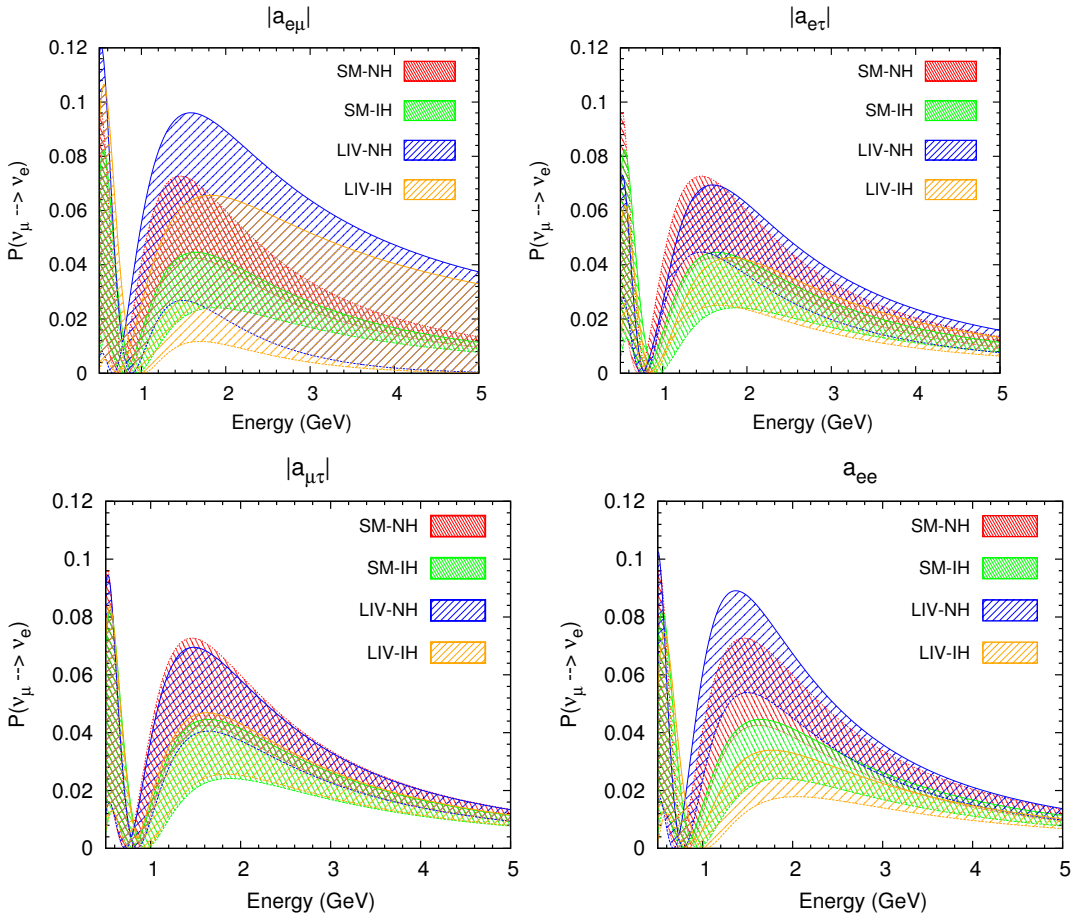

FIGURE 5.6: The oscillation probability for NOνA experiment as a function of energy in presence of non-diagonal LIV parameters $|a_{e\mu}|, |a_{e\tau}|$ and $|a_{\mu\tau}|$ are shown in top-let, top-right and bottom-left panels, respectively. The effect of diagonal LIV parameter a_{ee} shown in bottom-right panel.

amplitude of all the non-diagonal LIV elements as 2×10^{-23} GeV and diagonal LIV elements as 1×10^{-22} GeV. The red (green) band in the figure is for NH (IH) case with standard matter effect. There is some overlapped region between the two bands for some values of δ_{CP}, where determination of neutrino mass ordering is difficult. The blue and orange bands represent the NH and IH case in presence of the LIV parameters, respectively. It can be seen that the parameter $a_{e\mu}$ and a_{ee} have significant effect on the appearance probability energy spectrum compared to other two parameters. The two bands NH and IH shifted to higher values of probability and have more overlapped regions in presence of $a_{e\mu}$. The presence of a_{ee} shifted the NH band to higher values and IH band shifted to lower values of probabilities compared to standard case. Whereas the effects of $a_{e\tau}$ and $a_{\mu\tau}$ are negligibly small.

Next, we calculate the $\Delta\chi^2_{\rm MH}$ by comparing true event and test event spectra which are generated for the oscillation parameters in the Table 5.1 for each true value of δ_{CP}. In order to get the minimum deviation or $\Delta\chi^2_{\rm min}$, we do marginalization over δ_{CP}, θ_{23} and Δm^2_{31} in their allowed regions. In Fig. 5.7, we show the mass hierarchy sensitivity of NOνA experiment for standard paradigm and in presence of diagonal LIV parameter. The left (right) panel of the figure corresponds to the MH sensitivity for true NH (IH). It can be seen from the figure that for standard matter effect case (black curve), the test hierarchy can be ruled out in upper half plane (UHP) ($0 < \delta_{CP} < \pi$) and lower half plane (LHP) ($-\pi < \delta_{CP} < 0$) for true NH and IH, respectively above 2σ C.L.. The other half plane is unfavourable for mass hierarchy determination. The parameter a_{ee} is found to give significant enhancement from the standard case compared to $a_{\mu\mu}$.

It should also be emphasized that mass hierarchy can be measured precisely above 3σ C.L. for most of the δ_{CP} region in presence of a_{ee} for true value in both NH and IH.

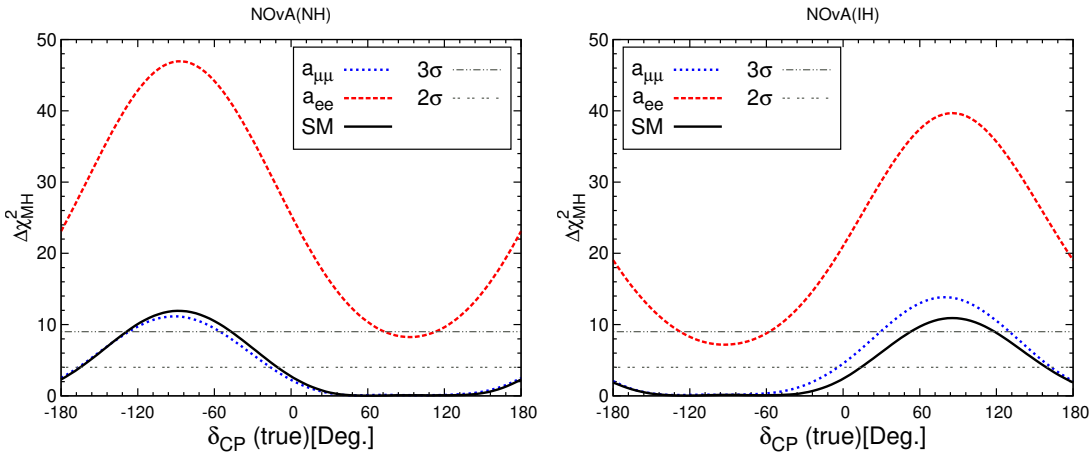

FIGURE 5.7: Mass hierarchy sensitivity as function of δ_{CP} for NOνA experiment. Left (right) panel is for NH (IH) as true value. Black curve represents the standard matter effect case without any LIV parameter. Red and blue dotted curves represent the sensitivity in the presence of diagonal parameters a_{ee}, and $a_{\mu\mu}$, respectively.

The MH sensitivity in presence non-diagonal Lorentz violating parameters $a_{\alpha\beta}$ is shown in Fig. 5.8. As the non-diagonal LIV parameters introduce new phases, we do marginalization over new phases in their allowed range, i.e., $[-\pi, \pi]$ while obtaining the MH sensitivity. In all the three cases, the MH sensitivity expands around the MH sensitivity in the standard three flavor framework. From the

figure, it can be seen that the non-diagonal LIV parameters significantly affect the sensitivity which crucially depends on the value of new phase. Similar analysis can be studied considering IH as the true hierarchy.

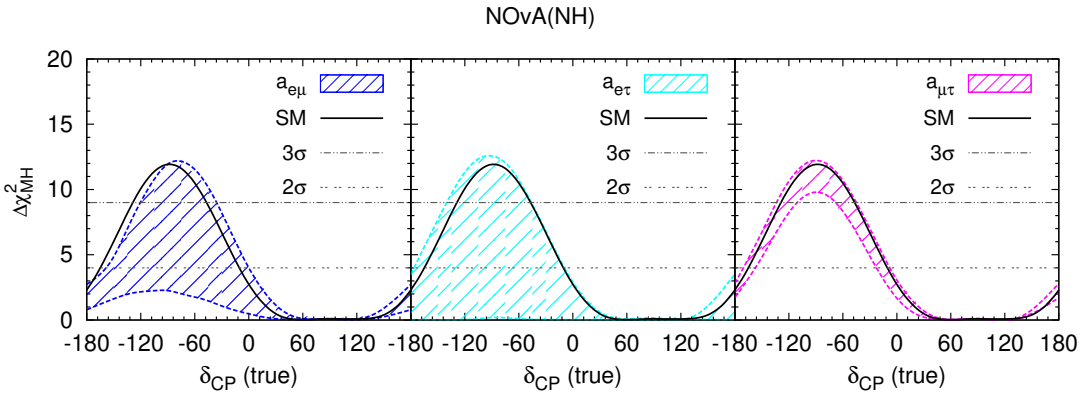

FIGURE 5.8: Mass hierarchy sensitivity as a function of δ_{CP} for NOνA experiment in presence of $a_{\alpha\beta}$. Black curve represents the standard matter effect case without any LIV parameter. Left, middle and right panels represent the sensitivity in presence of non-diagonal parameters $a_{e\mu}$, $a_{e\tau}$ and $a_{\mu\tau}$, respectively.

5.6.3 Correlations between Lorentz Invariance Violating parameters with δ_{CP} and θ_{23}

In this section, we show the correlation between the LIV parameters and the standard oscillation parameters θ_{23} and δ_{CP} in $|a_{\alpha\beta}| - \theta_{23}$ and $|a_{\alpha\beta}| - \delta_{CP}$ planes. Fig. 5.9 (5.10) shows the correlation for a_{ee}, $a_{\mu\mu}$, $a_{\tau\tau}$, $|a_{e\mu}|$, $|a_{e\tau}|$, $|a_{\mu\tau}|$ and θ_{23} (δ_{CP}), at 1σ, 2σ, 3σ C.L. in two dimensional plane. In both figures upper (lower) panel is for a_{ee}, $a_{\mu\mu}$ and $a_{\tau\tau}$ ($|a_{e\mu}|$, $|a_{e\tau}|$, $|a_{\mu\tau}|$). In order to obtain these correlations, we set the true value of LIV parameters to zero and the standard oscillation parameters as given in Table 5.1. Further, we do marginalization over $\sin^2\theta_{23}$, δ_{CP}, and Δm^2_{31} for both hierarchies. In the case of non-diagonal LIV parameters, $|a_{e\mu}|, |a_{e\tau}|, |a_{\mu\tau}|$, we also do marginalization over the additional phase $\phi_{\alpha\beta}$. From the plots it can be noticed that precise determination of θ_{23} will provide useful information about the possible interplay of LIV physics.

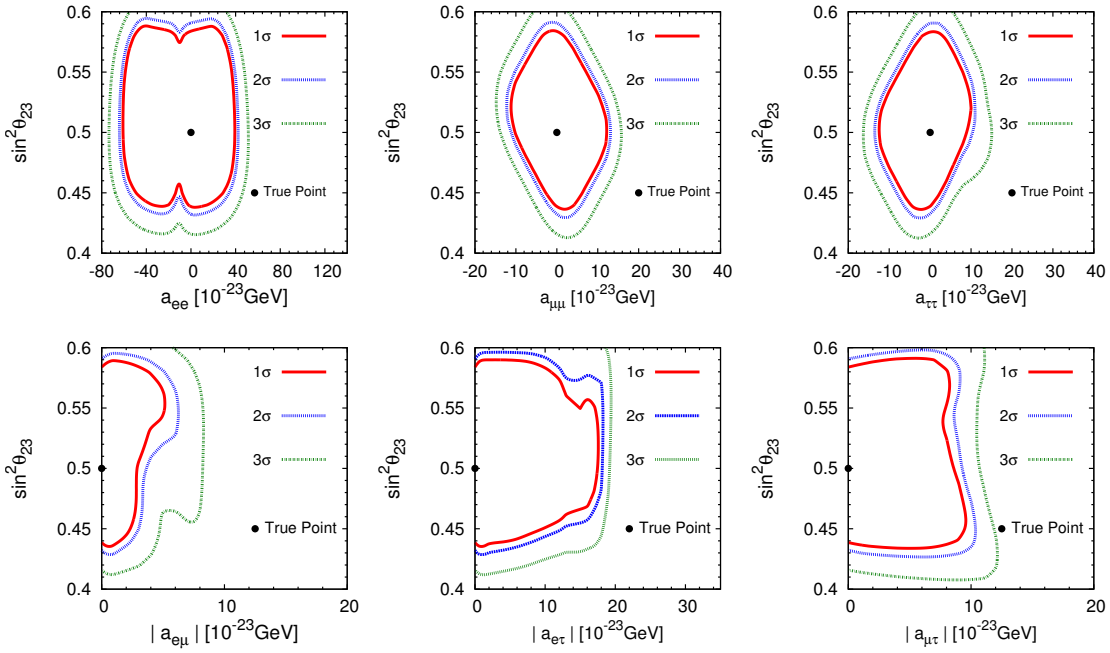

FIGURE 5.9: Correlation between LIV parameters and θ_{23} in $|a_{\alpha\beta}| - \sin^2\theta_{23}$ plane at 1σ, 2σ and 3σ C.L. for NOνA experiment.

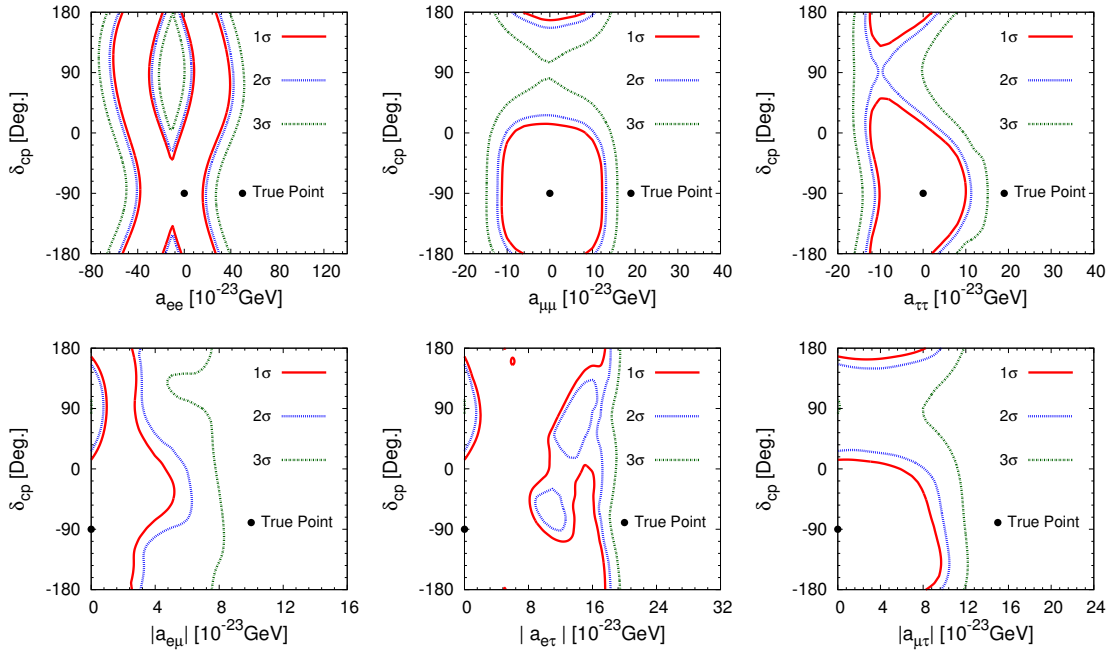

FIGURE 5.10: Correlation between LIV parameters and δ_{CP} in $|a_{\alpha\beta}| - \delta_{CP}$ plane at 1σ, 2σ and 3σ C.L. for NOνA experiment.

5.7 Summary and Conclusion

It is well known that, neutrino oscillation physics has entered a precision era, and the currently running accelerator based long-baseline experiment NOνA is expected to shed light on the current unknown parameters in the standard oscillation framework, such as the mass ordering as well as the leptonic CP phase δ_{CP}. However, the possible interplay of potential new physics scenarios can hinder the clean determination of these parameters. Lorentz invariance is one of the fundamental properties of space time in the standard version of relativity. Nevertheless, the possibility of small violation of this fundamental symmetry has been explored in various extensions of the SM in recent times and a variety of possible experiments for the search of such signals have been proposed over the years. In this context, the study of neutrino properties can also provide a suitable testing ground to look for the effects of LIV parameters as neutrino phenomenology is extremely rich and spans over a very wide range of energies. In this work, we have studied in detail the impact of Lorentz Invariance violating parameters on the currently running long-baseline experiments T2K and NOνA and our findings are summarized below.

- Considering the effect of only one LIV parameter at a time, we have obtained the sensitivity limits on these parameters for the currently running long baseline experiments T2K and NOνA. We found that the limits obtained from T2K are much weaker than that of NOνA and the synergy of T2K and NOνA can significantly improve the sensitivities.

- We have also explored the phenomenological consequences introduced in the neutrino oscillation physics due to the presence of Lorentz-Invariance violation on the sensitivity studies of long-baseline experiments by considering NOνA as a case study. We mainly focused on how the oscillation probabilities, which govern the neutrino flavor transitions, get modified in presence of different LIV parameters. In particular, we have considered the impact of the LIV parameters $|a_{e\mu}|$, $|a_{e\tau}|$, $|a_{\mu\tau}|$, a_{ee}, $a_{\mu\mu}$ and $a_{\tau\tau}$. We found that the parameters $|a_{e\mu}|$, $|a_{e\tau}|$ and a_{ee} significantly affect the $\nu_\mu \to \nu_e$ transition probability $P_{\mu e}$, while the effect of $|a_{\mu\tau}|$, $a_{\mu\mu}$, $a_{\tau\tau}$ on the survival probability $P_{\mu\mu}$ is minimal. We also found that $|a_{e\mu}|$ creates a distortion on the appearance probability.

- We further investigated the impact of LIV parameters on the determination of mass hierarchy and CP violation discovery potential and found that the presence of LIV parameters significantly affect these sensitivities. In fact, the mass hierarchy sensitivity and CPV sensitivity are enhanced or deteriorated significantly in presence of LIV parameters as these sensitivities crucially depend on the new CP-violating phase of these parameters.

- We also obtained the correlation plots between $\sin^2\theta_{23}$ and $|a_{\alpha\beta}|$ as well as between δ_{CP} and $|a_{\alpha\beta}|$. From these confidence regions, it can be ascertained that it is possible to obtain the limits on the LIV parameters once $\sin^2\theta_{23}$ is precisely determined.

In conclusion, we found that T2K and NOνA have the potential to explore the new physics associated with Lorentz invariance violation and can provide constraints on these parameters.

Chapter 6

Summary and Conclusion

Neutrinos inspire the scientific community to do fundamental research to explore their distinctive features. Since several decades varieties of neutrino experiments putting tremendous efforts to unravel the nature of neutrinos. So far, we have convincing evidence for neutrino oscillation from various well established experiments. Neutrino oscillation stipulates non-zero masses and mixing for neutrinos, which gives a clear indication of Physics beyond the SM. Many pragmatic theoretical frameworks have been developed to explain the origin of neutrino masses and mixing phenomena. Data collected by different neutrino experiment over the last couple of decades meticulously measured the oscillation parameters with great precision, except a few. The current sensitivity for δ_{CP} measurement is not significant enough. Also, there are several other unknowns in the neutrino sector, like the mass ordering, octant of θ_{23} and CP violation, which are yet to be established. Answers to all these unrevealed questions can be extracted from long-baseline experiments by focusing on the ν_μ to ν_e oscillation channel in both neutrino and anti-neutrino mode. In addition to this, long-baseline experiments can provide the information on impact of various BSM physics, such as existence of sterile neutrinos, non-standard interactions (NSI), CPT violation, Lorentz invariance violation, neutrino decay, etc. This thesis discusses the effects of many interesting BSM physics on the measurement of neutrino oscillation parameters at the currently running as well as future long-baseline experiments. This chapter summarises the research work that has been carried out in this thesis.

In order to simulate these long-baseline experiments, we use General Long Baseline Experiment Simulator (GLoBES), which is a C library based software package.

Additionally, snu file has been used to study sterile neutrinos and NSI effects. We have proceeded with the primary motivation to explore the implications of various BSM effects at probability as well as event levels. In our works, we have explicitly studied various oscillation probabilities in standard case and in presence of BSM physics. Event level studies show the effects of BSM physics on oscillation parameters and on current unknowns in neutrino sector. In order to illustrate this, we have obtained Mass Hierarchy (MH) and CP Violation (CPV) sensitivities by calculating χ^2 by pull method as mentioned in GLoBES.

Chapter-1 contains a brief introduction to the particle content of the standard model and the associated gauge symmetries. After that, the historical development of neutrino is discussed briefly. Also, an introduction to neutrinos in and beyond the SM is discussed in detail. Before concluding the chapter, a brief discussion about neutrinoless double beta decay is presented and concluded with a quick overview of the thesis.

Second chapter of thesis describes the neutrino oscillation. It started with neutrino mixing and then discusses oscillation in vacuum both in two and three flavor scenarios. Further the oscillation in matter is also presented. Evidence of neutrino oscillation is discussed briefly from solar and atmospheric neutrino anomalies. Various neutrino oscillation experiments such as solar, atmospheric, and accelerator-based, are discussed comprehensively. Prior to conclusion of this chapter, current status of neutrino oscillation has been described.

Chapter-3 is dedicated to impact of sterile neutrino on long-baseline experiment and on neutrinoless double beta decay. It started with the basic introduction to sterile neutrino from the anomalous results reported by short-baseline, reactor and Gallium experiments. Including one eV-scale sterile neutrino to the standard active neutrinos, the scenario became $3+1$. Extensive discussion on $3+1$ scenario and the new oscillation framework have been manifested. It has been shown that, at probability level the impact of sterile neutrino can be observable for the currently running long-baseline experiments NOvA and T2K. Presence of sterile neutrino consequences new kind of degeneracies between the oscillation parameters which can hamper the precise measurement of standard three flavor oscillation parameters. In this regard, degeneracies among the oscillation parameters have been shown for NOvA experiment in biprobability and probability as a function of δ_{CP}. Effects of sterile neutrinos are not only observable at probability but also at event level. For that, we have shown the allowed regions between θ_{23} and δ_{CP}

in standard case and in presence of sterile neutrino for NOvA and combination of NOvA and T2K, for different octant and hierarchy combinations. Effect of sterile neutrino is clearly visible and results deterioration of degeneracy resolution capability of the experiment. Combination of the two experiments can probe the degeneracies in a better way. Further the MH sensitivities have been shown in standard three flavor case and in presence of sterile for NOvA and synergy of NOvA and T2K. From standard case the wrong mass hierarchy can be ruled out at 2σ C.L. in the favourable region of δ_{CP} i.e., lower (upper) half plane of δ_{CP} for NH (IH). The active-sterile neutrino mixing generates new kind of degeneracies among the oscillation parameters causing a notable decline in the favourable region of CP phase for NOvA experiment. However, NOvA and T2K experiments together can enhance the MH sensitivity in presence of sterile neutrino. Combination of both experiments can also increase the δ_{CP} coverage. Further we have investigated the hypothesis of maximum CP violation with the true δ_{CP}. Addition of sterile neutrino brings two more CP phases, can cause CP violation. The two new CP phases δ_{14} and δ_{34} have large impact on maximum CP violation. The eV-scale sterile neutrino can have visible footprint on the rare process neutrinoless double beta decay resulting a significant increase in the effective mass parameter $|M_{ee}|$ for IH case in presence of sterile neutrino. This increment in $|M_{ee}|$ can be within the sensitivity reach of KamLAND-Zen experiment. Also a discussion on the sensitivity reach of future ^{136}Xe experiments for exploring the presence of eV-scale sterile neutrino is presented. The Majorana nature of neutrino can be revealed with a sensitive exposure of $\sim 10^4$ $\mathrm{kg_{iso}yr}$.

Chapter-4 of the thesis is based on the study of CPT violation in neutrino oscillation experiments. SM is an effective field theory at low energy, originated from the unified picture of gravity and quantum physics at Planck scale. Experimental observations of Planck scale physics are important to understand its correlation with the SM. Violation of CPT symmetry can be one of such type of signals. CPT symmetry being a fundamental symmetry of nature demands the particles and anti-particles to have same mass and lifetime. No such strong evidence for CPT violation from experimental observation has been observed so far. Though, from Kaon and lepton sectors, constraints are there on the CPT violation, but they are not very stringent. The bounds from Kaon sector are relatively weak compared to the bounds from neutrino sector. In addition, neutrinos are more fundamental particles than Kaons, so they provide a better platform to investigate CPT symmetry.

The long-baseline neutrino oscillation experiments can be an efficient tool to probe the CPT symmetry violation. As neutrinos have to propagate a very long distance, any tiny deviation due to the CPT violation during their propagation can be observable. In this context, we have done a model independent study on CPT violation for future long-baseline experiments: T2HK, T2HKK, ESSnuSB and DUNE. We have obtained bounds on the CPT violating parameters, i.e., the difference between neutrino and antineutrino parameters, which are parametrized as $|\delta_{CP} - \overline{\delta}_{CP}| = \Delta(\delta_{CP}), |\Delta m^2_{31} - \Delta\overline{m}^2_{31}| = \Delta(\Delta m^2_{31})$ and $|\sin^2\theta_{23} - \sin^2\overline{\theta}_{23}| = \Delta(\theta_{23})$. T2HK, T2HKK and DUNE experiments are more sensitive to the CPT violating parameters $\Delta(\Delta m^2_{31})$ and $\Delta(\theta_{23})$. These experiments will highly improvise existing bounds on CPT violation from Kaon sector. While ESSnuSB and T2HKK have significant CPT violating sensitivities for $\Delta(\delta_{CP})$ as both of these experiments are tuned to search for neutrino oscillation at second maxima, and hence can explore δ_{CP} better than other experiments. Further, discovery of CPT violation sensitivities and sensitivities to constrain CPT violation parameters are obtained for the T2HK, T2HKK, ESSnuSB and DUNE experiments individually and combination of experiments such as DUNE+T2HKK and DUNE+ESSnuSB for neutrino and antineutrino cases separately. One of the important observation is that the proposed long-baseline experiments within their run time can probe CPT violation, if it exists in nature. In conclusion, the future long-baseline experiments have potential to explore the CPT violation to a great extent.

Chapter-5 discusses the CPT violation through violation of Lorentz invariance at currently running long-baseline experiment. As we know CPT violation is one of the ways to study Planck scale physics, experimental observation of such signals is quite important. As we know, CPT symmetry is based on the Hermiticity, Locality and Lorentz invariance of the theory. Lorentz violation can be a consequence of CPT violation and can be delved by long-baseline experiments. In this study, we have added the simplest dimension-four CPT and Lorentz violating terms to the SM Lagrangian. The newly added parameters can be real and complex. The expression of Hamiltonian for LIV parameters is analogous to the Hamiltonian of Neutral Current NSI and hence, there are correlations between the NSI and LIV parameters. So, the implementation of LIV is quiet similar to NSI using snu file with GLoBES. These LIV parameters significantly affect the oscillation probabilities of NOvA experiment. Also for the first time, we have obtained the sensitivity limits on the LIV parameters from currently running long baseline experiment NOvA and T2K. Combined results of NOvA and T2K experiments

can improve the sensitivity limits of LIV parameters. In addition to this, the effect of LIV parameters on mass hierarchy and CP violating sensitivities have been investigated for NOvA experiment. LIV parameters can enhance or deteriorate the sensitivities depending upon the new complex CP phases of LIV parameters. Also the correlations of the LIV parameters with $\sin^2\theta_{23}$ and δ_{CP} have been obtained. In conclusion, both NOvA and T2K can explore Lorentz violation effect and can obtain stringent constraints on these parameters.

Presence of various new physics can hamper the landmark achievement regarding the measurement of neutrino oscillation. Hence, BSM physics like sterile neutrino, scalar and vector NSI, LIV, decoherence, long range force, etc. can be studied in numerous way at several long baseline experiments. Considering some physics beyond SM, current tension between NOvA and T2K for δ_{CP} can be solved. Eventually, with clear-cut idea about neutrino flux, huge neutrino detector and having large statistics long baseline experiments can explain the unknowns of neutrino sector. Many more discoveries of new physics will appear in the future from the neutrino sector.

Appendix A

Details of χ^2 analysis

A.1 Calculation of χ^2

In our analysis, we have performed the χ^2 analysis by comparing true (observed) event spectra $N_i^{\rm true}$ with test (predicted) event spectra $N_i^{\rm test}$, and its general form is given by

$$\chi^2_{\rm stat}(\vec{p}_{\rm true}, \vec{p}_{\rm test}) = -\sum_{i\in {\rm bins}} 2\Big[N_i^{\rm test} - N_i^{\rm true} - N_i^{\rm true} \ln\left(\frac{N_i^{\rm test}}{N_i^{\rm true}}\right)\Big], \tag{A.1}$$

where $\vec{p}$ is the array of standard neutrino oscillation parameters. However, for numerical calculation of χ^2, we also include the systematic errors using pull method. This is usually done with the help of nuisance systematic parameters as discussed in the GLoBES manual. In presence of systematics, the predicted event spectra modify as $N_i^{\rm test} \rightarrow N_i^{'\ {\rm test}} = N_i^{\rm test}(1 + \sum_{j=1}^{n} \pi_i^j \xi_j^2)$, where π_i^j is the systematic error associated with signals and backgrounds and ξ_j is the pull. Therefore, the Poissonian χ^2 becomes

$$\chi^2(\vec{p}_{\rm true}, \vec{p}_{\rm test}, \vec{\xi}) = -\min_{\vec{\xi_j}} \sum_{i\in {\rm bins}} 2\Big[N_i^{'\ {\rm test}} - N_i^{\rm true} - N_i^{\rm true} \ln\left(\frac{N_i^{'\ {\rm test}}}{N_i^{\rm true}}\right)\Big] + \sum_{j=1}^{n} \xi_j^2. \tag{A.2}$$

Suppose $\vec{q}$ is the oscillation parameter in presence of Lorentz invariance violating parameters. Then the sensitivity of LIV parameter $a_{\alpha\beta}$ can be evaluated as

$$\Delta\chi^2(a_{\alpha\beta}^{\rm test}) = \chi^2_{\rm SO} - \chi^2_{\rm LIV}\ , \tag{A.3}$$

where $\chi^2_{\rm SO} = \chi^2(\vec{p}_{\rm true}, \vec{p}_{\rm test})$, $\chi^2_{\rm LIV} = \chi^2(\vec{p}_{\rm true}, \vec{q}_{\rm test})$. We obtain minimum $\Delta\chi^2(a^{\rm test}_{\alpha\beta})$ by doing marginalization over $\sin^2\theta_{23}$, δm^2_{31}, and $\delta_{\rm CP}$. Further, the sensitivities of current unknowns in neutrino oscillation is discussed in following section.

A.2 CP violation sensitivity

$$\Delta\chi^2_{\rm CPV}(\delta^{\rm true}_{CP}) = \min[\chi^2(\delta^{\rm true}_{CP}, \delta^{\rm test}_{CP} = 0), \chi^2(\delta^{\rm true}_{CP}, \delta^{\rm test}_{CP} = \pi)]. \tag{A.4}$$

For obtaining minimum $\chi^2_{\rm CPV}$ marginalization is done over the oscillation parameters $\sin^2\theta_{23}$ and Δm^2_{31}. While including the non-diagonal Lorentz violating parameters $a_{\alpha\beta}$, we also marginalize over its corresponding phase $\phi_{\alpha\beta}$.

A.3 Mass Hierarchy sensitivity

$$\Delta\chi^2_{\rm MH} = \chi^2_{\rm NH} - \chi^2_{\rm IH} \quad \text{(for true normal ordering)}, \tag{A.5}$$

$$\Delta\chi^2_{\rm MH} = \chi^2_{\rm IH} - \chi^2_{\rm NH} \quad \text{(for true inverted ordering)}. \tag{A.6}$$

We obtain minimum $\chi^2_{\rm MH}$ by doing marginalization over the oscillation parameters $\sin^2\theta_{23}$, Δm^2_{31}, and δ_{CP} in the range [0.4:0.6], [2.36:2.64]$\times 10^{-3}$ eV^2 and [$-180°$,$180°$], respectively.

Appendix B

Detail discussion of Lorentz Invariance Violation

Observation of violation or Lorentz symmetry can change the year long well developed notation of space and time. Non-observation of Lorentz violation restrict the asymmetry to be very small. Lorentz transformation can be categorised as particle Lorentz transformation and observer Lorentz transformation. The Lorentz invariance is the consistency of the theory under particle Lorentz transformation, where Lorentz transformation applied on the fields of the theory. While in observer Lorentz transformation implies the laws of Physics are independent of the co-ordinate system. It can be understood by inserting some tensors which will couple to the SM operators. For a particular frame of reference these tensors are treated as some function and treated as backgrounds for the rest of the reference frame. When Lorentz transformation is applied on the particle, i.e., the properties of particles such as spin and magnetic moment are boosted or rotated, the coupling of backgrounds to particles changes without affecting the background. As a result, Lorentz symmetry breaks under particle Lorentz transformation. But under observer Lorentz transformation, both backgrounds and the properties of the considered particles change as a consequence of Lorentz invariance of the theory. Lorentz invariance violation can happen in a spontaneous way when the tensor field in vacuum gets some non-zero vacuum expectation values [121].

However, Lorentz violation can happen in an explicit breaking process. Spontaneous breaking of Lorentz symmetry believed to be suppressed by a Planck mass scale. Standard model extension (SME) is a broad theory includes the Lorentz

violation of all particles. It includes all possible terms for CPT violation and LIV. Possible re-normalizable LIV terms in Lagrangian can be written as [226]

$$\mathcal{L}' \supseteq \frac{\eta}{(m_p)^k} \langle T \rangle \, \Gamma \bar{\psi} (i\partial)^k \psi + h.c., \tag{B.1}$$

where η is the dimensionless coupling constant, m_p is the Planck mass, $\langle T \rangle$ is the VEV for the tensors, Γ is the notation for the tensors and k is an integral power term which defines the re-normalizable condition. Considering only re-normalizable gauge invariant terms for the value of $K \leqslant 1$, effective Lagrangian can be written as the combination of CPT violating and conserving terms [227]

$$\begin{aligned}
\mathcal{L}' &= \frac{1}{2}\left(\mathcal{L}'_{\text{CPT violating}} + \mathcal{L}'_{\text{CPT conserving}}\right), && \text{(B.2)}\\
\mathcal{L}'_{\text{CPT violating}} &= p_\mu \bar{\psi}\gamma^\mu\psi + q_\mu \bar{\psi}\gamma_5\gamma^\mu\psi + h.c., && \text{(B.3)}\\
\mathcal{L}'_{\text{CPT conserving}} &= i r_{\mu\nu} \bar{\psi}\gamma^\mu\partial^\nu\psi + i s_{\mu\nu} \bar{\psi}\gamma_5\gamma^\mu\partial^\nu\psi + h.c., && \text{(B.4)}\\
&= \frac{1}{4} r_{\mu\nu} \bar{\psi}\gamma^\mu\gamma^\nu(i\not{\partial})\psi + \frac{1}{4} s_{\mu\nu} \bar{\psi}\gamma_5\gamma^\mu\gamma^\nu(i\not{\partial})\psi + h.c., && \text{(B.5)}
\end{aligned}$$

where p_μ and q_μ are CPT violating and Lorentz violating parameters while $r_{\mu\nu}$ and $s_{\mu\nu}$ are CPT conserving Lorentz violating parameters. CPT conserving Lagrangian demands the tensors $r_{\mu\nu}$ and $s_{\mu\nu}$ are to be antisymmetric. For weak interactions of neutrinos, charge conjugation of Lagrangian should be invariant which consequences,

$$\begin{aligned}
p_\mu &= -C p_\mu^T C^{-1}, && \text{(B.6)}\\
q_\mu &= C q_\mu^T C^{-1}, && \text{(B.7)}\\
r_{\mu\nu} &= C r_{\mu\nu}^T C^{-1}, && \text{(B.8)}\\
s_{\mu\nu} &= -C s_{\mu\nu}^T C^{-1}. && \text{(B.9)}
\end{aligned}$$

These LIV parameters are very insignificant for experimental observation. Needs redefinition of LIV parameters as left and right handed parameters similar to existence of left handed neutrino and right handed anti-neutrino,

$$\begin{aligned}
a_L &= p + q, && \text{(B.10)}\\
a_R &= p - q, && \text{(B.11)}\\
c_L &= r + s, && \text{(B.12)}\\
c_R &= r - s. && \text{(B.13)}
\end{aligned}$$

Using the Equation B.6 and B.7, one can calculate the relation between the left and right handed parameters as

$$\langle a_L \rangle = \left\langle \Psi \middle| a_L \middle| \Psi \right\rangle = \left\langle \middle| \Psi C a_L^T C^{-1} \middle| \Psi \right\rangle , \tag{B.14}$$

$$\langle a_L \rangle = \left\langle \Psi \middle| C p^T C^{-1} + C q^T C^{-1} \middle| \Psi \right\rangle = \left\langle \Psi \middle| -p+q \middle| \Psi \right\rangle , \tag{B.15}$$

$$= -\left\langle \Psi \middle| p-q \middle| \Psi \right\rangle = -\left\langle \Psi^c \middle| C a_R C \middle| \Psi^c \right\rangle , \tag{B.16}$$

$$= -\langle a_R \rangle . \tag{B.17}$$

Similarly for the c_L and c_R using Equation B.8 and B.9 ,

$$\langle c_L \rangle = \left\langle \Psi \middle| c_L \middle| \Psi \right\rangle = \left\langle \middle| \Psi C c_L^T C^{-1} \middle| \Psi \right\rangle , \tag{B.18}$$

$$\langle c_L \rangle = \left\langle \Psi \middle| C r^T C^{-1} + C s^T C^{-1} \middle| \Psi \right\rangle = \left\langle \Psi \middle| r-s \middle| \Psi \right\rangle , \tag{B.19}$$

$$= \left\langle \Psi \middle| r-s \middle| \Psi \right\rangle = \left\langle \Psi^c \middle| C c_R C \middle| \Psi^c \right\rangle , \tag{B.20}$$

$$= -\langle c_R \rangle . \tag{B.21}$$

From Equation B.17 and B.21, it is clear that under charge conjugation if we are transforming neutrino to anti-neutrino, the CPT conserving LIV parameters (c) do not change the sign while CPT violating parameters (a) change their sign. This property is useful during calculation of neutrino oscillation for neutrino and anti-neutrino cases.

Bibliography

[1] S. L. Glashow, "*Partial Symmetries of Weak Interactions*," Nucl. Phys. **22** (1961) 579–588.

[2] A. Salam and J. C. Ward, "*Weak and electromagnetic interactions*," Nuovo Cim. **11** (1959) 568–577.

[3] S. Weinberg, "*A Model of Leptons*," Phys. Rev. Lett. **19** (1967) 1264–1266.

[4] F. Englert and R. Brout, "*Broken Symmetry and the Mass of Gauge Vector Mesons*," Phys. Rev. Lett. **13** (1964) 321–323.

[5] P. W. Higgs, "*Broken symmetries, massless particles and gauge fields*," Phys. Lett. **12** (1964) 132–133.

[6] P. W. Higgs, "*Broken Symmetries and the Masses of Gauge Bosons*," Phys. Rev. Lett. **13** (1964) 508–509.

[7] G. S. Guralnik, C. R. Hagen, and T. W. B. Kibble, "*Global Conservation Laws and Massless Particles*," Phys. Rev. Lett. **13** (1964) 585–587.

[8] S. M. Bilenky, "*Neutrino. History of a unique particle*," Eur. Phys. J. H **38** (2013) 345–404, `arXiv:1210.3065`.

[9] F. Reines and C. L. Cowan, "*Detection of the free neutrino*," Phys. Rev. **92** (1953) 830–831.

[10] S. Weinberg, "*Baryon and Lepton Nonconserving Processes*," Phys. Rev. Lett. **43** (1979) 1566–1570.

[11] P. Minkowski, "$\mu \to e\gamma$ *at a Rate of One Out of* 10^9 *Muon Decays?*," Phys. Lett. B **67** (1977) 421–428.

[12] R. N. Mohapatra and G. Senjanovic, "*Neutrino Mass and Spontaneous Parity Nonconservation*," Phys. Rev. Lett. **44** (1980) 912.

[13] R. N. Mohapatra and P. B. Pal, *Massive neutrinos in physics and astrophysics*, vol. 41. 1991.

[14] E. Ma, "*Neutrino Mass: Mechanisms and Models*," arXiv:0905.0221.

[15] E. Ma and U. Sarkar, "*Neutrino masses and leptogenesis with heavy Higgs triplets*," Phys. Rev. Lett. **80** (1998) 5716–5719, arXiv:hep-ph/9802445.

[16] A. Abada, C. Biggio, F. Bonnet, M. B. Gavela, and T. Hambye, "*mu —> e gamma and tau —> l gamma decays in the fermion triplet seesaw model*," Phys. Rev. D **78** (2008) 033007, arXiv:0803.0481.

[17] A. G. Dias, C. A. de S. Pires, P. S. Rodrigues da Silva, and A. Sampieri, "*A Simple Realization of the Inverse Seesaw Mechanism*," Phys. Rev. D **86** (2012) 035007, arXiv:1206.2590.

[18] A. Zee, "*A Theory of Lepton Number Violation, Neutrino Majorana Mass, and Oscillation*," Phys. Lett. B **93** (1980) 389. [Erratum: Phys.Lett.B 95, 461 (1980)].

[19] A. Zee, "*Quantum Numbers of Majorana Neutrino Masses*," Nucl. Phys. B **264** (1986) 99–110.

[20] K. S. Babu, "*Model of 'Calculable' Majorana Neutrino Masses*," Phys. Lett. B **203** (1988) 132–136.

[21] E. Ma, "*Verifiable radiative seesaw mechanism of neutrino mass and dark matter*," Phys. Rev. D **73** (2006) 077301, arXiv:hep-ph/0601225.

[22] S. R. Elliott, A. A. Hahn, and M. K. Moe, "*Direct Evidence for Two Neutrino Double Beta Decay in* ^{82}*Se*," Phys. Rev. Lett. **59** (1987) 2020–2023.

[23] **NEMO**, R. Arnold *et al.*, "*Double beta decay of Se-82*," Nucl. Phys. A **636** (1998) 209–223.

[24] **KamLAND-Zen**, A. Gando *et al.*, "*Search for Majorana Neutrinos near the Inverted Mass Hierarchy Region with KamLAND-Zen*," Phys. Rev. Lett. **117** (2016) no. 8, 082503, arXiv:1605.02889. [Addendum: Phys.Rev.Lett. 117, 109903 (2016)].

[25] **GERDA**, M. Agostini *et al.*, "*Improved Limit on Neutrinoless Double-β Decay of ^{76}Ge from GERDA Phase II*," Phys. Rev. Lett. **120** (2018) no. 13, 132503, arXiv:1803.11100.

[26] **EXO-200**, J. B. Albert *et al.*, "*Search for Majorana neutrinos with the first two years of EXO-200 data*," Nature **510** (2014) 229–234, arXiv:1402.6956.

[27] **CUORE**, C. Alduino *et al.*, "*First Results from CUORE: A Search for Lepton Number Violation via $0\nu\beta\beta$ Decay of ^{130}Te*," Phys. Rev. Lett. **120** (2018) no. 13, 132501, arXiv:1710.07988.

[28] M. Doi, T. Kotani, and E. Takasugi, "*Double beta Decay and Majorana Neutrino*," Prog. Theor. Phys. Suppl. **83** (1985) 1.

[29] W. C. Haxton and G. J. Stephenson, "*Double beta Decay*," Prog. Part. Nucl. Phys. **12** (1984) 409–479.

[30] **GERDA**, M. Agostini *et al.*, "*Results on Neutrinoless Double-β Decay of ^{76}Ge from Phase I of the GERDA Experiment*," Phys. Rev. Lett. **111** (2013) no. 12, 122503, arXiv:1307.4720.

[31] **EXO-200**, J. B. Albert *et al.*, "*Search for Majorana neutrinos with the first two years of EXO-200 data*," Nature **510** (2014) 229–234, arXiv:1402.6956.

[32] B. Pontecorvo, "*Neutrino Experiments and the Problem of Conservation of Leptonic Charge*," Zh. Eksp. Teor. Fiz. **53** (1967) 1717–1725.

[33] M. C. Gonzalez-Garcia and Y. Nir, "*Neutrino Masses and Mixing: Evidence and Implications*," Rev. Mod. Phys. **75** (2003) 345–402, arXiv:hep-ph/0202058.

[34] P. Hernandez, "*Neutrino physics*," in *5th CERN - Latin American School of High-Energy Physics*. 10, 2010. arXiv:1010.4131.

[35] I. Esteban, M. C. Gonzalez-Garcia, M. Maltoni, T. Schwetz, and A. Zhou, "*The fate of hints: updated global analysis of three-flavor neutrino oscillations*," JHEP **09** (2020) 178, arXiv:2007.14792.

[36] L. Wolfenstein, "*Neutrino Oscillations in Matter*," Phys. Rev. D **17** (1978) 2369–2374.

[37] L. Wolfenstein, "*Neutrino Oscillations and Stellar Collapse*," Phys. Rev. D **20** (1979) 2634–2635.

[38] S. P. Mikheyev and A. Y. Smirnov, "*Resonance Amplification of Oscillations in Matter and Spectroscopy of Solar Neutrinos*," Sov. J. Nucl. Phys. **42** (1985) 913–917.

[39] S. P. Mikheev and A. Y. Smirnov, "*Resonant amplification of neutrino oscillations in matter and solar neutrino spectroscopy*," Nuovo Cim. C **9** (1986) 17–26.

[40] T. Ohlsson and H. Snellman, "*Three flavor neutrino oscillations in matter*," J. Math. Phys. **41** (2000) 2768–2788, `arXiv:hep-ph/9910546`. [Erratum: J.Math.Phys. 42, 2345 (2001)].

[41] M. Freund, "*Analytic approximations for three neutrino oscillation parameters and probabilities in matter*," Phys. Rev. D **64** (2001) 053003, `arXiv:hep-ph/0103300`.

[42] E. K. Akhmedov, R. Johansson, M. Lindner, T. Ohlsson, and T. Schwetz, "*Series expansions for three flavor neutrino oscillation probabilities in matter*," JHEP **04** (2004) 078, `arXiv:hep-ph/0402175`.

[43] M. Freund, M. Lindner, S. T. Petcov, and A. Romanino, "*Very long baseline neutrino oscillation experiments and the MSW effect*," Nucl. Instrum. Meth. A **451** (2000) 18–35.

[44] S. K. Agarwalla, "*Physics Potential of Long-Baseline Experiments*," Adv. High Energy Phys. **2014** (2014) 457803, `arXiv:1401.4705`.

[45] H. A. Bethe and C. L. Critchfield, "*The formation of deuterium by proton combination*," Phys. Rev. **54** (1938) 248–254.

[46] **BOREXINO**, M. Agostini *et al.*, "*Comprehensive measurement of pp-chain solar neutrinos*," Nature **562** (2018) no. 7728, 505–510.

[47] H. A. Bethe, "*Energy production in stars*," Phys. Rev. **55** (1939) 434–456.

[48] W. C. Haxton, "*Solar neutrinos: Models, observations, and new opportunities*," Publ. Astron. Soc. Austral. **25** (2008) 44–51, `arXiv:0710.2295`.

[49] L. Miramonti, "*Solar neutrino detection*," AIP Conf. Proc. **1123** (2009) no. 1, 166–173, arXiv:0901.3443.

[50] A. M. Serenelli, W. C. Haxton, and C. Pena-Garay, "*Solar models with accretion. I. Application to the solar abundance problem*," Astrophys. J. **743** (2011) 24, arXiv:1104.1639.

[51] B. T. Cleveland, T. Daily, R. Davis, Jr., J. R. Distel, K. Lande, C. K. Lee, P. S. Wildenhain, and J. Ullman, "*Measurement of the solar electron neutrino flux with the Homestake chlorine detector*," Astrophys. J. **496** (1998) 505–526.

[52] C. Pena-Garay and A. Serenelli, "*Solar neutrinos and the solar composition problem*," arXiv:0811.2424.

[53] **GNO**, M. Altmann *et al.*, "*Complete results for five years of GNO solar neutrino observations*," Phys. Lett. B **616** (2005) 174–190, arXiv:hep-ex/0504037.

[54] **SAGE**, J. N. Abdurashitov *et al.*, "*Measurement of the solar neutrino capture rate with gallium metal. III: Results for the 2002–2007 data-taking period*," Phys. Rev. C **80** (2009) 015807, arXiv:0901.2200.

[55] **Super-Kamiokande**, K. Abe *et al.*, "*Solar Neutrino Measurements in Super-Kamiokande-IV*," Phys. Rev. D **94** (2016) no. 5, 052010, arXiv:1606.07538.

[56] N. Vinyoles, A. M. Serenelli, F. L. Villante, S. Basu, J. Bergström, M. C. Gonzalez-Garcia, M. Maltoni, C. Peña Garay, and N. Song, "*A new Generation of Standard Solar Models*," Astrophys. J. **835** (2017) no. 2, 202, arXiv:1611.09867.

[57] **SNO**, B. Aharmim *et al.*, "*Combined Analysis of all Three Phases of Solar Neutrino Data from the Sudbury Neutrino Observatory*," Phys. Rev. C **88** (2013) 025501, arXiv:1109.0763.

[58] C. V. Achar *et al.*, "*Detection of muons produced by cosmic ray neutrinos deep underground*," Phys. Lett. **18** (1965) 196–199.

[59] **Kamiokande-II**, K. S. Hirata *et al.*, "*Experimental Study of the Atmospheric Neutrino Flux*," Phys. Lett. B **205** (1988) 416.

[60] D. Casper *et al.*, "*Measurement of atmospheric neutrino composition with IMB-3*," Phys. Rev. Lett. **66** (1991) 2561–2564.

[61] **Frejus**, K. Daum *et al.*, "*Determination of the atmospheric neutrino spectra with the Frejus detector*," Z. Phys. C **66** (1995) 417–428.

[62] **NUSEX**, M. Aglietta *et al.*, "*Experimental study of atmospheric neutrino flux in the NUSEX experiment*," EPL **8** (1989) 611–614.

[63] **Kamiokande-II**, K. S. Hirata *et al.*, "*Observation of a small atmospheric muon-neutrino / electron-neutrino ratio in Kamiokande*," Phys. Lett. B **280** (1992) 146–152.

[64] **Kamiokande**, Y. Fukuda *et al.*, "*Atmospheric muon-neutrino / electron-neutrino ratio in the multiGeV energy range*," Phys. Lett. B **335** (1994) 237–245.

[65] **Super-Kamiokande**, Y. Fukuda *et al.*, "*Evidence for oscillation of atmospheric neutrinos*," Phys. Rev. Lett. **81** (1998) 1562–1567, arXiv:hep-ex/9807003.

[66] J. A. Formaggio and G. P. Zeller, "*From eV to EeV: Neutrino Cross Sections Across Energy Scales*," Rev. Mod. Phys. **84** (2012) 1307–1341, arXiv:1305.7513.

[67] J. L. Hewett *et al.*, "*Planning the Future of U.S. Particle Physics (Snowmass 2013): Chapter 2: Intensity Frontier*," in *Community Summer Study 2013: Snowmass on the Mississippi*. 1, 2014. arXiv:1401.6077.

[68] **Borexino**, C. Arpesella *et al.*, "*First real time detection of Be-7 solar neutrinos by Borexino*," Phys. Lett. B **658** (2008) 101–108, arXiv:0708.2251.

[69] **OPERA**, N. Agafonova *et al.*, "*Final Results of the OPERA Experiment on ν_τ Appearance in the CNGS Neutrino Beam*," Phys. Rev. Lett. **120** (2018) no. 21, 211801, arXiv:1804.04912. [Erratum: Phys.Rev.Lett. 121, 139901 (2018)].

[70] **IceCube**, M. G. Aartsen *et al.*, "*Measurement of Atmospheric Tau Neutrino Appearance with IceCube DeepCore*," Phys. Rev. D **99** (2019) no. 3, 032007, arXiv:1901.05366.

[71] **Double Chooz**, F. Ardellier *et al.*, "*Double Chooz: A Search for the neutrino mixing angle theta(13)*," arXiv:hep-ex/0606025.

[72] **Daya Bay**, X. Guo *et al.*, "*A Precision measurement of the neutrino mixing angle θ_{13} using reactor antineutrinos at Daya-Bay*," arXiv:hep-ex/0701029.

[73] **RENO**, J. K. Ahn *et al.*, "*RENO: An Experiment for Neutrino Oscillation Parameter θ_{13} Using Reactor Neutrinos at Yonggwang*," arXiv:1003.1391.

[74] **NEOS**, Y. J. Ko *et al.*, "*Sterile Neutrino Search at the NEOS Experiment*," Phys. Rev. Lett. **118** (2017) no. 12, 121802, arXiv:1610.05134.

[75] D. Beavis, A. Carroll, I. Chiang, and E. Collaboration, "*Long baseline neutrino oscillation experiment at the AGS. Physics design report*,". https://www.osti.gov/biblio/52878.

[76] X. Qian and P. Vogel, "*Neutrino Mass Hierarchy*," Prog. Part. Nucl. Phys. **83** (2015) 1–30, arXiv:1505.01891.

[77] R. N. Mohapatra *et al.*, "*Theory of neutrinos: A White paper*," Rept. Prog. Phys. **70** (2007) 1757–1867, arXiv:hep-ph/0510213.

[78] G. Barenboim, L. Borissov, and J. D. Lykken, "*CPT Violating Neutrinos in the Light of KamLAND*," arXiv:hep-ph/0212116.

[79] **MINOS**, P. Adamson *et al.*, "*Measurement of Neutrino and Antineutrino Oscillations Using Beam and Atmospheric Data in MINOS*," Phys. Rev. Lett. **110** (2013) no. 25, 251801, arXiv:1304.6335.

[80] G. L. Fogli, E. Lisi, A. Marrone, D. Montanino, A. Palazzo, and A. M. Rotunno, "*Global analysis of neutrino masses, mixings and phases: entering the era of leptonic CP violation searches*," Phys. Rev. D **86** (2012) 013012, arXiv:1205.5254.

[81] M. C. Gonzalez-Garcia, M. Maltoni, and T. Schwetz, "*Global Analyses of Neutrino Oscillation Experiments*," Nucl. Phys. B **908** (2016) 199–217, arXiv:1512.06856.

[82] M. Fukugita and T. Yanagida, "*Baryogenesis Without Grand Unification*," Phys. Lett. B **174** (1986) 45–47.

[83] A. S. Joshipura, E. A. Paschos, and W. Rodejohann, "*A Simple connection between neutrino oscillation and leptogenesis*," JHEP **08** (2001) 029, arXiv:hep-ph/0105175.

[84] S. S. Chatterjee and A. Palazzo, "*Nonstandard Neutrino Interactions as a Solution to the NOνA and T2K Discrepancy*," Phys. Rev. Lett. **126** (2021) no. 5, 051802, arXiv:2008.04161.

[85] **LSND**, A. Aguilar-Arevalo *et al.*, "*Evidence for neutrino oscillations from the observation of $\bar{\nu}_e$ appearance in a $\bar{\nu}_\mu$ beam*," Phys. Rev. D **64** (2001) 112007, arXiv:hep-ex/0104049.

[86] **MiniBooNE**, A. A. Aguilar-Arevalo *et al.*, "*Improved Search for $\bar{\nu}_\mu \to \bar{\nu}_e$ Oscillations in the MiniBooNE Experiment*," Phys. Rev. Lett. **110** (2013) 161801, arXiv:1303.2588.

[87] G. Barenboim, C. A. Ternes, and M. Tórtola, "*Neutrinos, DUNE and the world best bound on CPT invariance*," Phys. Lett. B **780** (2018) 631–637, arXiv:1712.01714.

[88] M. A. Tórtola, G. Barenboim, and C. A. Ternes, "*CPT and CP, an entangled couple*," JHEP **07** (2020) 155, arXiv:2005.05975.

[89] J. S. Diaz, V. A. Kostelecky, and M. Mewes, "*Perturbative Lorentz and CPT violation for neutrino and antineutrino oscillations*," Phys. Rev. D **80** (2009) 076007, arXiv:0908.1401.

[90] **Super-Kamiokande**, S. Fukuda *et al.*, "*Solar B-8 and hep neutrino measurements from 1258 days of Super-Kamiokande data*," Phys. Rev. Lett. **86** (2001) 5651–5655, arXiv:hep-ex/0103032.

[91] **SNO**, Q. R. Ahmad *et al.*, "*Measurement of the rate of $\nu_e + d \to p + p + e^-$ interactions produced by ^8B solar neutrinos at the Sudbury Neutrino Observatory*," Phys. Rev. Lett. **87** (2001) 071301, arXiv:nucl-ex/0106015.

[92] **SNO**, Q. R. Ahmad *et al.*, "*Direct evidence for neutrino flavor transformation from neutral current interactions in the Sudbury Neutrino Observatory*," Phys. Rev. Lett. **89** (2002) 011301, arXiv:nucl-ex/0204008.

[93] **SNO**, Q. R. Ahmad *et al.*, "*Measurement of day and night neutrino energy spectra at SNO and constraints on neutrino mixing parameters*," Phys. Rev. Lett. **89** (2002) 011302, arXiv:nucl-ex/0204009.

[94] **Super-Kamiokande**, Y. Fukuda *et al.*, "*Neutrino induced upward stopping muons in Super-Kamiokande*," Phys. Lett. **B467** (1999) 185–193, arXiv:hep-ex/9908049.

[95] **Super-Kamiokande**, S. Fukuda *et al.*, "*Tau neutrinos favored over sterile neutrinos in atmospheric muon-neutrino oscillations*," Phys. Rev. Lett. **85** (2000) 3999–4003, arXiv:hep-ex/0009001.

[96] **CHOOZ**, M. Apollonio *et al.*, "*Initial results from the CHOOZ long baseline reactor neutrino oscillation experiment*," Phys. Lett. **B420** (1998) 397–404, arXiv:hep-ex/9711002.

[97] **Daya Bay**, F. P. An *et al.*, "*Observation of electron-antineutrino disappearance at Daya Bay*," Phys. Rev. Lett. **108** (2012) 171803, arXiv:1203.1669.

[98] **Double Chooz**, Y. Abe *et al.*, "*Indication of Reactor $\bar{\nu}_e$ Disappearance in the Double Chooz Experiment*," Phys. Rev. Lett. **108** (2012) 131801, arXiv:1112.6353.

[99] **RENO**, J. K. Ahn *et al.*, "*Observation of Reactor Electron Antineutrino Disappearance in the RENO Experiment*," Phys. Rev. Lett. **108** (2012) 191802, arXiv:1204.0626.

[100] **KamLAND**, T. Araki *et al.*, "*Measurement of neutrino oscillation with KamLAND: Evidence of spectral distortion*," Phys. Rev. Lett. **94** (2005) 081801, arXiv:hep-ex/0406035.

[101] **KamLAND**, K. Eguchi *et al.*, "*First results from KamLAND: Evidence for reactor anti-neutrino disappearance*," Phys. Rev. Lett. **90** (2003) 021802, arXiv:hep-ex/0212021.

[102] **KamLAND**, S. Abe *et al.*, "*Precision Measurement of Neutrino Oscillation Parameters with KamLAND*," Phys. Rev. Lett. **100** (2008) 221803, arXiv:0801.4589.

[103] **OPERA**, N. Agafonova *et al.*, "*Final Results of the OPERA Experiment on ν_τ Appearance in the CNGS Neutrino Beam*," Phys. Rev. Lett. **120** (2018) no. 21, 211801, arXiv:1804.04912. [Erratum: Phys. Rev. Lett.121,no.13,139901(2018)].

[104] **T2K**, K. Abe *et al.*, "*Indication of Electron Neutrino Appearance from an Accelerator-produced Off-axis Muon Neutrino Beam*," Phys. Rev. Lett. **107** (2011) 041801, arXiv:1106.2822.

[105] **NOvA**, P. Adamson *et al.*, "*First measurement of electron neutrino appearance in NOvA*," Phys. Rev. Lett. **116** (2016) no. 15, 151806, arXiv:1601.05022.

[106] **LSND**, A. Aguilar-Arevalo *et al.*, "*Evidence for neutrino oscillations from the observation of anti-neutrino(electron) appearance in a anti-neutrino(muon) beam*," Phys. Rev. **D64** (2001) 112007, arXiv:hep-ex/0104049.

[107] **MiniBooNE**, A. A. Aguilar-Arevalo *et al.*, "*Improved Search for $\bar{\nu}_\mu \to \bar{\nu}_e$ Oscillations in the MiniBooNE Experiment*," Phys. Rev. Lett. **110** (2013) 161801, arXiv:1303.2588.

[108] **MiniBooNE**, A. A. Aguilar-Arevalo *et al.*, "*Significant Excess of ElectronLike Events in the MiniBooNE Short-Baseline Neutrino Experiment*," Phys. Rev. Lett. **121** (2018) no. 22, 221801, arXiv:1805.12028.

[109] T. Lasserre, "*Testing the Reactor and Gallium Anomalies with Intense (Anti)Neutrino Emitters*," Nucl. Phys. Proc. Suppl. **235-236** (2013) 214–219, arXiv:1209.5090.

[110] G. Mention, M. Fechner, T. Lasserre, T. A. Mueller, D. Lhuillier, M. Cribier, and A. Letourneau, "*The Reactor Antineutrino Anomaly*," Phys. Rev. **D83** (2011) 073006, arXiv:1101.2755.

[111] **NEOS**, Y. J. Ko *et al.*, "*Sterile Neutrino Search at the NEOS Experiment*," Phys. Rev. Lett. **118** (2017) no. 12, 121802, arXiv:1610.05134.

[112] **DANSS**, I. Alekseev *et al.*, "*Search for sterile neutrinos at the DANSS experiment*," Phys. Lett. **B787** (2018) 56–63, arXiv:1804.04046.

[113] **PROSPECT**, J. Ashenfelter *et al.*, "*First search for short-baseline neutrino oscillations at HFIR with PROSPECT*," Phys. Rev. Lett. **121** (2018) no. 25, 251802, arXiv:1806.02784.

[114] D. Lhuillier, "*Future short-baseline sterile neutrino searches with reactors*," AIP Conf. Proc. **1666** (2015) no. 1, 180003.

[115] **GALLEX**, P. Anselmann *et al.*, "*First results from the Cr-51 neutrino source experiment with the GALLEX detector*," Phys. Lett. **B342** (1995) 440–450.

[116] **GALLEX**, W. Hampel *et al.*, "*Final results of the Cr-51 neutrino source experiments in GALLEX*," Phys. Lett. **B420** (1998) 114–126.

[117] F. Kaether, W. Hampel, G. Heusser, J. Kiko, and T. Kirsten, "*Reanalysis of the GALLEX solar neutrino flux and source experiments*," Phys. Lett. **B685** (2010) 47–54, arXiv:1001.2731.

[118] D. Abdurashitov *et al.*, "*The Russian-American gallium experiment (SAGE) Cr neutrino source measurement*," Phys. Rev. Lett. **77** (1996) 4708–4711.

[119] C. Giunti, M. Laveder, Y. F. Li, Q. Y. Liu, and H. W. Long, "*Update of Short-Baseline Electron Neutrino and Antineutrino Disappearance*," Phys. Rev. **D86** (2012) 113014, arXiv:1210.5715.

[120] C. Giunti and M. Laveder, "*Statistical Significance of the Gallium Anomaly*," Phys. Rev. **C83** (2011) 065504, arXiv:1006.3244.

[121] K. N. Abazajian *et al.*, "*Light Sterile Neutrinos: A White Paper*," arXiv:1204.5379.

[122] **SAGE**, J. N. Abdurashitov *et al.*, "*Measurement of the solar neutrino capture rate with gallium metal. III: Results for the 2002–2007 data-taking period*," Phys. Rev. **C80** (2009) 015807, arXiv:0901.2200.

[123] **ALEPH, DELPHI, L3, OPAL, SLD, LEP Electroweak Working Group, SLD Electroweak Group, SLD Heavy Flavour Group**, S. Schael *et al.*, "*Precision electroweak measurements on the Z resonance*," Phys. Rept. **427** (2006) 257–454, arXiv:hep-ex/0509008.

[124] **MINOS+**, P. Adamson *et al.*, "*Search for sterile neutrinos in MINOS and MINOS+ using a two-detector fit*," Phys. Rev. Lett. **122** (2019) no. 9, 091803, arXiv:1710.06488.

[125] **NOvA**, M. A. Acero *et al.*, "*New constraints on oscillation parameters from ν_e appearance and ν_μ disappearance in the NOvA experiment*," Phys. Rev. **D98** (2018) 032012, arXiv:1806.00096.

[126] **MicroBooNE**, P. Abratenko *et al.*, "*Search for an Excess of Electron Neutrino Interactions in MicroBooNE Using Multiple Final-State Topologies*," Phys. Rev. Lett. **128** (2022) no. 24, 241801, arXiv:2110.14054.

[127] P. B. Denton, "*Sterile Neutrino Searches with MicroBooNE: Electron Neutrino Disappearance*," arXiv:2111.05793.

[128] D. Dutta, R. Gandhi, B. Kayser, M. Masud, and S. Prakash, "*Capabilities of long-baseline experiments in the presence of a sterile neutrino*," JHEP **11** (2016) 122, arXiv:1607.02152.

[129] S. K. Agarwalla, S. S. Chatterjee, and A. Palazzo, "*Signatures of a Light Sterile Neutrino in T2HK*," JHEP **04** (2018) 091, arXiv:1801.04855.

[130] S. Gupta, Z. M. Matthews, P. Sharma, and A. G. Williams, "*The Effect of a Light Sterile Neutrino at NOνA and DUNE*," Phys. Rev. **D98** (2018) no. 3, 035042, arXiv:1804.03361.

[131] M. Ghosh, S. Gupta, Z. M. Matthews, P. Sharma, and A. G. Williams, "*Study of parameter degeneracy and hierarchy sensitivity of NOνA in presence of sterile neutrino*," Phys. Rev. **D96** (2017) no. 7, 075018, arXiv:1704.04771.

[132] S. K. Agarwalla, S. S. Chatterjee, A. Dasgupta, and A. Palazzo, "*Discovery Potential of T2K and NOvA in the Presence of a Light Sterile Neutrino*," JHEP **02** (2016) 111, arXiv:1601.05995.

[133] A. Palazzo, "*3-flavor and 4-flavor implications of the latest T2K and NOνA electron (anti-)neutrino appearance results*," Phys. Lett. **B757** (2016) 142–147, arXiv:1509.03148.

[134] **T2K**, D. Dewhurst, "*Searches for Sterile Neutrinos Using the T2K Off-Axis Near Detector*," in *Proceedings, Topical Research Meeting on Prospects in Neutrino Physics (NuPhys2014): London, UK, December 15-17, 2014*. 2015. arXiv:1504.08237.

[135] B. Bhattacharya, A. M. Thalapillil, and C. E. M. Wagner, "*Implications of sterile neutrinos for medium/long-baseline neutrino experiments and the determination of θ_{13}*," Phys. Rev. **D85** (2012) 073004, arXiv:1111.4225.

[136] A. Chatla, S. Rudrabhatla, and B. A. Bambah, "*Degeneracy Resolution Capabilities of NOνA and DUNE in the Presence of Light Sterile Neutrino*," Adv. High Energy Phys. **2018** (2018) 2547358, arXiv:1804.02818.

[137] S. Choubey, D. Dutta, and D. Pramanik, "*Imprints of a light Sterile Neutrino at DUNE, T2HK and T2HKK*," Phys. Rev. **D96** (2017) no. 5, 056026, arXiv:1704.07269.

[138] S. K. Agarwalla, S. S. Chatterjee, and A. Palazzo, "*Physics Reach of DUNE with a Light Sterile Neutrino*," JHEP **09** (2016) 016, arXiv:1603.03759.

[139] J. M. Berryman, A. de Gouva, K. J. Kelly, and A. Kobach, "*Sterile neutrino at the Deep Underground Neutrino Experiment*," Phys. Rev. **D92** (2015) no. 7, 073012, arXiv:1507.03986.

[140] S. Choubey, D. Dutta, and D. Pramanik, "*Measuring the Sterile Neutrino CP Phase at DUNE and T2HK*," Eur. Phys. J. **C78** (2018) no. 4, 339, arXiv:1711.07464.

[141] R. Gandhi, B. Kayser, M. Masud, and S. Prakash, "*The impact of sterile neutrinos on CP measurements at long baselines*," JHEP **11** (2015) 039, arXiv:1508.06275.

[142] P. F. de Salas, D. V. Forero, C. A. Ternes, M. Tortola, and J. W. F. Valle, "*Status of neutrino oscillations 2018: 3σ hint for normal mass ordering and improved CP sensitivity*," Phys. Lett. **B782** (2018) 633–640, arXiv:1708.01186.

[143] W. Li, J. Ling, F. Xu, and B. Yue, "*Matter Effect of Light Sterile Neutrino: An Exact Analytical Approach*," JHEP **10** (2018) 021, arXiv:1808.03985.

[144] I. Esteban, M. C. Gonzalez-Garcia, A. Hernandez-Cabezudo, M. Maltoni, and T. Schwetz, "*Global analysis of three-flavour neutrino oscillations: synergies and tensions in the determination of θ_{23}, δ_{CP}, and the mass ordering*," JHEP **01** (2019) 106, arXiv:1811.05487.

[145] S. Gariazzo, C. Giunti, M. Laveder, and Y. F. Li, "*Updated Global 3+1 Analysis of Short-BaseLine Neutrino Oscillations*," JHEP **06** (2017) 135, arXiv:1703.00860.

[146] P. Huber, M. Lindner, and W. Winter, "*Simulation of long-baseline neutrino oscillation experiments with GLoBES (General Long Baseline Experiment Simulator)*," Comput. Phys. Commun. **167** (2005) 195, arXiv:hep-ph/0407333.

[147] P. Huber, J. Kopp, M. Lindner, M. Rolinec, and W. Winter, "*New features in the simulation of neutrino oscillation experiments with GLoBES 3.0: General Long Baseline Experiment Simulator*," Comput. Phys. Commun. **177** (2007) 432–438, arXiv:hep-ph/0701187.

[148] J. Kopp, "*Efficient numerical diagonalization of hermitian 3 x 3 matrices*," Int. J. Mod. Phys. C **19** (2008) 523–548, arXiv:physics/0610206.

[149] S. C, K. N. Deepthi, and R. Mohanta, "*A comprehensive study of the discovery potential of NOvA, T2K and T2HK experiments*," Adv. High Energy Phys. **2016** (2016) 9139402, arXiv:1408.6071.

[150] **T2K**, K. Abe *et al.*, "*Combined Analysis of Neutrino and Antineutrino Oscillations at T2K*," Phys. Rev. Lett. **118** (2017) no. 15, 151801, arXiv:1701.00432.

[151] **T2K**, K. Abe *et al.*, "*Neutrino oscillation physics potential of the T2K experiment*," PTEP **2015** (2015) no. 4, 043C01, arXiv:1409.7469.

[152] G.-Y. Huang and S. Zhou, "*Impact of an eV-mass sterile neutrino on the neutrinoless double-beta decays: A Bayesian analysis*," Nucl. Phys. **B945** (2019) 114691, arXiv:1902.03839.

[153] **Planck**, P. A. R. Ade *et al.*, "*Planck 2015 results. XIII. Cosmological parameters*," Astron. Astrophys. **594** (2016) A13, arXiv:1502.01589.

[154] M. Agostini, G. Benato, and J. Detwiler, "*Discovery probability of next-generation neutrinoless double- β decay experiments*," Phys. Rev. D **96** (2017) no. 5, 053001, arXiv:1705.02996.

[155] K. N. Vishnudath, S. Choubey, and S. Goswami, "*New sensitivity goal for neutrinoless double beta decay experiments*," Phys. Rev. **D99** (2019) no. 9, 095038, arXiv:1901.04313.

[156] **nEXO**, S. A. Kharusi *et al.*, "*nEXO Pre-Conceptual Design Report*," arXiv:1805.11142.

[157] G. Lders, "*Proof of the TCP theorem*," Annals of Physics **2** (1957) no. 1, 1–15. https://www.sciencedirect.com/science/article/pii/0003491657900325.

[158] V. A. Kostelecky and M. Mewes, "*Lorentz and CPT violation in the neutrino sector*," Phys. Rev. D **70** (2004) 031902, arXiv:hep-ph/0308300.

[159] V. A. Kostelecky and M. Mewes, "*Lorentz and CPT violation in neutrinos*," Phys. Rev. D **69** (2004) 016005, arXiv:hep-ph/0309025.

[160] H. Minakata and S. Uchinami, "*Testing CPT symmetry with supernova neutrinos*," Phys. Rev. D **72** (2005) 105007, arXiv:hep-ph/0505133.

[161] A. de Gouvea and Y. Grossman, "*A Three-flavor, Lorentz-violating solution to the LSND anomaly*," Phys. Rev. D **74** (2006) 093008, arXiv:hep-ph/0602237.

[162] J. S. Diaz and A. Kostelecky, "*Lorentz- and CPT-violating models for neutrino oscillations*," Phys. Rev. D **85** (2012) 016013, arXiv:1108.1799.

[163] A. Kostelecky and M. Mewes, "*Neutrinos with Lorentz-violating operators of arbitrary dimension*," Phys. Rev. D **85** (2012) 096005, arXiv:1112.6395.

[164] J. S. Díaz, T. Katori, J. Spitz, and J. M. Conrad, "*Search for neutrino-antineutrino oscillations with a reactor experiment*," Phys. Lett. B **727** (2013) 412–416, arXiv:1307.5789.

[165] M. Jacobson and T. Ohlsson, "*Extrinsic CPT violation in neutrino oscillations in matter*," Phys. Rev. D **69** (2004) 013003, arXiv:hep-ph/0305064.

[166] **Super-Kamiokande**, K. Abe *et al.*, "*Test of Lorentz invariance with atmospheric neutrinos*," Phys. Rev. D **91** (2015) no. 5, 052003, arXiv:1410.4267.

[167] C. A. Argüelles, T. Katori, and J. Salvado, "*New Physics in Astrophysical Neutrino Flavor*," Phys. Rev. Lett. **115** (2015) 161303, arXiv:1506.02043.

[168] J. S. Diaz and T. Schwetz, "*Limits on CPT violation from solar neutrinos*," Phys. Rev. D **93** (2016) no. 9, 093004, arXiv:1603.04468.

[169] R. Majhi, S. Chembra, and R. Mohanta, "*Exploring the effect of Lorentz invariance violation with the currently running long-baseline experiments*," Eur. Phys. J. C **80** (2020) no. 5, 364, arXiv:1907.09145.

[170] D. Kaur, "*Model-independent test for CPT violation using long-baseline and atmospheric neutrino experiments*," Phys. Rev. D **101** (2020) no. 5, 055017, arXiv:2004.00349.

[171] B. Schwingenheuer *et al.*, "*CPT tests in the neutral kaon system*," Phys. Rev. Lett. **74** (1995) 4376–4379.

[172] A. Capolupo, S. M. Giampaolo, and G. Lambiase, "*Decoherence in neutrino oscillations, neutrino nature and CPT violation*," Phys. Lett. B **792** (2019) 298–303, arXiv:1807.07823.

[173] S. M. Bilenky and S. T. Petcov, "*Massive Neutrinos and Neutrino Oscillations*," Rev. Mod. Phys. **59** (1987) 671. [Erratum: Rev.Mod.Phys. 61, 169 (1989), Erratum: Rev.Mod.Phys. 60, 575–575 (1988)].

[174] **Hyper-Kamiokande**, K. Abe *et al.*, "*Physics potentials with the second Hyper-Kamiokande detector in Korea*," PTEP **2018** (2018) no. 6, 063C01, arXiv:1611.06118.

[175] S. K. Agarwalla, S. S. Chatterjee, and A. Palazzo, "*Signatures of a Light Sterile Neutrino in T2HK*," JHEP **04** (2018) 091, arXiv:1801.04855.

[176] **Hyper-Kamiokande**, K. Abe *et al.*, "*Hyper-Kamiokande Design Report*," arXiv:1805.04163.

[177] **ESSnuSB**, E. Baussan *et al.*, "*A very intense neutrino super beam experiment for leptonic CP violation discovery based on the European*

spallation source linac," Nucl. Phys. B **885** (2014) 127–149, arXiv:1309.7022.

[178] **DUNE**, R. Acciarri *et al.*, "*Long-Baseline Neutrino Facility (LBNF) and Deep Underground Neutrino Experiment (DUNE): Conceptual Design Report, Volume 2: The Physics Program for DUNE at LBNF*," arXiv:1512.06148.

[179] A. de Gouvêa and K. J. Kelly, "*Neutrino vs. Antineutrino Oscillation Parameters at DUNE and Hyper-Kamiokande*," Phys. Rev. D **96** (2017) no. 9, 095018, arXiv:1709.06090.

[180] P. Arias, J. Gamboa, J. Lopez-Sarrion, F. Mendez, and A. K. Das, "*CPT / Lorentz invariance violation and neutrino oscillation*," Phys. Lett. **B650** (2007) 401–406, arXiv:hep-ph/0608007.

[181] X. Zhang and B.-Q. Ma, "*Testing Lorentz invariance and CPT symmetry using gamma-ray burst neutrinos*," Phys. Rev. **D99** (2019) no. 4, 043013, arXiv:1810.03571.

[182] R. G. Lang, H. Martínez-Huerta, and V. de Souza, "*Improved limits on Lorentz invariance violation from astrophysical gamma-ray sources*," Phys. Rev. **D99** (2019) no. 4, 043015, arXiv:1810.13215.

[183] **SNO**, B. Aharmim *et al.*, "*Tests of Lorentz invariance at the Sudbury Neutrino Observatory*," Phys. Rev. **D98** (2018) no. 11, 112013, arXiv:1811.00166.

[184] M. Mewes, "*Signals for Lorentz violation in gravitational waves*," Phys. Rev. **D99** (2019) no. 10, 104062, arXiv:1905.00409.

[185] **LIGO Scientific, Virgo**, A. Samajdar, "*Constraints on Lorentz Invariance Violations from Gravitational Wave Observations*," in *8th Meeting on CPT and Lorentz Symmetry (CPT'19) Bloomington, Indiana, USA, May 12-16, 2019*. 2019. arXiv:1906.05933.

[186] H. Martínez-Huerta, "*Lorentz violation constraints with astroparticle physics*," in *8th Meeting on CPT and Lorentz Symmetry (CPT'19) Bloomington, Indiana, USA, May 12-16, 2019*. 2019. arXiv:1906.06293.

[187] Y. Huang, H. Li, and B.-Q. Ma, "*Consistent Lorentz violation features from near-TeV IceCube neutrinos*," Phys. Rev. **D99** (2019) no. 12, 123018, arXiv:1906.07329.

[188] P. Satunin, "*New constraints on Lorentz Invariance violation from Crab Nebula spectrum beyond* 100 *TeV*," Eur. Phys. J. **C79** (2019) no. 12, 1011, arXiv:1906.08221.

[189] **IceCube**, T. Katori, C. A. Argüelles, K. Farrag, and S. Mandalia, "*Test of Lorentz Violation with Astrophysical Neutrino Flavor in IceCube*," in *8th Meeting on CPT and Lorentz Symmetry (CPT'19) Bloomington, Indiana, USA, May 12-16, 2019*. 2019. arXiv:1906.09240.

[190] **Muon g-2**, B. Quinn, "*CPT- and Lorentz-Violation Tests with Muon g-2*," in *8th Meeting on CPT and Lorentz Symmetry (CPT'19) Bloomington, Indiana, USA, May 12-16, 2019*. 2019. arXiv:1907.00162. http://lss.fnal.gov/archive/2019/conf/fermilab-conf-19-303-e.pdf.

[191] **Particle Data Group**, M. Tanabashi *et al.*, "*Review of Particle Physics*," Phys. Rev. **D98** (2018) no. 3, 030001.

[192] T. Ohlsson and S. Zhou, "*Extrinsic and Intrinsic CPT Asymmetries in Neutrino Oscillations*," Nucl. Phys. **B893** (2015) 482–500, arXiv:1408.4722.

[193] J. M. Carmona, J. L. Cortes, A. K. Das, J. Gamboa, and F. Mendez, "*Matter-antimatter asymmetry without departure from thermal equilibrium*," Mod. Phys. Lett. **A21** (2006) 883–892, arXiv:hep-th/0410143.

[194] G. Barenboim, M. Masud, C. A. Ternes, and M. Tórtola, "*Exploring the intrinsic Lorentz-violating parameters at DUNE*," Phys. Lett. **B788** (2019) 308–315, arXiv:1805.11094.

[195] B. Rebel and S. Mufson, "*The Search for Neutrino-Antineutrino Mixing Resulting from Lorentz Invariance Violation using neutrino interactions in MINOS*," Astropart. Phys. **48** (2013) 78–81, arXiv:1301.4684.

[196] V. Antonelli, L. Miramonti, and M. D. C. Torri, "*Neutrino oscillations and Lorentz Invariance Violation in a Finslerian Geometrical model*," Eur. Phys. J. **C78** (2018) no. 8, 667, arXiv:1803.08570.

[197] M. D. C. Torri, V. Antonelli, and L. Miramonti, "*Homogeneously Modified Special relativity (HMSR)*," Eur. Phys. J. **C79** (2019) no. 9, 808, arXiv:1906.05595.

[198] **IceCube**, C. A. Argüelles, "*Search for Lorentz Violation Using High-Energy Atmospheric Neutrinos In IceCube*," in *8th Meeting on CPT and Lorentz Symmetry (CPT'19) Bloomington, Indiana, USA, May 12-16, 2019*. 2019. arXiv:1907.04244.

[199] **IceCube**, M. G. Aartsen *et al.*, "*Neutrino Interferometry for High-Precision Tests of Lorentz Symmetry with IceCube*," Nature Phys. **14** (2018) no. 9, 961–966, arXiv:1709.03434.

[200] W.-M. Dai, Z.-K. Guo, R.-G. Cai, and Y.-Z. Zhang, "*Lorentz invariance violation in the neutrino sector: a joint analysis from big bang nucleosynthesis and the cosmic microwave background*," Eur. Phys. J. **C77** (2017) no. 6, 386, arXiv:1701.02553.

[201] T. Katori, C. A. Argüelles, and J. Salvado, "*Test of Lorentz Violation with Astrophysical Neutrino Flavor*," in *Proceedings, 7th Meeting on CPT and Lorentz Symmetry (CPT 16): Bloomington, Indiana, USA, June 20-24, 2016*, pp. 209–212. 2017. arXiv:1607.08448.

[202] J.-J. Wei, X.-F. Wu, H. Gao, and P. Mészáros, "*Limits on the Neutrino Velocity, Lorentz Invariance, and the Weak Equivalence Principle with TeV Neutrinos from Gamma-Ray Bursts*," JCAP **1608** (2016) no. 08, 031, arXiv:1603.07568.

[203] Z.-Y. Wang, R.-Y. Liu, and X.-Y. Wang, "*Testing the equivalence principle and Lorentz invariance with PeV neutrinos from blazar flares*," Phys. Rev. Lett. **116** (2016) no. 15, 151101, arXiv:1602.06805.

[204] **Super-Kamiokande**, K. Abe *et al.*, "*Test of Lorentz invariance with atmospheric neutrinos*," Phys. Rev. **D91** (2015) no. 5, 052003, arXiv:1410.4267.

[205] A. Chatterjee, R. Gandhi, and J. Singh, "*Probing Lorentz and CPT Violation in a Magnetized Iron Detector using Atmospheric Neutrinos*," JHEP **06** (2014) 045, arXiv:1402.6265.

[206] **LSND, MiniBooNE, Double Chooz**, T. Katori, "*Tests of Lorentz and CPT violation with neutrinos*," PoS **ICHEP2012** (2013) 008, arXiv:1211.7129.

[207] J. S. Diaz, "*Testing Lorentz and CPT invariance with neutrinos*," Symmetry **8** (2016) no. 10, 105, arXiv:1609.09474.

[208] J. S. Diaz, "*Neutrinos as probes of Lorentz invariance*," Adv. High Energy Phys. **2014** (2014) 962410, arXiv:1406.6838.

[209] S.-F. Ge and H. Murayama, "*Apparent CPT Violation in Neutrino Oscillation from Dark Non-Standard Interactions*," arXiv:1904.02518.

[210] A. Higuera, "*Results and Prospects from the Daya Bay Reactor Neutrino Experiment*," in *Proceedings, 7th Meeting on CPT and Lorentz Symmetry (CPT 16): Bloomington, Indiana, USA, June 20-24, 2016*, pp. 77–80. 2017. arXiv:1607.07324.

[211] **Double Chooz**, Y. Abe *et al.*, "*First Test of Lorentz Violation with a Reactor-based Antineutrino Experiment*," Phys. Rev. **D86** (2012) 112009, arXiv:1209.5810.

[212] T. Katori and J. Spitz, "*Testing Lorentz Symmetry with the Double Chooz Experiment*," in *Proceedings, 6th Meeting on CPT and Lorentz Symmetry (CPT 13): Bloomington, Indiana, USA, June 17-21, 2013*, pp. 9–12. 2014. arXiv:1307.5805.

[213] S. Kumar Agarwalla and M. Masud, "*Can Lorentz invariance violation affect the sensitivity of deep underground neutrino experiment?*," Eur. Phys. J. C **80** (2020) no. 8, 716, arXiv:1912.13306.

[214] T. Ohlsson, "*Status of non-standard neutrino interactions*," Rept. Prog. Phys. **76** (2013) 044201, arXiv:1209.2710.

[215] J. Liao, D. Marfatia, and K. Whisnant, "*Degeneracies in long-baseline neutrino experiments from nonstandard interactions*," Phys. Rev. **D93** (2016) no. 9, 093016, arXiv:1601.00927.

[216] J. Kopp, M. Lindner, T. Ota, and J. Sato, "*Non-standard neutrino interactions in reactor and superbeam experiments*," Phys. Rev. **D77** (2008) 013007, arXiv:0708.0152.

[217] A. Chatterjee, F. Kamiya, C. A. Moura, and J. Yu, "*Impact of Matter Density Profile Shape on Non-Standard Interactions at DUNE*," arXiv:1809.09313.

[218] M. Esteves Chaves, D. Rossi Gratieri, and O. L. G. Peres, "*Improvements on perturbative oscillation formulas including non-standard neutrino Interactions*," arXiv:1810.04979.

[219] K. N. Deepthi, S. Goswami, and N. Nath, "*Can nonstandard interactions jeopardize the hierarchy sensitivity of DUNE?*," Phys. Rev. **D96** (2017) no. 7, 075023, arXiv:1612.00784.

[220] K. N. Deepthi, S. Goswami, and N. Nath, "*Challenges posed by non-standard neutrino interactions in the determination of δ_{CP} at DUNE*," Nucl. Phys. **B936** (2018) 91–105, arXiv:1711.04840.

[221] U. K. Dey, N. Nath, and S. Sadhukhan, "*Non-Standard Neutrino Interactions in a Modified ν2HDM*," Phys. Rev. **D98** (2018) no. 5, 055004, arXiv:1804.05808.

[222] O. Yasuda, "*On the exact formula for neutrino oscillation probability by Kimura, Takamura and Yokomakura*," arXiv:0704.1531.

[223] M. Masud, A. Chatterjee, and P. Mehta, "*Probing CP violation signal at DUNE in presence of non-standard neutrino interactions*," J. Phys. **G43** (2016) no. 9, 095005, arXiv:1510.08261.

[224] M. Masud and P. Mehta, "*Nonstandard interactions and resolving the ordering of neutrino masses at DUNE and other long baseline experiments*," Phys. Rev. **D94** (2016) no. 5, 053007, arXiv:1606.05662.

[225] M. Masud and P. Mehta, "*Nonstandard interactions spoiling the CP violation sensitivity at DUNE and other long baseline experiments*," Phys. Rev. **D94** (2016) 013014, arXiv:1603.01380.

[226] V. A. Kostelecky and R. Potting, "*Expectation values, Lorentz invariance, and CPT in the open bosonic string*," Phys. Lett. B **381** (1996) 89–96, arXiv:hep-th/9605088.

[227] D. Colladay and V. A. Kostelecky, "*Lorentz violating extension of the standard model*," Phys. Rev. D **58** (1998) 116002, arXiv:hep-ph/9809521.

List of Publications

Thesis Publications

1. ***"Exploring the effect of Lorentz invariance violation with the currently running long-baseline experiments"***, **R. Majhi**, S. Chembra and R. Mohanta, Eur. Phys. J. C **80**, no.5, 364 (2020) [arXiv:1907.09145 [hep-ph]].

2. ***"Light sterile neutrinos and their implications on currently running long-baseline and neutrinoless double beta decay experiments"***, **R. Majhi**, S. Chembra and R. Mohanta, J. Phys. G **47**, no.9, 095002 (2020) [arXiv:1911.10952 [hep-ph]].

3. ***"Constraining CPT violation with Hyper-Kamiokande and ESSnuSB"***, **R. Majhi**, D. K. Singha, K. N. Deepthi and R. Mohanta, Phys. Rev. D **104**, no.5, 055002 (2021) doi:10.1103/PhysRevD.104.055002 [arXiv:2101.08202 [hep-ph]].

Other Publications

1. ***"Optimal configuration of Protvino to ORCA experiment for hierarchy and non-standard interactions,"*** D. K. Singha, M. Ghosh, **R. Majhi** and R. Mohanta, JHEP **05** (2022), 117 doi:10.1007/JHEP05(2022)117 [arXiv:2112.04876 [hep-ph]].

2. ***"Vector leptoquark U_3 and CP violation at T2K, NOvA experiments,"*** **R. Majhi**, D. K. Singha, K. N. Deepthi and R. Mohanta, [arXiv:2205.04269 [hep-ph]].

Conference Proceedings

1. ***"Impact of Active-Sterile Neutrino Mixing at Currently Running Long-Baseline Experiments"***, **R. Majhi**, S. Chembra and R. Mohanta, Springer Proc. Phys. **234**, 341-345 (2019)

2. ***"Lorentz Invariance Violation and Long Baseline Experiments"***, **R. Majhi**, S. Chembra and R. Mohanta, Springer Proc. Phys. **248**, 349-353 (2020)

3. ***"Physics Potential of Long-Baseline Neutrino Oscillation Experiments in Presence of Sterile Neutrino"***, **R. Majhi**, S. Chembra and R. Mohanta, Springer Proc. Phys. **261**, 521-527 (2021)

EXPLORING PHYSICS BEYOND THE STANDARD MODEL WITH NEUTRINO OSCILLATION

by Rudra Majhi

Submission date: 19-Aug-2022 03:15PM (UTC+0530)
Submission ID: 1884313931
File name: Rudra_Majhi.pdf (33.9M)
Word count: 33671
Character count: 160019

EXPLORING PHYSICS BEYOND THE STANDARD MODEL WITH NEUTRINO OSCILLATION

ORIGINALITY REPORT

47%	45%	41%	3%
SIMILARITY INDEX	INTERNET SOURCES	PUBLICATIONS	STUDENT PAPERS

PRIMARY SOURCES

1	arxiv.org Internet Source	28%
2	export.arxiv.org Internet Source	8%
3	Rudra Majhi, Soumya Chembra, Rukmani Mohanta. "Exploring the effect of Lorentz invariance violation with the currently running long-baseline experiments", The European Physical Journal C, 2020 Publication	3%
4	hdl.handle.net Internet Source	1%
5	Rudra Majhi, C Soumya, Rukmani Mohanta. "Light sterile neutrinos and their implications on currently running long-baseline and neutrinoless double-beta decay experiments", Journal of Physics G: Nuclear and Particle Physics, 2020 Publication	1%

Rukmani Mohanta
Dr. Rukmani Mohanta
Professor
School of Physics
UNIVERSITY OF HYDERABAD
Hyderabad-500 046.

6	Rudra Majhi, Dinesh Kumar Singha, K. N. Deepthi, Rukmani Mohanta. " Constraining violation with Hyper-Kamiokande and ESSnuSB ", Physical Review D, 2021 Publication	<1 %
7	RUDRA MAJHI, Soumya C, R Mohanta. "Light sterile neutrinos and their implications on currently running long-baseline and neutrinoless double beta decay experiments", Journal of Physics G: Nuclear and Particle Physics, 2020 Publication	<1 %
8	Submitted to KTH - The Royal Institute of Technology Student Paper	<1 %
9	P A Zyla, R M Barnett, J Beringer, O Dahl et al. "Review of Particle Physics", Progress of Theoretical and Experimental Physics, 2020 Publication	<1 %
10	Submitted to Tezpur University - CN-173457 Student Paper	<1 %
11	physicslearning2.colorado.edu Internet Source	<1 %
12	epdf.pub Internet Source	<1 %
13	home.phy.iitb.ac.in Internet Source	<1 %

Rukmani Mohanta

Dr. Rukmani Mohanta
Professor
School of Physics
UNIVERSITY OF HYDERABAD
Hyderabad-500 046.

Rukmani Mohanta

Dr. Rukmani Mohanta
Professor
School of Physics
UNIVERSITY OF HYDERABAD
Hyderabad-500 046.

14	link.springer.com Internet Source	<1 %
15	theor.jinr.ru Internet Source	<1 %
16	Submitted to University College London Student Paper	<1 %
17	etheses.dur.ac.uk Internet Source	<1 %
18	indico.fnal.gov Internet Source	<1 %
19	"Introduction to the Physics of Massive and Mixed Neutrinos", 'Springer Science and Business Media LLC', 2018 Internet Source	<1 %
20	Submitted to Higher Education Commission Pakistan Student Paper	<1 %
21	www.duo.uio.no Internet Source	<1 %
22	Submitted to University of Glasgow Student Paper	<1 %
23	"XXIII DAE High Energy Physics Symposium", Springer Science and Business Media LLC, 2021 Publication	<1 %

24	A Bandyopadhyay. "Physics at a future Neutrino Factory and super-beam facility", Reports on Progress in Physics, 10/01/2009 Publication	<1 %
25	Juan Pedro Ochoa-Ricoux. "A Search for Muon Neutrino to Electron Neutrino Oscillations in the MINOS Experiment", Springer Science and Business Media LLC, 2011 Publication	<1 %
26	ebin.pub Internet Source	<1 %
27	digitalassets.lib.berkeley.edu Internet Source	<1 %
28	www2.warwick.ac.uk Internet Source	<1 %
29	Submitted to Imperial College of Science, Technology and Medicine Student Paper	<1 %
30	Submitted to University of Edinburgh Student Paper	<1 %
31	mdpi-res.com Internet Source	<1 %
32	C Soumya, Mohanta Rukmani. "Non-unitary lepton mixing in an inverse seesaw and its impact on the physics potential of long-	<1 %

	baseline experiments", Journal of Physics G: Nuclear and Particle Physics, 2018 Publication	
33	mafiadoc.com Internet Source	<1 %
34	Submitted to Indian Institute of Technology Guwahati Student Paper	<1 %
35	Sanjib Kumar Agarwalla. "Physics Potential of Long-Baseline Experiments", Advances in High Energy Physics, 2014 Publication	<1 %
36	Submitted to University of Wollongong Student Paper	<1 %
37	eprints.hec.gov.pk Internet Source	<1 %
38	library.oapen.org Internet Source	<1 %
39	sro.sussex.ac.uk Internet Source	<1 %
40	"Workshop on Frontiers in High Energy Physics 2019", Springer Science and Business Media LLC, 2020 Publication	<1 %
41	Michael F. L'Annunziata. "The atomic nucleus, nuclear radiation, and the interaction of	<1 %

radiation with matter", Elsevier BV, 2020
Publication

42	R.D. McKeown, P. Vogel. "Neutrino masses and oscillations: triumphs and challenges", Physics Reports, 2004 Publication	<1 %
43	Sanjib Kumar Agarwalla, Sudipta Das, Alessio Giarnetti, Davide Meloni. "Model-independent constraints on non-unitary neutrino mixing from high-precision long-baseline experiments", Journal of High Energy Physics, 2022 Publication	<1 %
44	Submitted to University of Sheffield Student Paper	<1 %
45	www.escholar.manchester.ac.uk Internet Source	<1 %
46	www.pd.infn.it Internet Source	<1 %
47	K. A. Olive. "Introduction to Supersymmetry: Astrophysical and Phenomenological Constraints", Les Houches - Ecole d'Ete de Physique Theorique, 2000 Publication	<1 %
48	Submitted to The University of Manchester Student Paper	<1 %

49	www.ino.tifr.res.in Internet Source	<1 %
50	www.science.gov Internet Source	<1 %
51	Jaydeep Datta, Mohammad Nizam, Ali Ajmi, S. Uma Sankar. "Matter vs vacuum oscillations in atmospheric neutrinos", Nuclear Physics B, 2020 Publication	<1 %
52	Irene Tamborra. "Neutrino and antineutrino spectral splits from collective effects in supernovae", Journal of Physics Conference Series, 01/01/2010 Publication	<1 %
53	Submitted to Nanyang Technological University, Singapore Student Paper	<1 %
54	etheses.bham.ac.uk Internet Source	<1 %
55	hal-amu.archives-ouvertes.fr Internet Source	<1 %
56	Submitted to King's College Student Paper	<1 %
57	publikationen.bibliothek.kit.edu Internet Source	<1 %

58	zone.biblio.laurentian.ca Internet Source	<1 %
59	"XXII DAE High Energy Physics Symposium", Springer Science and Business Media LLC, 2018 Publication	<1 %
60	jyx.jyu.fi Internet Source	<1 %
61	nbn-resolving.de Internet Source	<1 %
62	Alain Mazure. "From telescopes to accelerators", Matter Dark Matter and Anti-Matter, 2012 Publication	<1 %
63	B. Ananthanarayan. "Pentaquarks: Do they exist?", Resonance, 01/2006 Publication	<1 %
64	Lothar Oberauer, Aldo Ianni, Aldo Serenelli. "Solar Neutrino Physics", Wiley, 2020 Publication	<1 %
65	Philip Rodrigues. "A Sterile-Neutrino Search with the MINOS Experiment", 'Office of Scientific and Technical Information (OSTI)', 2011 Internet Source	<1 %
66	cds.cern.ch Internet Source	

		<1%
67	webthesis.biblio.polito.it Internet Source	<1%
68	www.arxiv-vanity.com Internet Source	<1%

Exclude quotes	On	Exclude matches	< 14 words
Exclude bibliography	On		

Plagiarism-free statement

This is to certify that the thesis entitled "Exploring Physics Beyond the Standard Model with Neutrino Oscillation" has been screened by the Turnitin software at the Indira Gandhi Memorial Library (IGML), University of Hyderabad. The software shows 47% similarity index out of which, 36% came from the candidate's pre published version of research articles related to this thesis. Also, 3%, 2% and 1% similarity index came from his published research articles in European Physical Journal C(2020), Journal of Physics G (2020) and Physical Review D (2021), respectively. The remaining effective similarity is 4% after excluding his research articles is below 10% stipulated by the University guidelines. These similarities came from sources or articles in which the software detected mostly generic terms, standard notations, standard equations, standard symbols and common terminologies frequently used in the field. Therefore, this thesis is free from plagiarism.

Rukmani Mohanta

Prof. Rukmani Mohanta
(Thesis Supervisor)

Dr. Rukmani Mohanta
Professor
School of Physics
UNIVERSITY OF HYDERABAD
Central University P.O.
Hyderabad-500 046.


ν_μ
ν_τ
ν_e